Department of Construction Sciences

Solid Mechanics

ISRN LUTFD2/TFHF-26/5001-SE(1-150)

Evaluation and Development of Fatigue Design Methods for Tightening Bolts

Master's Dissertation by

Tony Nguyen

Supervisors:
Anders Lüning, Alfa Laval
Erik Jacobsson, Division of Solid Mechanics Lund University
Daniel Hård, Division of Solid Mechanics Lund University

Examiner:
Håkan Hallberg, Division of Solid Mechanics Lund University

Printed by Media-Tryck AB, Lund, Sweden
For information, address:
Division of Solid Mechanics, Lund University, Box 118, SE-221 00 Lund, Sweden
Webpage: www.solid.lth.se

Abstract

This thesis investigates fatigue assessment of tightening bolts in gasketed plate heat exchangers, with particular focus on the discrepancy between conservative code-based predictions and the long service lives observed in practice. The work addresses two fatigue contributions: high-cycle operational loading and larger-amplitude assembly loading. For the operational loading, the study examines whether the statistical interpretation of existing bolt fatigue data may be overly conservative. For the assembly loading, a local strain-based assessment route is explored using analytical modelling and finite element analysis. A structured literature review, finite element modelling, and a proposed experimental test strategy are combined to establish a technically defensible basis for a more representative fatigue evaluation of tightening bolts in this application.

Sammanfattning

Detta examensarbete behandlar utmattningsbedömning av åtdragningsbultar i packningsförsedda plattvärmeväxlare, med särskilt fokus på skillnaden mellan konservativa kodbaserade livslängdsprognoser och den långa livslängd som observerats i praktiken. Arbetet behandlar två utmattningsbidrag: högcyklisk driftbelastning och monteringsbelastning med större amplitud. För driftbelastningen undersöks om den statistiska tolkningen av befintliga utmattningsdata för bultar är onödigt konservativ. För monteringsbelastningen studeras i stället en lokal töjningsbaserad metod med hjälp av analytisk modellering och finita elementanalys. Genom en strukturerad litteraturstudie, finita elementmodellering och ett föreslaget experimentellt testupplägg etableras en tekniskt välgrundad grund för en mer representativ utmattningsbedömning av åtdragningsbultar i denna tillämpning.

Acknowledgements

I would like to express my sincere gratitude to my supervisors, colleagues at Alfa Laval, and the Division of Solid Mechanics at LTH for their guidance and support throughout this project. Special thanks to my family and friends for their continuous encouragement.

Nomenclature

Symbols

Symbol	Description	Unit
A	Cross-sectional area	mm^2
A_0	Material constant for plasticity correction	-
A_b	Major-diameter area	mm^2
A_s	Tensile stress area	mm^2
b	Basquin exponent	-
C	Fatigue design curve constant (Class number)	-
C_1, C_2	Fatigue design curve constants for specific cycle ranges	-
C_d	Parameter defining the S_r-N relationship for d std. dev.	-
C_o	Parameter defining the mean line S_r-N relationship	-
c	Fatigue ductility exponent	-
D	Damage (Miner's rule)	-
D_ass	Damage from assembly cycles	-
D_f	Fatigue damage index	-
D_op	Damage from operational cycles	-
d	Bolt diameter / Major diameter / Number of standard deviations (context)	$\frac{\text{mm}}{-}$
d_1, d_3	Minor diameter of external thread	mm
d_2	Basic pitch diameter of external thread	mm
E	Young's modulus	GPa
F	Force (general) / Test factor (context)	$\frac{\text{N}}{-}$
F_m	Mean force	N
F_a	Force amplitude	N
F_B	Bolt force	N
f_b	Overall bolt correction factor	—
F_e	Thickness correction calculation factor	—
f_e	Thickness correction factor	—
f_m	Mean stress correction factor	-
F_s	Surface finish factor (constant part)	-
f_s	Surface finish correction factor	-
f_{T^*}	Temperature correction factor	—
f_u	Overall correction factor for unwelded components	-
H	Height of the fundamental triangle of the thread	mm
K	Monotonic strength coefficient	-
k	One-sided tolerance factor	-
K'	Cyclic strength coefficient	-
k_e	Plasticity correction factor	-
K_t	Theoretical stress concentration factor	-

K_f	Fatigue (effective) stress concentration factor	-
K_σ	Stress concentration factor	-
K_ε	Strain concentration factor	-
k_{tb}	Thickness reduction factor for bolts	-
M	Mean stress sensitivity	-
m	Gasket maintenance factor / Inverse slope of the S-N curve	-
m_1, m_2	Inverse slopes of the fatigue design curves	-
N	Number of cycles / Allowable number of cycles	cycles
n	Number of test results	-
n_1, n_i	Actual or specified number of cycles	cycles
N_1, N_i	Allowable number of cycles at stress level i	cycles
$N_{\text{c,gm}}$	Geometric mean number of cycles	cycles
N_f	Cycles to failure	cycles
N_{ass}	Predicted assembly fatigue life	cycles
N_{EN}	Allowable number of cycles from selected EN 13445 S– N curve	cycles
N_{init}	Cycles to initiate a fatigue crack	cycles
N_{prop}	Cycles to propagate it subcritically	cycles
N_{req}	Required fatigue life	cycles
N_t	Transition life	cycles
n_{ass}	Specified number of assembly cycles	cycles
n_f	Cyclic strain hardening exponent	-
n_m	Strain hardening exponent	-
n_{op}	Specified number of operational cycles	cycles
P	Thread pitch	mm
P_{min}	Minimum pressure	MPa
P_{s}	Cyclic pressure amplitude / test pressure	MPa
R	Stress ratio, $R = \sigma_{\text{min}}/\sigma_{\text{max}}$	-
$R_{p0.2}$	0.2% offset yield strength	MPa
$R_{p0.2/T^*}$	0.2% offset yield strength at evaluation temperature	MPa
R_{z}	Peak-to-valley height for surface finish	µm
r	Notch radius	mm
S	Stress range / stress level / bolt fatigue strength (context)	MPa
s	Estimated standard deviation	cycles
S_a	Stress amplitude	MPa
S_{B}	Fatigue strength for bolts	MPa
SD	Standard deviation of log N	-
S_m	Mean stress	MPa
S_{max}	Maximum stress	MPa
S_{min}	Minimum stress	MPa
S_{r}	Applied stress range (BS 7608)	MPa
T^*	Evaluation temperature	$°C$
T_{max}	Maximum metal temperature	°C
T_{min}	Minimum metal temperature	°C
t	Bolt diameter / thickness	mm

t_{B}	Reference bolt diameter	mm
t_{eff}	Effective bolt diameter	mm
W_{M1}	Tension of bolts in service	N
W_{M2}	Tension of bolts at assembly	N
y	Initial gasket stress at assembly	MPa
γ	Material fitting parameter	-
$\hat{\mu}$	Fitted mean logarithmic fatigue life	cycles
Ω	Degree of bending	-
σ	Stress (general)	MPa
σ_a	Stress amplitude	MPa
σ_{ar}	Stress amplitude for zero mean stress	MPa
σ_e	Endurance limit (fatigue limit)	MPa
$\overline{\sigma}_{\mathrm{eq}}$	Mean equivalent stress	MPa
$\overline{\sigma}_{\mathrm{eq,r}}$	Reduced mean equivalent stress	MPa
σ'_f	Fatigue strength coefficient (Basquin)	MPa
σ_{max}	Maximum stress	MPa
σ_m	Mean stress	MPa
σ_{min}	Minimum stress	MPa
σ_{peak}	Peak stress	MPa
σ_{struc}	Structural stress	MPa
σ_{total}	Total stress	MPa
σ_{TS}	Ultimate tensile strength	MPa
σ_y	Yield strength	MPa
σ_0	Nominal stress	MPa
$\tilde{\sigma}_f$	True fracture strength	MPa
ΔK_{B}	Stress intensity factor range	$\mathrm{MPa}\sqrt{\mathrm{m}}$
ΔL	Change in bolt length	mm
ΔP	Cyclic pressure range	MPa
$\Delta\sigma$	Stress range, $\sigma_{\mathrm{max}} - \sigma_{\mathrm{min}}$	MPa
$\Delta\sigma^{\infty}$	Range of the fully reversed stress	MPa
$\Delta\sigma_{\mathrm{D}}$	Endurance limit for unwelded material	MPa
$\Delta\sigma_{\mathrm{eq,total}}$	Total equivalent stress range	MPa
$\Delta\sigma_{\mathrm{eq,struc}}$	Structural equivalent stress range corrected for plasticity	MPa
$\Delta\sigma_{\mathrm{eq,l,mechanical}}$	Pseudo-elastic structural stress range for unwelded parts	MPa
$\Delta\sigma_f$	Effective total stress range	MPa
$\Delta\sigma_{\mathrm{R}}$	Reference stress range	MPa
ε	Strain (general)	–
$\Delta\varepsilon_e$	Elastic strain range	–
$\Delta\varepsilon_p$	Plastic strain range	–
$\Delta\varepsilon$	Total strain range	–
$\Delta\tilde{\varepsilon}$	Total true (stabilized) strain range	–
ε'_f	Fatigue ductility coefficient	–

Abbreviations

Abbrev.	Meaning
ASME	American Society of Mechanical Engineers
BISO	Bilinear Isotropic Hardening
BKIN	Bilinear Kinematic Hardening
CEN	European Committee for Standardization
EN 13445	Unfired pressure vessels (European standard)
FE	Finite Element
FEA	Finite Element Analysis
GPHE	Gasketed Plate Heat Exchanger
HCF	High-cycle fatigue
ISO	International Organization for Standardization
LCF	Low-cycle fatigue
PED	Pressure Equipment Directive (2014/68/EU)
S–N	Stress-life (Wöhler) curve
TWI	The Welding Institute
UTS	Ultimate tensile strength
Wöhler	Fatigue testing method / Wöhler curve

Contents

1

Introduction

1.1 Background

Alfa Laval's gasketed plate heat exchangers (GPHEs) are clamped by tightening bolts located along the edges of the frame plates, Figure 1.1. The primary function of the bolts is to maintain compression of the plate package and gasket interfaces during operation. During their service life, the tightening bolts are subjected to two distinct types of repeated load variations that must be assessed with respect to fatigue. The first is *operational loading*, which consists of high-cycle stress fluctuations driven by internal pressure variations during continuous service. The second is *assembly loading*, characterized by low-cycle, large-amplitude stress excursions occurring when the heat exchanger is tightened, un-tightened, and re-tightened during maintenance procedures.

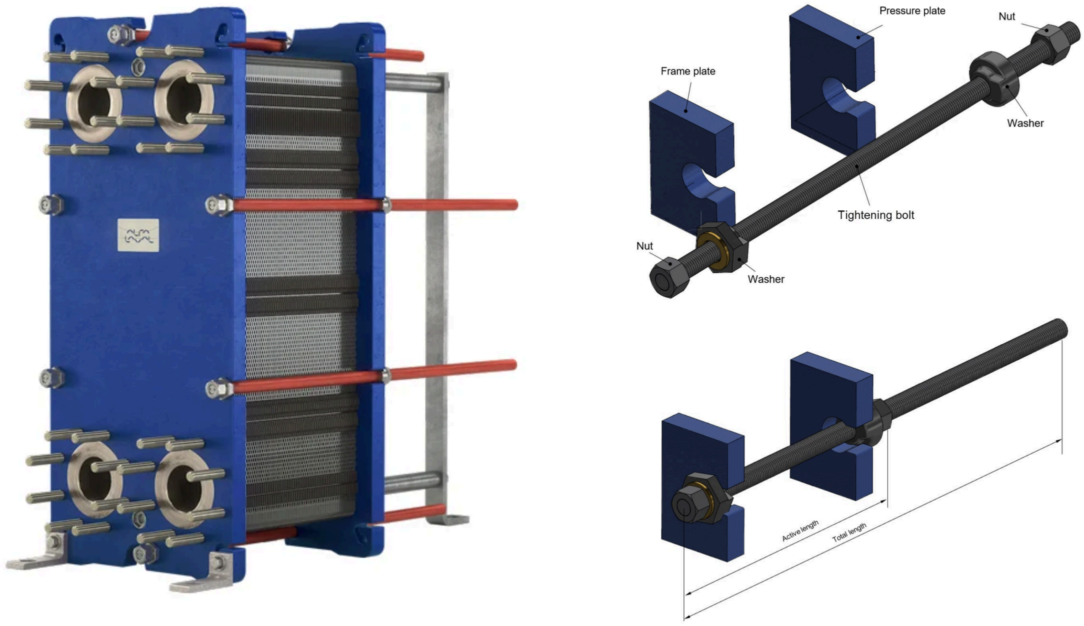

(a) Gasketed plate heat exchanger. (b) Tightening bolt construction.

Figure 1.1: Alfa Laval GPHE and tightening bolt construction.

Under EN 13445-3, bolt fatigue is evaluated using standardized stress–life (S–N) curves derived from axially loaded bolt test data and reduced to conservative design levels. This approach is intended to provide safe and broadly applicable design rules. However, extensive Alfa Laval field experience indicates that the tightening bolts in GPHE applications last far longer than direct application of the code curves would suggest. Over decades of service, no fatigue failures have been observed in situations where the code-based assessment would imply a much shorter life.

In representative assembly loading calculations, direct application of the current EN 13445 bolt fatigue curve may lead to predicted lives on the order of only 10^3–10^4 assembly cycles, depending on the precise load definition and correction assumptions adopted. By contrast, Alfa Laval field experience indicates no known fatigue failures of tightening bolts in comparable applications over many decades of service. While exact service histories are not disclosed here, the observed endurance in practice is clearly much greater than the order of magnitude implied by the direct code-based calculation.

This discrepancy suggests that the current code-based fatigue representation may not be fully representative of the loading and response of tightening bolts in this specific application.

In addition, the GPHE tightening bolts are large, high-strength, standardized fasteners manufactured by thread rolling and heat treatment.

1.2 Research problem and thesis approach

The fatigue assessment problem studied in this thesis is that the loading of Alfa Laval tightening bolts cannot be represented adequately by a single conventional interpretation of the standardized bolt fatigue curve. The direct code-based fatigue prediction for the extreme case can be limited to only a few thousand assembly cycles, whereas the observed service performance indicates substantially greater endurance without known fatigue failures, Figure 1.2.

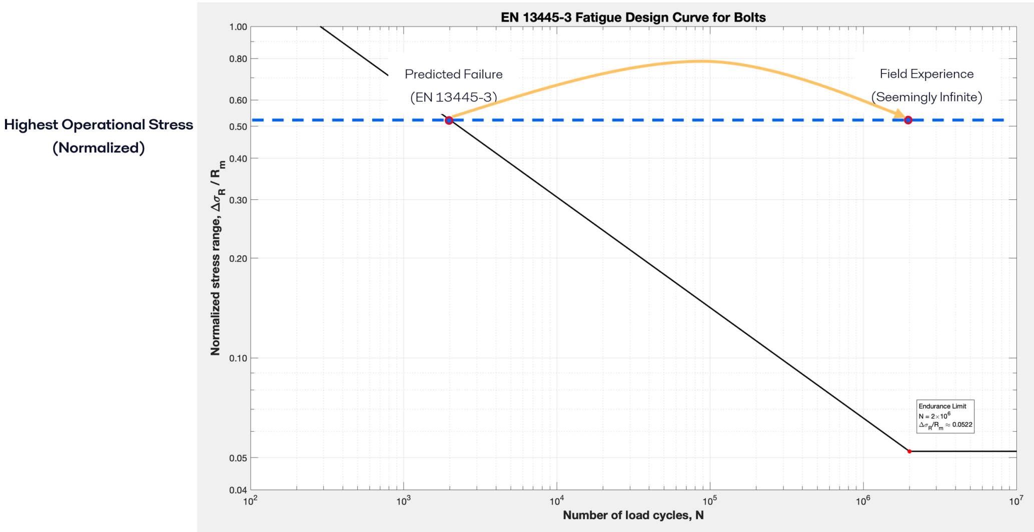

Figure 1.2: Current discrepancy between the predicted fatigue life and field experience.

For the operational loading, the main issue is not necessarily the absence of fatigue data, but rather how the existing data behind current bolt design curves are interpreted statistically. Previous work, in [1] and [2], has suggested that the current treatment may be unnecessarily conservative for threaded fasteners, particularly in the high-cycle regime relevant to operational loading. One part of the present thesis therefore investigates whether the standardized bolt fatigue data, together with published literature, support a less conservative and more representative interpretation for the operational loading.

For the assembly loading, the issue is different. Here the relevant cycle may be a large zero-based excursion from an unloaded or disassembled state to full tightening and subsequent peak operating load, Figure 1.3. Such a cycle is not well represented by the conventional pretensioned axial bolt fatigue tests on which code-based S–N curves are largely founded. For this loading class, a local elastoplastic assessment route is therefore considered more appropriate, based on finite element analysis, strain–life concepts, and a proposed test strategy for large-amplitude zero-based loading.

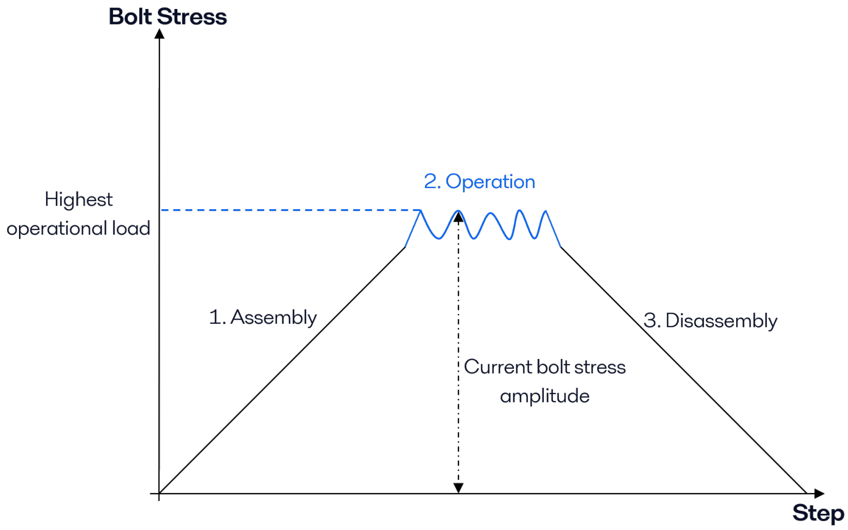

Figure 1.3: Bolt load cycle for some Alfa Laval GPHEs.

1.3 Scope

The work focuses on axial loading and local stress or strain effects in tightening bolts for GPHEs under both operational loading and assembly loading. Particular emphasis is placed on the first engaged thread root, where fatigue crack initiation is expected to occur. The thesis combines literature review, analytical modelling, finite element analysis, and experimental planning.

2

Fatigue Theory

Relevant fatigue theory includes the basic mechanisms of fatigue crack initiation and growth, the stress–life and strain–life approaches, mean stress effects, cumulative damage, and the influence of notches. Since the present work focuses on threaded bolts, particular importance is placed on notch sensitivity, local strain methods, and elastoplastic notch-root behaviour using Ramberg–Osgood and Neuber analysis. Mechanisms associated with overloads and crack-growth retardation are also briefly included, since they may influence the interpretation of severe loading events.

2.1 Fatigue of Materials

In 1874, German engineer H. Gerber, began developing methods for fatigue design [3]. Gerber contributed to the development of methods for fatigue life calculations for different mean levels of cyclic stresses. Later, Goodman also addressed related issues in 1899. The progression of fatigue damage may be described in terms of five stages. The first stage consists of sub-structural and microstructural changes that lead to the nucleation of permanent damage and is not shown explicitly in Figure 2.1. The subsequent macroscopic stages correspond to those illustrated in the figure,

1. the creation of microscopic cracks;
2. the growth and coalescence of microscopic flaws to form a dominant crack, commonly marking the transition from crack initiation to crack propagation;
3. stable propagation of the dominant macro-crack; and
4. structural instability or complete fracture.

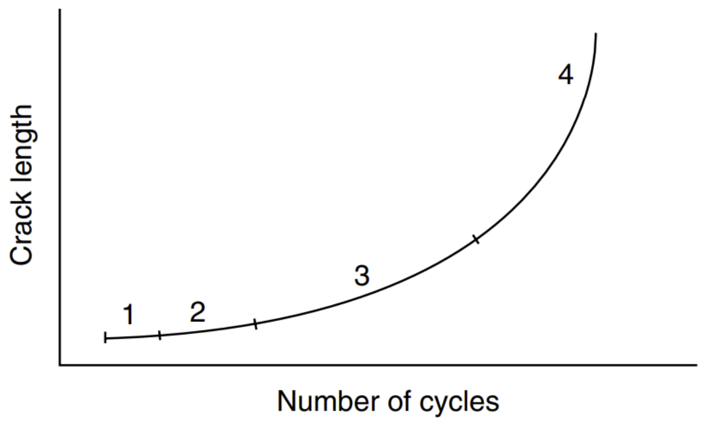

Figure 2.1: Fatigue failure sequence in a bolt under cyclic tensile loading. The figure illustrates the macroscopic stages of failure: (1) crack initiation, (2) crack growth, (3) crack propagation, and (4) final rupture. Adapted from [4].

The total fatigue life, N_f, may be expressed as the sum of the number of cycles required to initiate a fatigue crack, N_{init}, and the number of cycles required to propagate it subcritically to a final crack size, N_{prop},

$$N_f = N_{\text{init}} + N_{\text{prop}}. \tag{2.1}$$

Two classical approaches are commonly used to characterize fatigue life: the stress–life approach, in which life is related to the cyclic stress range (S–N), and the strain–life approach, in which life is related to the cyclic strain range, typically the total strain range or its elastic and plastic components.

2.2 Stress-life Approach

The S–N approach was introduced by Wöhler in the 1860s. This empirical approach is used widely in fatigue analysis, mostly in applications where low-amplitude cyclic stresses induce primarily elastic deformaiton in a component which is designed for long life – high cycle fatigue (HCF) applications.

2.2.1 Fatigue Limit

Some materials exhibit a fatigue behavior with a stress plateu level, below which the specimen can be cycled indefinitely without causing failure, called the fatigue limit or endurance limit, denoted by σ_e. For most steels and copper alloys the endurance limit is typically 35% to 50% of the tensile strength, σ_{TS}. The extrapolated intercept of the S–N curve with the ordinate stress amplitude, σ_a, is σ_{TS} at one-quarter of the first fatigue cycle, $N = 1/4$, as shown in Figure 2.2.

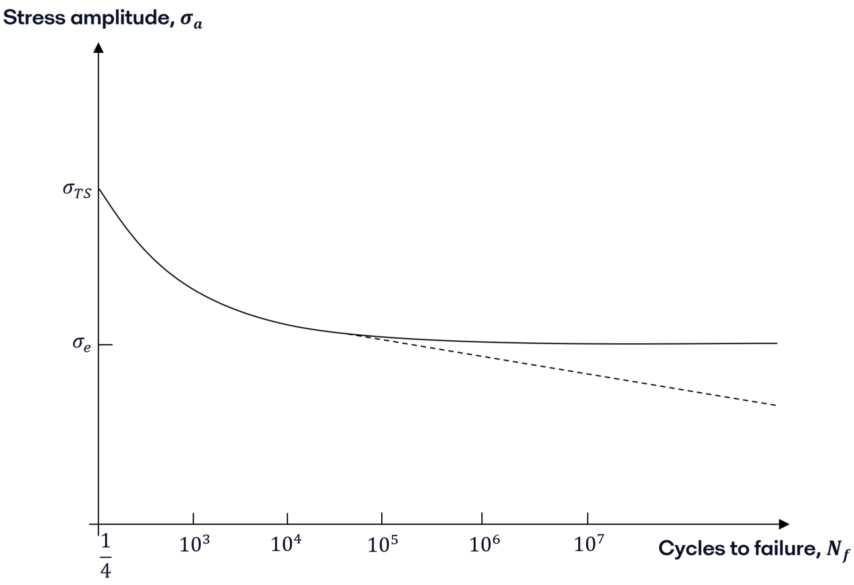

Figure 2.2: Typical S–N diagram

A number of high strength steels, aluminum alloys and other materials do not generally exhibit a fatigue limit. Instead σ_a continues to decrease with increasing number of cycles. In this case, an endurance limit is defined as the stress amplitude which the specimen can support for predefined number of cycles. Plotting using a log-log scale, with the true stress amplitude as a function of the number of cycles to failure, a linear relationship is commonly observed. Basquin's expression relates σ_a to the number of load reversals to failure, $2N_f$, for zero mean stress.

$$\sigma_{ar} = \sigma_f' \left(2N_f\right)^b \tag{2.2}$$

where σ_{ar} is the stress amplitude for zero mean stress, σ_f' is the fatigue strength coefficient and b is known as the fatigue strength exponent or Basquin exponent, which for most metals, is in the range of -0.05 to -0.12.

2.2.2 Mean Stress Effect on Fatigue Life

The mean stress is known to play an important role in influencing the fatigue behavior of engineering materials. Definitions of the stress range, the stress amplitude, the mean stress, and the load ratio are given as

$$\Delta\sigma = \sigma_{\max} - \sigma_{\min}, \quad \sigma_a = \frac{\sigma_{\max} - \sigma_{\min}}{2}, \quad \sigma_m = \frac{\sigma_{\max} + \sigma_{\min}}{2}, \quad R = \frac{\sigma_{\min}}{\sigma_{\max}}, \tag{2.3}$$

where $\sigma_{\max}$ and $\sigma_{\min}$ denote the maximum and minimum stresses within a loading cycle, respectively. When the stress amplitude from a uniaxial fatigue test is plotted against the number of cycles to failure, the resulting S–N curve is generally not unique but depends on the applied mean stress level. In other words, the position of the S–N curve shifts with mean stress. Typically, fatigue life decreases as the mean stress increases.

Constant-life diagrams account for mean stress effects in fatigue by representing combinations of mean stress and stress amplitude that correspond to the same fatigue life. The best-known constant-life relations are those of Gerber, Goodman, and Soderberg, and may be expressed as

$$\text{Soderberg relation:} \quad \sigma_a = \sigma_{ar}\left[1 - \frac{\sigma_\mathrm{m}}{\sigma_y}\right], \tag{2.4}$$

$$\text{Modified Goodman relation:} \quad \sigma_a = \sigma_{ar}\left[1 - \frac{\sigma_\mathrm{m}}{\sigma_\mathrm{TS}}\right], \tag{2.5}$$

$$\text{Gerber relation:} \quad \sigma_a = \sigma_{ar}\left[1 - \left(\frac{\sigma_\mathrm{m}}{\sigma_\mathrm{TS}}\right)^2\right], \tag{2.6}$$

where σ_a is the stress amplitude denoting the fatigue strength for a nonzero mean stress, σ_{ar} is the stress amplitude for a fixed life for a fully-reversed loading, i.e. $\sigma_\mathrm{m} = 0$ and $R = -1$, and σ_y and σ_TS are the yield strength and the ultimate tensile strength of the material, respectively.

Suresh provides a general rule-of-thumb for the application of constant-life models. In general form, the relationship may be expressed as

$$\frac{\sigma_a}{\sigma_{ar}} = f(\sigma_m). \tag{2.7}$$

The same form is also used for the endurance limit, for which σ_a and σ_{ar} are replaced by σ_e and σ_{er}, respectively.

1. Equation (2.4) provides a conservative estimate of fatigue life for most engineering alloys.
2. Equation (2.5) matches experimental results rather closely for brittle metals, but is conservative for ductile alloys.
3. Equation (2.6) is good for ductile alloys for tensile mean stresses, however, it does not distinguish between the difference in fatigue life due to tensile and compressive mean stresses.

Additional curves mentioned in [5], are the Morrow line, ASME-Elliptic, Smith-Watson-Topper criterion and the closely related Walker criterion.

The Morrow line is identical in nature to the Goodman line, except it replaces σ_TS as the x-axis intersect with the true fracture strength $\tilde{\sigma}_f$, or the fatigue strength coefficient σ_f', where σ_f'/E is the ordinate intercept of the elastic-strain line.

The ASME-elliptic criterion uses an elliptic equation to attempt to mix the qualities of Gerber and the Soderberg criteria to fit the fatigue data and check for yielding at the same time. It is sometimes conservative and sometimes nonconservative, for both fatigue and yielding.

The Smith-Watson-Topper (SWT) criterion is very good for aluminum and usually is reasonably good for steels, while having the advantage of simplicity in only needing two stress components.

The Walker criterion is considered the best match to experimental predictions for the equivalent fully reversed stress when the material fitting parameter γ is known. For steels, the estimate $\gamma = -0.0002\sigma_{TS} + 0.8818$ can be used.

$$\text{Morrow relation} \quad \sigma_a = \sigma_{ar}\left[1 - \frac{\sigma_\mathrm{m}}{\sigma'_f}\right] \tag{2.8}$$

$$\text{ASME-elliptic} \quad \left(\frac{\sigma_a}{\sigma_{ar}}\right)^2 = 1 - \left(\frac{\sigma_\mathrm{m}}{\sigma_\mathrm{y}}\right)^2 \tag{2.9}$$

$$\text{SWT relation} \quad \sigma_{ar} = \sqrt{(\sigma_\mathrm{m} + \sigma_a)\sigma_a} \tag{2.10}$$

$$\text{Walker relation} \quad \sigma_{ar} = (\sigma_\mathrm{m} + \sigma_a)^{1-\gamma}\sigma_a^\gamma \tag{2.11}$$

The different curves are shown and highlighted in Figure 2.3.

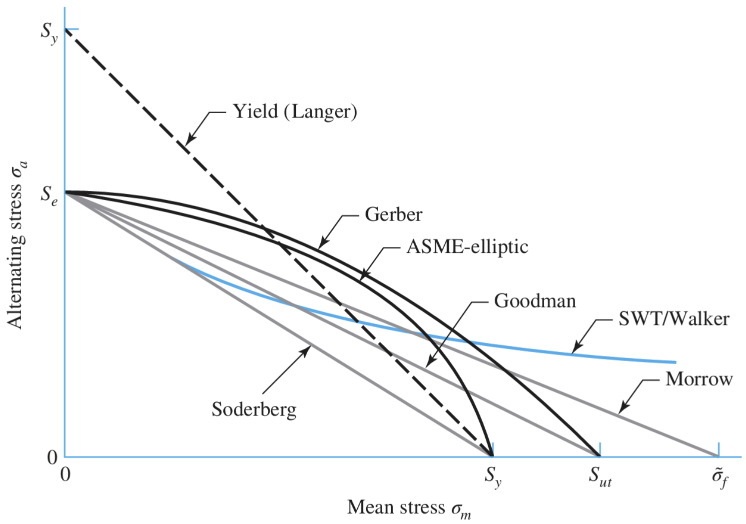

Figure 2.3: Constant-life diagram for fatigue limits. If service conditions (σ_a, σ_m) are below this line, then an infinite life is predicted [5].

The Basquin relation in Equation (2.2) describes the fully reversed stress amplitude and is therefore most directly associated with the case of zero mean stress. More generally, mean stress effects may be introduced through a constant-life relation of the form

$$\frac{\sigma_a}{\sigma_\mathrm{ar}} = f(\sigma_m), \tag{2.12}$$

where σ_ar is the fully reversed fatigue strength corresponding to the same fatigue life. Using Basquin's relation,

$$\sigma_{\mathrm{ar}} = \sigma'_f \left(2N_f\right)^b, \tag{2.13}$$

gives

$$\sigma_a = \sigma'_f \left(2N_f\right)^b f(\sigma_m). \tag{2.14}$$

To visualize the impact of mean stress across the entire finite life regime, these constant-life models can be expanded into three-dimensional surfaces. By evaluating the permissible stress amplitude σ_a as a simultaneous function of the applied mean stress σ_m and the number of cycles N_f, a complete physical operating envelope is generated.

Figure 2.4 illustrates these three-dimensional fatigue life surfaces for the Soderberg, Modified Goodman, and Gerber criteria. The surfaces clearly demonstrate how the allowable cyclic stress amplitude is mathematically forced to collapse as the static mean stress approaches the material's yield or ultimate tensile limits.

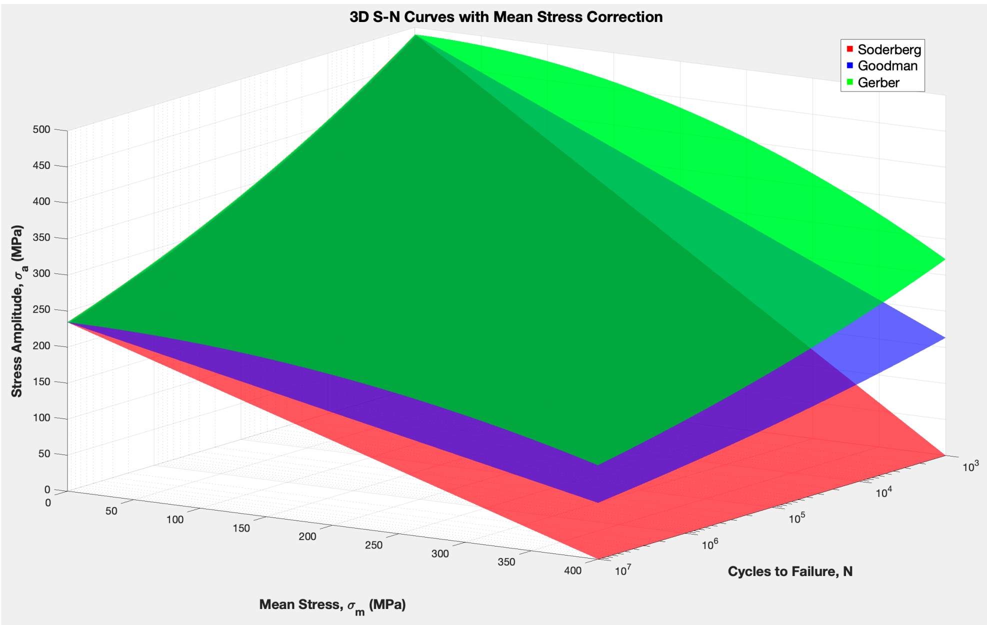

Figure 2.4: Three-dimensional fatigue life surfaces illustrating the relationship between cycles to failure (N), mean stress (σ_m), and permissible stress amplitude (σ_a) for the Soderberg, Modified Goodman, and Gerber criteria.

Similarly, Figure 2.5 maps the finite life surfaces for the Morrow, ASME-Elliptic, and Smith-Watson-Topper (SWT) models. Viewing these criteria across three axes provides a comprehensive physical intuition of how each mathematical model uniquely penalizes the presence of mean stress over the structural life of the component.

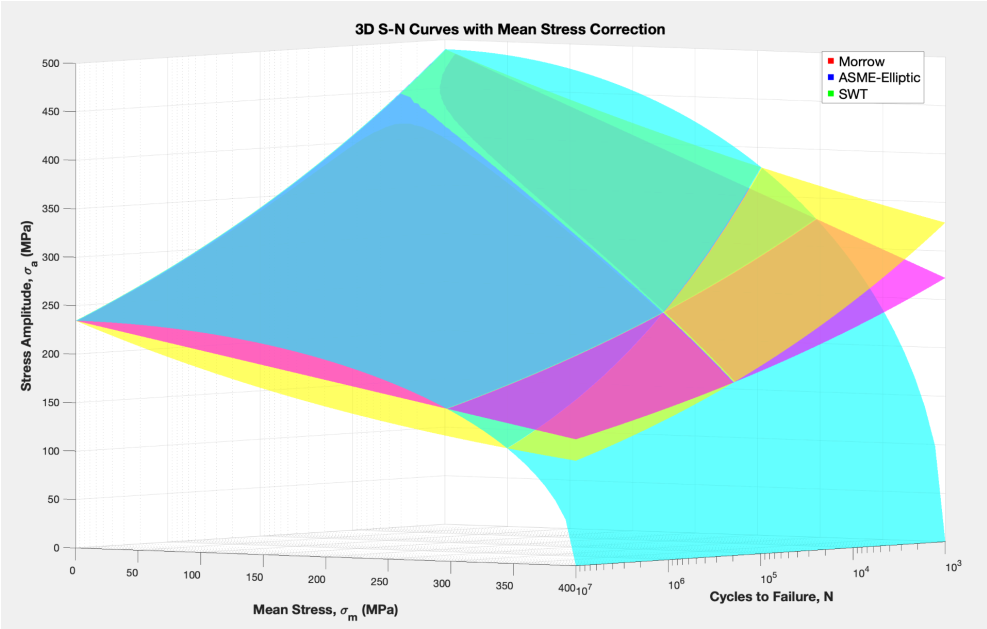

Figure 2.5: Three-dimensional fatigue life surfaces demonstrating the mean stress sensitivity of the Morrow, ASME-Elliptic, and Smith-Watson-Topper (SWT) criteria across the finite life regime.

Different mean stress correction models correspond to different choices of the function $f(\sigma_m)$. The modification proposed by Morrow is one such special case.

For the Morrow relation, the effect of mean stress is introduced by replacing σ'_f with $\sigma'_f - \sigma_m$, giving

$$\sigma_a = (\sigma'_f - \sigma_m)(2N_f)^b. \tag{2.15}$$

The number of cycles to fatigue failure for any nonzero mean stress, N_f, is then

$$N_f = \left[1 - \frac{\sigma_\mathrm{m}}{\sigma'_f}\right] \cdot N_f \mid_{\sigma_\mathrm{m}=0}, \tag{2.16}$$

where $N_f \mid_{\sigma_\mathrm{m}=0}$ is the number of cycles to failure for zero mean stress.

2.2.3 Cumulative Damage

In practice, engineering components are subjected to varying cyclic stress amplitudes, mean stresses and loading frequencies. The Palmgren–Miner cumulative damage rule provides a simple criterion for predicting the extent of fatigue damage induced by a particular block of constant amplitudes cyclic stresses, in a loading sequence consisting of various blocks of different stress amplitudes. In this linear damage rule, it is assumed that

1. The number of stress cycles imposed on a component, as a percentage of the fatigue life of the same equivalent amplitude, gives the fraction of damage.

2. The order that the stress blocks of different amplitudes are imposed does not affect the fatigue life.
3. Failure occurs when the linear sum of the damage from each load level reaches critical level.

The Palmgren–Miner damage rule states that failure occurs when

$$\sum_{i=1}^{m} \frac{n_i}{N_{\mathrm{f}i}} = 1 \tag{2.17}$$

where n_i is the number of cycles corresponding to the ith block of the constant stress amplitude $\sigma_{\mathrm{a}i}$ in a sequence of m blocks, and $N_{\mathrm{f}i}$ is the number of cycles to failure at $\sigma_{\mathrm{a}i}$.

Damage accumulation and failure under variable amplitude loading conditions are dictated by several concurrent mechanisms and that the linear damage rule may lead to inaccurate predictions of variable amplitude fatigue behavior in many cases. For example, the Palmgren–Miner damage rule predicts increased fatigue damage with increasing cyclic stress amplitude, even though it is well established that tensile overloads applied to notched and cracked metallic materials can reduce the rate of fatigue crack growth.

2.2.3.1 Surface Treatment Effects

Fatigue cracks often nucleate on the free surface of a component, so the manner in which the surface is prepared during manufacturing is crucial in dictating the intiation life for fatigue cracks. Residual stresses from the fabrication or surface and heat treatments, when superinposed with the applied fatigue loads, alter the mean level of the fatigue cycle and the fatigue life for crack nucleation. Compressive residual stresses are favorable as, generally, residual stresses affect the fatigue behavior of materials in the same way as the static mechanical stresses superimposed on a cyclic stress amplitude.

2.2.4 Stress Concentration

The theoretical stress-concentration factor K_t is defined for static loading conditions as

$$K_t = \frac{\sigma_{\mathrm{max,elastic}}}{\sigma_0}, \tag{2.18}$$

where nominal stress, $\sigma_0 = F/A_s$, is calculated using the applied force and tensile stress area [5]. Here, F is the load and the tensile stress area, A_s, is later shown and calculated in Equation (2.21).

For fatigue analysis, a fatigue stress concentration factor K_f is defined based on the fatigue strengths of notch free versus notched specimens at long-life conditions under fully reversed loading as

$$K_f = \frac{\text{Fatigue strength of notch-free specimen}}{\text{Fatigue strength of notched specimen}}. \tag{2.19}$$

In this context, fatigue strength refers to the stress amplitude required to cause failure at a given fatigue life.

Thus, K_f is a reduced K_t used for fatigue situations and is used in place of K_t as a stress increaser of the nominal stress,

$$\sigma_{\text{max,fatigue}} = K_f \sigma_0. \tag{2.20}$$

2.2.4.1 Tensile Stress Area

The tensile stress area, A_s, is the effective cross-sectional area used to calculate the nominal axial stress in the threaded part of a bolt. It is smaller than the shank area because the thread reduces the load-carrying section. In the present work, the tensile stress area is used to define the nominal bolt stress, the nominal thread stress, and the reference stress quantities appearing in both the analytical fatigue calculations and the finite element validation. It depends on the thread geometry and is calculated according to ISO 898-1 Section 9.1.6.1 [6] according to

$$A_{s,\text{nom}} = \frac{\pi}{4}\left(\frac{d_2 + d_3}{2}\right)^2 \tag{2.21}$$

where $A_{s,\text{nom}}$ is the nominal tensile stress area, d_2 is the basic pitch diameter of the external thread, d_3 is the basic minor diameter of the external thread, and P is the thread pitch. For ISO metric threads,

$$d_2 = d - 0.649519P, \tag{2.22}$$

where d is the nominal thread diameter. The dimensions d_2, d_3, and the fundamental thread profile are defined in ISO 68-1 and ISO 724. These dimensions are illustrated in Figure 2.6. The figure is reproduced from SS-ISO 724:2023 with due permission from SIS, Swedish Institute for Standards where the complete standard can be purchased.

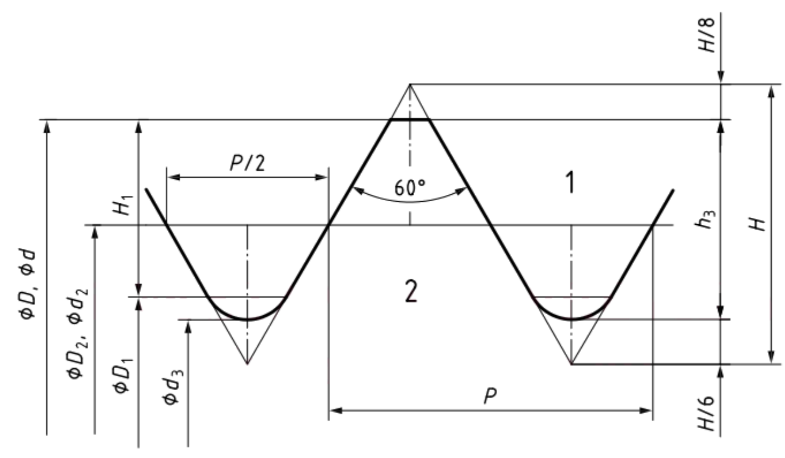

Figure 2.6: Basic dimensions on design profiles. [7]

For standard coarse-pitch and fine-pitch metric threads, tabulated values of the tensile stress area are provided directly in ISO 898-1. In the present work, the nominal tensile stress area calculated from Equation (2.21), or taken from the corresponding standard table, is thereafter denoted simply by A_s and used as the reference area for nominal stress calculations.

2.2.4.2 Combined Effect of Notches and Mean Stresses

With the instantaneous value S, the mean value S_m, and the amplitude S_a of the nominal cyclic stress in the member away from the notch, the local stress amplitude and mean stress at the notch root may be estimated from the fatigue notch factor K_f as

$$\sigma_a = K_f S_a, \quad \sigma_\mathrm{m} = K_f S_\mathrm{m}, \tag{2.23}$$

where the peak value of $K_f S$ is always smaller than the yield strength of the material σ_y in both tension and compression [3].

2.3 Strain-life approach

It was proposed that the fatigue life could be characterized using the plastic strain amplitude. The logarithm of the plastic strain amplitude, $\Delta\varepsilon_\mathrm{p}/2$, plotted against the logarithm of the number of load reversals to failure, $2N_f$, provided a linear relationship for metallic materials

$$\frac{\Delta\varepsilon_\mathrm{p}}{2} = \varepsilon_\mathrm{f}'\left(2N_f\right)^c, \tag{2.24}$$

where ε_f' is the fatigue ductility coefficient and c is the fatigue ductility exponent. Generally, ε_f is a approximately equal to the true fracture ductility ε_f in monotonic tension, and c is in the range of -0.5 to -0.7 for most metals.

2.3.1 Cyclic Hysteresis Loop

Strain cycling may lead to changes in the monotonic material properties, such as cyclic hardening or softening, however with relatively few cycles the material response settles into a stable cyclic hysteresis loop such as in Figure 2.7 [5]. The geometric and physical characteristics of this stabilized loop form the foundational basis for local strain-life fatigue testing and life-prediction algorithms. As illustrated in Figure 2.7, the total width of the loop represents the total true strain range ($\Delta\tilde{\varepsilon}$), while its total height defines the true stress range ($\Delta\tilde{\sigma}$). The total true strain amplitude, $\Delta\tilde{\varepsilon}/2$ is comprised of an elastic component, $\Delta\tilde{\varepsilon}_e/2$, and a plastic component, $\Delta\tilde{\varepsilon}_p/2$. So for each strain reversal, a strain-life fatigue test produces two data points, both elastic and plastic.

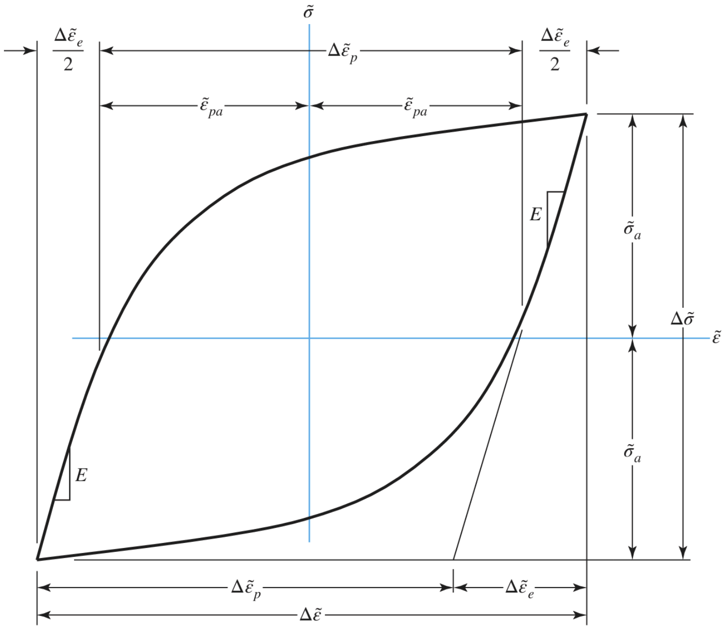

Figure 2.7: A stabilized cyclic stress-strain hysteresis loop under completely reversed strain-controlled conditions. The loop geometry defines the total true stress range ($\Delta\tilde{\sigma}$) and total true strain range ($\Delta\tilde{\varepsilon}$). The width at the mean stress axis explicitly isolates the plastic strain range ($\Delta\tilde{\varepsilon}_p$), while the linear unloading slope corresponds to the elastic modulus (E). [5]

2.3.2 Separation of Low-cycle and High-cycle Fatigue

The total strain amplitude in a constant strain amplitude test can be written as the sum of the elastic strain amplitude and plastic strain amplitude so that

$$\frac{\Delta\varepsilon}{2} = \frac{\Delta\varepsilon_{\mathrm{e}}}{2} + \frac{\Delta\varepsilon_{\mathrm{p}}}{2}. \tag{2.25}$$

It is noted that

$$\frac{\Delta\varepsilon_{\mathrm{e}}}{2} = \frac{\Delta\sigma}{2E} = \frac{\sigma_a}{E}, \tag{2.26}$$

where E is Young's modulus. Using Basquin's relation in Equation (2.2), it is found that

$$\frac{\Delta\varepsilon_{\mathrm{e}}}{2} = \frac{\sigma_f'}{E}\left(2N_f\right)^b. \tag{2.27}$$

Combining the Coffin-Manson relationship in Equation (2.24) with Equation (2.25) and Equation (2.27), yields

$$\frac{\Delta\varepsilon}{2} = \frac{\sigma_f'}{E}\left(2N_f\right)^b + \varepsilon_{\mathrm{f}}'\left(2N_f\right)^c. \tag{2.28}$$

This equation forms the basis for the strain-life approach to fatigue design and has found widespread application in industrial practice.

The strain-life relation is based on fully reversed tensile and compressive strain of equal amplitudes [5]. Strain-controlled cycling with a mean stress results in a relaxation of the mean stress for large strains, because of the plastic deformation. Thus, the stress tends to move toward centering around zero mean stress even as the strain cycles with a mean strain, where the mean strain has little effect.

2.3.3 Transition Life

It is useful to consider a transition life, N_t, which is defined as the number of reversals to failure at which the elastic and plastic strain amplitudes are equal. This intersection is seen in Figure 2.8. N_t is solved for from setting Equation (2.24) equal to Equation (2.27).

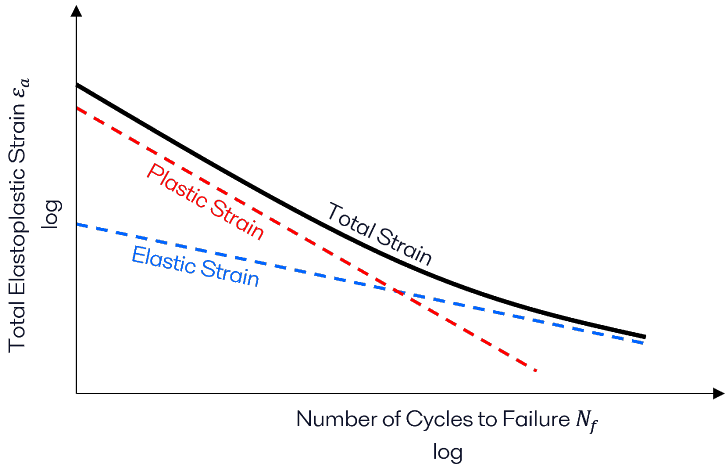

Figure 2.8: Strain-life curve (Coffin-Morrow)

The plastic strain term is more dominant than the elastic strain term at short fatigue lives, when $2N_f \ll 2N_t$, and the fatigue life of the material is controlled by ductility. With long fatigue lives, when $2N_f \gg 2N_t$, the elastic strain term is more dominant than the plastic strain term and the fatigue life is dictated by the rupture strength.

Mean stress effects have also been incorporated into the uniaxial strain-based characterization of fatigue life. By assuming that a tensile mean stress reduces fatigue strength σ'_f, such that

$$\sigma_a = \left(\sigma'_f - \sigma_{\mathrm{m}}\right)\left(2N_f\right)^b, \tag{2.29}$$

the strain life relation in Equation (2.28) can be rewritten as

$$\frac{\Delta\varepsilon}{2} = \frac{\sigma'_f - \sigma_{\mathrm{m}}}{E}\left(2N_f\right)^b + \varepsilon'_{\mathrm{f}}\left(2N_f\right)^c. \tag{2.30}$$

2.3.4 Local Strain Approach for Notched Members

The local strain approach relates deformation occuring in the immediate vicinity of a stress concentration to the remote stresses and strains using the constitutive response, and the analysis is divided into two steps.

1. The local stress and strain histories at the tip of the notch are determined from the imposed loads.
2. The expected fatigue life for the local stress and strain histories is determined.

The local stress and strain histories are determined from simple analytical expressions, detailed finite element simulations or experiments. Then the damage accumulation from the local stress and strain histories must also be estimated so that the safe fatigue life of the component can be assessed based on the low cycle fatigue properties measured on smooth laboratory test specimens.

2.3.5 Ramberg-Osgood Relationship

The Ramberg-Osgood relationship is a constitutive law to describe the monotonic stress-strain behavior of ductile solids under uniaxial tension,

$$\varepsilon = \frac{\sigma}{E} + \left(\frac{\sigma}{K}\right)^{\frac{1}{n_m}}, \tag{2.31}$$

where E is Young's modulus, K is a constant known as the monotonic strength coefficient, ε is the uniaxial strain, σ is the uniaxial stress, and n_m is the strain hardening exponent. The cyclic stress-strain response can then be represented by the relationship

$$\frac{\Delta\varepsilon}{2} = \frac{\Delta\sigma}{2E} + \left(\frac{\Delta\sigma}{2K'}\right)^{\frac{1}{n_f}}, \tag{2.32}$$

where K' is the cyclic strength coefficient and n_f is the cyclic strain hardening exponent.

2.3.6 Neuber Analysis

Stress and strain concentration factors are only directly applicable as elastic measures as long as the material response at the notch root remains elastic. Once yielding occurs, the local stress and strain concentration factors no longer remain equal to the purely elastic theoretical value and must instead be related through an elastoplastic notch rule.

The strain concentration factor, K_ε, is defined as the ratio of the maximum local strain, $\varepsilon_{\max}$, to the nominal strain, ε_0, i.e.

$$K_\varepsilon = \frac{\varepsilon_{\max}}{\varepsilon_0}. \tag{2.33}$$

Similarly, the stress concentration factor based on the actual local stress is

$$K_\sigma = \frac{\sigma_{\max}}{\sigma_0}. \tag{2.34}$$

For elastoplastic notch analysis, Neuber's rule assumes that the theoretical elastic stress concentration factor K_t is related approximately to the actual stress and strain concentration factors through

$$K_\sigma K_\varepsilon = K_t^2, \tag{2.35}$$

or equivalently,

$$K_t = \sqrt{K_\sigma K_\varepsilon}. \tag{2.36}$$

Substituting the definitions of K_σ and K_ε gives

$$\left(\frac{\sigma_{\max}}{\sigma_0}\right)\left(\frac{\varepsilon_{\max}}{\varepsilon_0}\right) = K_t^2, \tag{2.37}$$

which may be rearranged as

$$\sigma_{\max}\varepsilon_{\max} = K_t^2 \sigma_0 \varepsilon_0. \tag{2.38}$$

If the nominal response is elastic, such that

$$\varepsilon_0 = \frac{\sigma_0}{E}, \tag{2.39}$$

then Neuber's rule may also be written as

$$\sigma_{\max}\varepsilon_{\max} = K_t^2 \frac{\sigma_0^2}{E}. \tag{2.40}$$

For cyclic loading, an equivalent amplitude form is obtained by expressing the notch-root stress and strain in terms of stress and strain amplitudes. If $\Delta\sigma^\infty$ denotes the nominal applied elastic stress range, Neuber's rule may be written as

$$\Delta\sigma\Delta\varepsilon = \frac{(K_t \Delta\sigma^\infty)^2}{E}, \tag{2.41}$$

which is the equation of a rectangular hyperbola for fixed values of $K_t\Delta\sigma^\infty$.

This relation is commonly combined with a cyclic stress–strain law in order to estimate the local elastoplastic stress and strain at a notch root from the nominal elastic stress range. Using the cyclic Ramberg–Osgood relation,

$$\Delta\varepsilon = \frac{\Delta\sigma}{E} + \left(\frac{\Delta\sigma}{K'}\right)^{\frac{1}{n'}}, \tag{2.42}$$

gives

$$\Delta\sigma\Delta\varepsilon = \frac{(\Delta\sigma)^2}{E} + \Delta\sigma\left(\frac{\Delta\sigma}{K'}\right)^{\frac{1}{n'}}. \tag{2.43}$$

The local notch-root stress and strain amplitudes are then obtained from the simultaneous solution of the Neuber relation in Equation (2.41) and the cyclic stress–strain relation in Equation (2.43).

2.4 Crack Retardation from Tensile Overloads

Load excursions in the form of single tensile overloads or high-amplitude/low-amplitude block loading sequences can contribute to retardation of crack advance or even complete arrest of fatigue crack growth. At a baseline stress intensity factor range ΔK_B, the material exhibits a characteristic fatigue crack growth rate. When a tensile overload is applied, the ductile solid exhibits a small amount of temporarily accelerated crack growth, occurring mainly during application of the overload. The stretch zone is the marking on the fracture surface corresponding to the rapid crack extension during the overload cycle.

This accelerated crack growth may persist over many post-overload cycles if the overload causes a change in the microscopic or macroscopic fracture mode. In general, the burst of accelerated crack advance is followed by prolonged deceleration of crack growth when the post-overload crack is subjected to the same baseline ΔK_B as in the pre-overload regime. The delay distance is the crack-growth distance, a_d, over which the progressive reduction in crack velocity continues. After reaching a minimum, the crack growth rate begins to increase and eventually returns to the pre-overload baseline value.

2.4.1 Plasticity-Induced Crack Closure

The application of an overload produces a larger plastic stretch in the wake of the fatigue crack tip, while the fatigue crack propagates through the overload plastic zone. The attendent fracture surface contact causes an enhancement in the level of plasticity-induced crack closure in the post overload regime which promotes crack growth retardation. It would be reasonable to expect delayed retardation, since some crack growth through the overload plastic zone is needed for the residual plastic stretch to induce premature closure behind the crack tip.

2.4.2 Crack Tip Blunting

Post overload crack retardation could also be caused by the blunting of the crack tip by the overload cycle, which can persist during post overload crack growth. This retardation mechanism is that the blunted crack tip behaves like a notch with a less severe stress concentration than the originally sharp crack tip. It cannot, however, account for the existence of delayed retardation and cannot quantitatively rationalize the experimentally observed reductions in post overload crack growth.

2.4.3 Residual Compressive Stresses

Residual compressive stresses are produced by reverse yielding ahead of a fatigue crack loaded in cyclic tension. The size of the zone of residual compression is increased, when a tensile overload is applied.

2.4.4 Near-Threshold Mechanisms

A post overload intensity factor that is much lower than the nominal baseline value ΔK_{B} is achieved in fatigue cracks subjected to tensile overloads, the development of enhanced levels of plasticity-induced crack closure, residual compressive stresses or crack deflection. In these cases, additional mechanisms of fatigue crack growth retardation which are of significance to constant amplitude near-threshold fatigue, are also activated in the post overload regime. The activation of near-threshold mechanisms in the post-overload regime is not the primary cause of retardation but rather a process which prolongs retardation.

3

Statistical Evaluation of Fatigue Data

The statistical evaluation of fatigue data in the present work is based primarily on the framework described by Schneider and Maddox [8]. It provides the basis for fitting mean S–N relationships, treating censored data and run-outs, and deriving lower-bound design curves with defined statistical confidence.

3.1 Assumptions

It is assumed that there is an underlying relationship between $\log S$ and $\log N$ of the form

$$\log N = \log A - m \log S, \tag{3.1}$$

where m is the slope of the straight line in log–log space and $\log A$ is its intercept. The equivalent and more familiar form is

$$S^m N = A. \tag{3.2}$$

This assumption only holds true between certain limits on S. The lower limit on S is determined by the fatigue endurance limit while the upper limit is dependent on the static strength of the test specimen but is most commonly taken to be the maximum allowable static design stress.

It is also assumed that the fatigue life N for a given stress range S is log-normally distributed, that the standard deviation of $\log N$ does not vary with S, and that each test result is statistically independent of the others.

3.2 Fitting an S–N Curve

S–N data in their simplest form, comprise n data points of $\log S_\mathrm{i}$ and $\log N_\mathrm{i}$, where S_i is the stress range and N_i is the endurance in cycles.

Only using using the results from the failed specimens, the intercept log A and slope log m of the best-fit line through the data are estimated by ordinary linear regression. Normally, least squares estimation is the method used to estimate the slope and intercept coefficient.

3.3 Treatment of unfailed specimens and run-outs

When establishing the endurance limit of a component experimentally, it is generally assumed to be the highest applied stress range, for which a given applied mean stress or stress ratio, at and below which the test specimen endures a particular number of cycles without showing any evidence of fatigue cracking.

The standard S–N curve is typically modeled to descend to the endurance limit, at which point it abruptly levels off into a horizontal infinite-life plateau. In practice, however, fatigue test results normally follow an S–N curve that gradually changes slope in the region of the endurance limit. Test results from either failed or unfailed specimens that lie in this transition region nearing the endurance limit should not be combined with those obtained at higher stresses when estimating the best-fit linear S–N curve. As a guide, any result from notched or welded specimens that give $N < 2 \cdot 10^6$ cycles could be included, or $N < 10^6$ cycles in the case of results obtained from smooth specimens.

It may be necessary to model the S–N curve more precisely and include the transition regions at high and low applied stresses. In this case, the data corresponds to an S-shaped curve such as:

$$N = \frac{A \cdot \exp[-C(S - E)]}{S - E} - B \tag{3.3}$$

where A, B, C and E are constants.

Unfailed specimens provide essential data for estimating the best-fit S–N curve in two specific scenarios. The first involves tests that are deliberately halted before failure due to cycle or time limits. The second occurs in specimens with multiple potential failure sites, where failure at the primary location leaves the secondary sites unfailed.

3.4 Establishing a design curve

A distinction must be made between a fitted mean S–N curve and a design curve. The latter is intended to provide a lower-bound estimate of fatigue life with a specified statistical basis. Schneider and Maddox [8] discuss this in terms of prediction limits and tolerance limits.

For a fitted mean S–N line, lower prediction limits may be derived to estimate where a specified proportion of future observations is expected to lie. In engineering fatigue design, lower one-sided bounds are generally of greatest interest because a component surviving longer than predicted does not constitute a structural failure. This distinction relies on the assumption that the scatter of fatigue lives follows a normal distribution in the logarithmic domain. A two-sided 95% prediction interval captures the central 95% of the data, symmetrically excluding the lowest 2.5% and the highest 2.5% of the distribution. However, because the upper "safe" tail is acceptable in fatigue design, the lower boundary of that interval effectively bounds 97.5% of the population (the central 95% plus the upper 2.5%). Therefore, the lower one-sided 97.5% prediction limit is mathematically equivalent to the lower branch of a two-sided 95% prediction interval.

For small and medium datasets, however, it is often more appropriate to use a one-sided tolerance-limit approach when deriving a lower-bound design curve. In general form, this may be expressed as

$$\log N_{\text{design}} = \hat{\mu} - ks \tag{3.4}$$

where $\hat{\mu}$ is the fitted mean logarithmic fatigue life, s is the estimated standard deviation, and k is a one-sided tolerance factor depending on the sample size, the intended population coverage, and the required confidence level. This formulation is particularly useful when discussing what level of testing is required to support a new or modified design curve.

3.5 Interpretation of EN 13445 fatigue curves

For the present thesis, the most important statistical question is not how to fit an arbitrary S–N line, but how the existing EN 13445 bolt fatigue curve should be interpreted and how a possible supplementary curve might be derived.

According to Baylac and Koplewicz [9], the EN 13445 fatigue curves for bolting and weld details are based on statistical lower bounds to experimental datasets representing specified probabilities of survival. In the underlying treatment, mean S–N curves were fitted in log space and then reduced by a number of standard deviations in order to obtain conservative design lines. For bolt-related curves, this reduction has been interpreted as being approximately three standard deviations below the fitted mean, corresponding to a very high survival probability.

This interpretation is more conservative than the mean-minus-two-standard-deviation format often encountered in structural fatigue practice. The distinction is important in the present work, since one of the hypotheses is that the existing bolt fatigue curve may already be conservative in its statistical interpretation for the operational loading case.

3.6 Required sample size and statistical confidence

The number of fatigue tests required depends on the purpose of the program. A small dataset may be sufficient to identify the approximate slope and scatter of an S–N relationship or to determine whether a loading case differs clearly from an existing reference curve. A substantially larger dataset is required, however, if the aim is to establish a lower-bound design curve with stated statistical confidence.

Schneider and Maddox [8] show that the reduction from a fitted mean curve to a statistically defensible design curve depends explicitly on sample size. For limited datasets, this is typically handled through a one-sided tolerance-limit approach in Equation (3.4). For small values of the sample size n (the number of failed test specimens), the factor k becomes large, so the design curve must be placed substantially below the fitted mean.

A further practical point is whether the slope of the new S–N relationship is assumed to be the same as that of an existing reference curve. If the slope is fixed, the statistical burden is reduced. If both slope and intercept must be estimated from a small dataset, the uncertainty increases and the sample-size requirement becomes more demanding.

4

Fatigue Design Standards

The Danish adoption of the European standard, DS EN 13445-3 [10], together with Amendment A1 [11] defines the European rules for the fatigue assessment of unfired pressure vessels, covering welded components, unwelded components and axially loaded bolts. The fatigue provisions are contained in Clause 18 and are based on a stress-life (S–N) methodology combined with local stress concepts and cumulative damage assessment. For comparison, BS 7608 is also relevant in the present work, since it provides fatigue design guidance for steel structures and has influenced the interpretation of fatigue design curves used for bolts and other notched components. While EN 13445 forms the primary code basis for the present assessment, BS 7608 is used as a supporting reference in the discussion of fatigue curve derivation and statistical interpretation.

4.1 General fatigue framework

Clause 18 of EN 13445-3 establishes a structured fatigue assessment procedure comprising identification of fatigue-critical locations, determination of stress histories, cycle counting, selection of appropriate fatigue design curves, and cumulative damage evaluation using Miner's rule. A defining feature of EN 13445 is the explicit distinction between welded details, unwelded components and bolted joints, each of which is associated with specific stress definitions and fatigue design data.

Fatigue assessment is performed using an equivalent stress range derived from the multi-axial stress state, based on either the von Mises or Tresca criterion. Depending on the type of structural detail, nominal stresses, structural stresses, or structural hot-spot stresses may be employed. The standard explicitly supports the use of finite element analysis for determining stresses, with detailed guidance on modeling, stress linearization, and cycle counting provided in Annexes NA and NB in EN 13445-3.

4.2 Design Data

The fatigue strength of axially loaded bolts is expressed in terms of the ratio

$$\frac{\Delta\sigma}{R_m}, \tag{4.1}$$

where $\Delta\sigma$ is the maximum nominal stress range and R_m is the nominal ultimate tensile strength of bolt material.

The fatigue life is calculated from the single design curve with an endurance limit $\Delta\sigma_{\mathrm{D}}/R_m = 0.0522$ at $2 \cdot 10^6$ cycles

$$\left(\frac{\Delta\sigma_{\mathrm{R}}}{R_m}\right)^3 \cdot N = 285, \tag{4.2}$$

where $\Delta\sigma_{\mathrm{R}}$ is the reference stress range in the design curve. The design curve is shown in Figure 4.1.

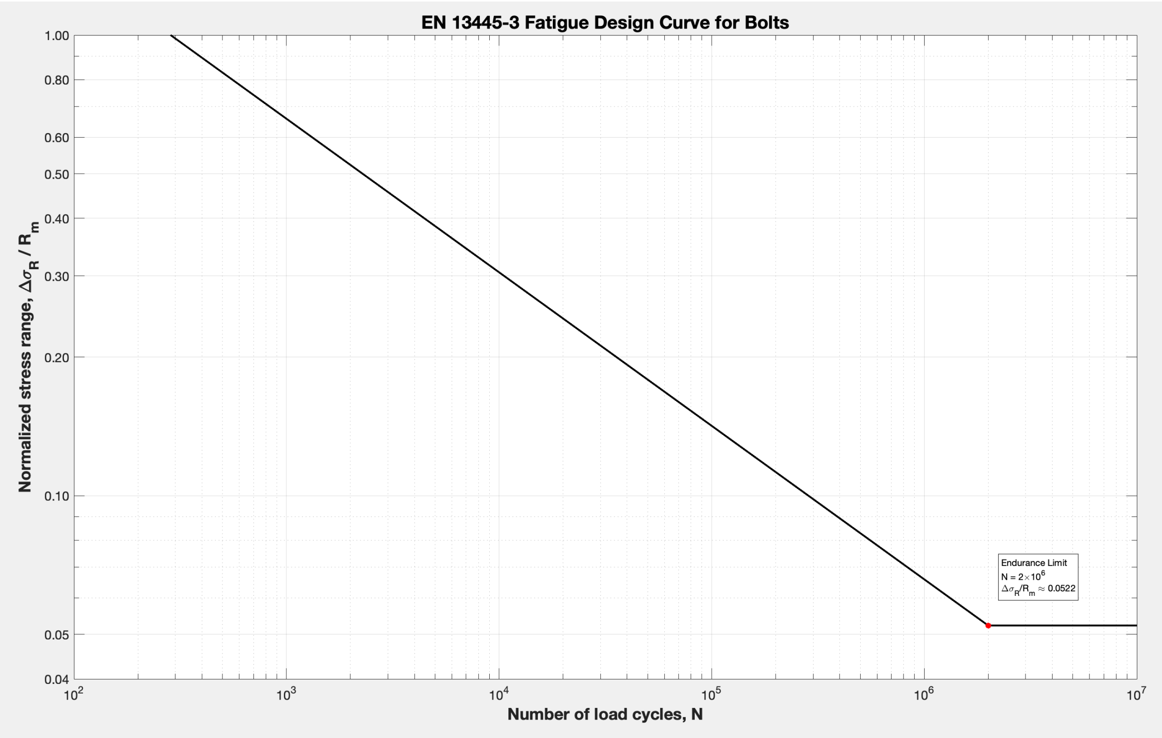

Figure 4.1: Fatigue design curve for bolts.

Equation (4.2) was derived from fatigue test data obtained from axially-loaded threaded connections.

The allowable number of load cycles, N, at a specified stress range, $\Delta\sigma$, above the endurance limit is calculated as

$$N = 285\left(\frac{R_m \cdot f_{\mathrm{b}}}{\Delta\sigma}\right)^3. \tag{4.3}$$

4.3 Fatigue Assessment of Bolts

Bolts are addressed separately in Subclause 18.12. The EN 13445 method is limited to axially loaded steel bolts and is based on a single normalized S–N curve expressed in terms of the ratio $\Delta\sigma/R_m$, where $\Delta\sigma$ is the nominal axial stress range on the minimum bolt cross-section and R_m is the ultimate tensile strength.

The EN 13445 bolt curve was derived directly from fatigue tests on real threaded bolts. The stress concentration effect at the first engaged thread is therefore implicitly included, and no explicit fatigue strength reduction factor is required. The curve represents a mean minus three standard deviations fit to the experimental database, corresponding to a failure probability of approximately 0.1% [9]. This does not imply that the overall design uncertainty in service is reduced to the same level, since additional effects outside the underlying laboratory database may influence practical fatigue performance.

The design curve does not include any correction for thread manufacturing method and is applicable to core diameters up to 25 mm, with a size correction applied for larger bolts. Although the curve is normalized by R_m, the ultimate tensile strength used in calculations is limited to a maximum of 785 MPa. The endurance limit is defined at $2 \cdot 10^6$ cycles.

The fatigue bolt design curve was adopted from the design curve for steel bolting in BS 7608, lowered to correspond to mean - 3 standard deviations of log N. The curve was directly based on fatigue data obtained from actual steel bolts, some under moderately high tensile mean stress.

4.3.1 Thickness Correction Factor

For bolt diameters greater than 25 mm, a size correction factor f_e is applied to account for the reduction in fatigue strength with increasing diameter. In practice, this acts as a modification of the fatigue strength associated with a given stress level, or equivalently as a correction to the effective stress used in the fatigue assessment. It is calculated as

$$f_\mathrm{e} = \begin{cases} F_\mathrm{e}^{(0.1\cdot\, \ln(N) - 0.465)} & \text{if } N < 2 \cdot 10^6 \text{ cycles} \\ F_\mathrm{e} \quad \text{if } N \geq 2 \cdot 10^6 \text{ cycles} \end{cases} \tag{4.4}$$

where

$$F_\mathrm{e} = \left(\frac{25\ \mathrm{mm}}{d_\mathrm{n}}\right)^{0.182}, \tag{4.5}$$

where d_n is the nominal bolt diameter. For bolt diameters smaller than or equal to 25 mm, $f_\mathrm{e} = 1$. Here, N is the allowable number of cycles associated to a stress level and is calculated by an iterative process. F_e is calculated inside a loop with only the use of stress range and fatigue, with other correction factors set to 1.

4.3.2 Temperature Correction Factor

For temperatures T^* exceeding 100°C, a temperature correction factor f_{T^*} is applied in the fatigue assessment to account for the reduction in fatigue strength at elevated temperature. It is calculated as

$$f_{T^*} = \begin{cases} 1.03 - 1.5 \cdot 10^{-4} T^* - 1.5 \cdot 10^{-6} T^{*2} & \text{for ferritic materials} \\ 1.043 - 4.3 \cdot 10^{-4} T^* & \text{for austenitic materials,} \end{cases} \tag{4.6}$$

where

$$T^* = 0.75 T_{\text{max}} + 0.25 T_{\text{min}}, \tag{4.7}$$

and where T_{max} and T_{min} are the maximum and minimum metal temperatures, respectively, experienced during the evaluated load cycle.

For temperatures, T^*, not exceeding 100°C, $f_{T^*} = 1$.

4.3.3 Overall Correction Factor for Bolts

The overall correction factor, f_b, is calculated as

$$f_b = f_e \cdot f_{T^*}. \tag{4.8}$$

This combined factor is used in the fatigue assessment to account for the joint influence of bolt diameter and temperature on fatigue strength.

4.3.4 OTO 97 067 - The Empirical Baseline

The standardized fatigue curves for threaded fasteners in current pressure vessel codes, including EN 13445, rely on legacy empirical testing. The most notable foundational work is the extensive experimental program documented in OTO 97 067 [12]. To establish a robust statistical baseline, these tests were conducted using a continuous distribution of load levels. While a comprehensive summary of the test matrices, rig setups, and detailed data tables is provided in Appendix A.1, several critical conclusions regarding bolt fatigue behaviour emerged from the results.

Regarding the variability in failure locations, the physical tests challenged the conventional fatigue assessment assumption that failure always occurs at the first engaged thread. Many specimens actually failed directly beneath the bolt head. For the 20 mm Grade 8.8 bolts, failure predominantly occurred at the cross-section entering the nut, although some rolled-thread specimens exhibited unusual failures at the very start of the threaded region.

Comparisons across 12 mm, 20 mm, and 36 mm diameters revealed a significant, albeit nonlinear and inconsistent, volumetric size effect. Increasing the diameter from 12 mm to 20 mm reduced fatigue life by approximately a factor of three, aligning with general fracture mechanics expectations. However, the 36 mm bolts unexpectedly demonstrated a life increase by a factor of 1.8 compared to the 20 mm bolts. This inconsistency highlighted that fatigue life is highly sensitive to the specific geometric proportions of the head-to-shank transitions and thread profiles, which can vary between manufacturing batches of different sizes.

The testing also highlighted the profound influence of heat treatment sequencing. Initial test series counterintuitively showed cut threads performing slightly better than rolled threads. Metallurgical examination revealed that these specific rolled bolts had been heat-treated after thread rolling, which thermally erased the beneficial compressive residual stresses at the thread root. When tested with bolts that were correctly thread-rolled after heat treatment, fatigue life dramatically increased by a factor of 4 to 10, confirming that manufacturing sequence is a critical determinant of fatigue performance.

Finally, the experimental program evaluated whether S–N curves should be presented in terms of normalized stress (stress/UTS) rather than absolute applied stress. When plotted using absolute stress ranges alone, different high-strength bolt grades yielded nearly identical fatigue results. This demonstrated that fatigue design rules for threaded fasteners should be based strictly on absolute stress amplitudes, rather than being scaled by ultimate tensile strength parameters.

4.4 Stresses for Fatigue Assessment of Unwelded Components

The fatigue assessment of unwelded components is based on the the effective stress range of each cycle calculated using the components of the total stresses at the location under consideration. The total equivalent stress range, $\Delta\sigma_{\mathrm{eq,total}}$, may be obtained either from a linear elastic FE stress analysis or from an analysis in which the structural stress range is amplified by a stress concentration factor to account for local discontinuities.

The standard provides formulas for calculating the effective stress range, distinguishing between approaches based on structural stresses (excluding local notches) and total stresses (including all discontinuities). The effective total stress range is given by, when calculated from structural stresses,

$$\Delta\sigma_f = \frac{K_f}{K_t} \cdot \Delta\sigma_{\mathrm{eq,total}}. \tag{4.9}$$

The total stresses for this calculation are determined from a model that incorporates the full effect of all structural discontinuities.

Here, the effective stress concentration factor, K_f, is given by

$$K_f = 1 + \frac{1.5(K_t - 1)}{1 + 0.5\mathrm{max}\left(1; K_t \cdot \frac{\Delta\sigma_{\mathrm{eq,struc}}}{\Delta\sigma_{\mathrm{D}}}\right)}, \tag{4.10}$$

where $\Delta\sigma_{\mathrm{D}}$ is the endurance limit for the unwelded material, and $\Delta\sigma_{\mathrm{eq,struc}}$ is the structural equivalent stress range corrected to account for plasticity. The reference value of $\Delta\sigma_{\text{eq,struc}}$ is taken from the basic fatigue curve at $10,000$ cycles, before any correction factors are applied.

The theoretical stress concentration factor K_t shall be determined from the values given in Annex ND for common stress concentrating features as

$$K_t = \frac{\sigma_{\text{total}}}{\sigma_{\text{struc}}}. \tag{4.11}$$

If the total stresses calculated directly by analysis or determined experimentally, the structural and peak stresses can be separated

$$\sigma_{\text{total}} = \sigma_{\text{struc}} + \sigma_{\text{peak}}. \tag{4.12}$$

Then from Equation (4.11),

$$K_t = 1 + \frac{\sigma_{\text{peak}}}{\sigma_{\text{struc}}}. \tag{4.13}$$

4.5 Fatigue Strength of Unwelded Components

The bolts could potentially also be interpreted as unwelded components with specific stress concentration correction factors.

4.5.1 Plasticity Correction

If the calculated pseudo-elastic structural stress range for unwelded parts exceeds twice the yield strength of the material, $\Delta\sigma_{\text{eq,l,mechanical}} > 2R_{p0.2/T^*}$, it is multiplied by a plasticity correction factor.

For mechanical loading, the correction factor is

$$k_{\text{e}} = 1 + A_0 \left(\Delta \frac{\sigma_{\text{eq,l,mechanical}}}{2R_{p0.2/T^*}} - 1 \right), \tag{4.14}$$

where $A_0 = 0.5$ for ferritic steels with $800 \leq R_{\text{m}} \leq 1000$ MPa, $A_0 = 0.4$ for ferritic steels with $R_{\text{m}} \leq 500$ MPa and for austenitic steels and $A_0 = 0.4 + \frac{(R_{\text{m}}-500)}{3000}$ for ferritic steels with $500 \leq R_{\text{m}} \leq 800$ MPa.

4.5.1.1 Surface finish correction factor

The surface finish correction factor, f_{s}, takes account of the component's surface finish and is calculated as

$$f_{\text{s}} = \begin{cases} F_{\text{s}}^{(0.1 \ln N - 0.465)} & \text{if } N < 2 \cdot 10^6 \text{ cycles} \\ F_{\text{s}} \quad \text{if } N \geq 2 \cdot 10^6 \text{ cycles} \end{cases} \tag{4.15}$$

where $F_{\text{s}} = 1 - 0.056(\ln R_{\text{z}})^{0.64} \cdot \ln R_m + 0.289(\ln R_{\text{z}})^{0.53}$, and R_{z} is the peak-to-valley height in microns. Here N is the allowable number of cycles associated to a stress level and is calculated iteratively. F_s is calculated inside a loop with only the use of stress range and fatigue curve, with other correction factors set to 1.

The base values for R_z are tabulated in Table 4.1, which are to be used if not otherwise specified. For polished surfaces with $R_z < 6\mu$m, it assumed that $f_s = 1$.

Table 4.1: Base values for peak-to-valley heights.

Surface condition	$\boldsymbol{R_z}$**, µm**
Rolled or extruded	200
Machined	50
Ground, free of notches	10

4.5.2 Mean Stress Correction Factor

The mean stress correction factor, f_m, takes account of the mean stress influence on the component fatigue strength.

4.5.2.1 Full Mean Stress Correction (Purely Elastic Behavior)

For $\Delta\sigma_{eq} \leq 2 \cdot R_{p0.2/T^*}$ and $|\sigma_{eqmax}| \leq R_{p0.2/T^*}$, f_m is determined for rolled and forged steel as a function of the mean stress sensitivity M from

$$f_m = \left[1 - \frac{M \cdot (2+M)}{1+M} \cdot \left(\frac{2\overline{\sigma}_{eq}}{\Delta\sigma_R}\right)\right]^{0.5} \quad \text{for} - R_{p0.2/T^*} \leq \overline{\sigma}_{eq} \leq \frac{\Delta\sigma_R}{2(1+M)}, \tag{4.16}$$

or

$$f_m = \frac{1+M/3}{1+M} - \frac{M}{3} \cdot \left(\frac{2\overline{\sigma}_{eq}}{\Delta\sigma_R}\right) \quad \text{for} \ \frac{\Delta\sigma_R}{2(1+M)} \leq \overline{\sigma}_{eq} \leq R_{p0.2/T^*}, \tag{4.17}$$

where for rolled and forged steel, $M = 0.00035R_m - 0.1$.

4.5.2.2 Reduced Mean Stress Correction (Partly Plastic Behavior)

For $\Delta\sigma_{eq} \leq 2 \cdot R_{p0.2/T^*}$ and $|\sigma_{eqmax}| \leq R_{p0.2/T^*}$, f_m is calculated using Equation (4.16) or Equation (4.17), with the reduced mean equivalent stress $\overline{\sigma}_{eq,r}$ being used instead of $\overline{\sigma}_{eq}$.

If $\overline{\sigma}_{eq} > 0$,

$$\overline{\sigma}_{eq,r} = R_{p0.2/T^*} - \frac{\Delta\sigma_{eq}}{2}. \tag{4.18}$$

If $\overline{\sigma}_{eq} < 0$,

$$\overline{\sigma}_{eq,r} = \frac{\Delta\sigma_{eq}}{2} - R_{p0.2/T^*}. \tag{4.19}$$

4.5.3 Overall Correction Factor for Unwelded Components

The overall correction factor for unwelded components, f_u is calculated according to

$$f_{\mathrm{u}} = f_{\mathrm{s}} \cdot f_{\mathrm{e}} \cdot f_{\mathrm{m}} \cdot f_{\mathrm{T^*}}, \tag{4.20}$$

where f_{e} and $f_{\mathrm{T^*}}$ are given in Section 4.3.1 and Section 4.3.2 respectively.

4.5.3.1 Design Data

The fatigue strenghts of unwelded components are expressed in terms of a series of $\Delta\sigma_{\mathrm{R}}$–$N$, each applicable to a particular tensile strength, R_m, of steel as shown in Figure 4.2.

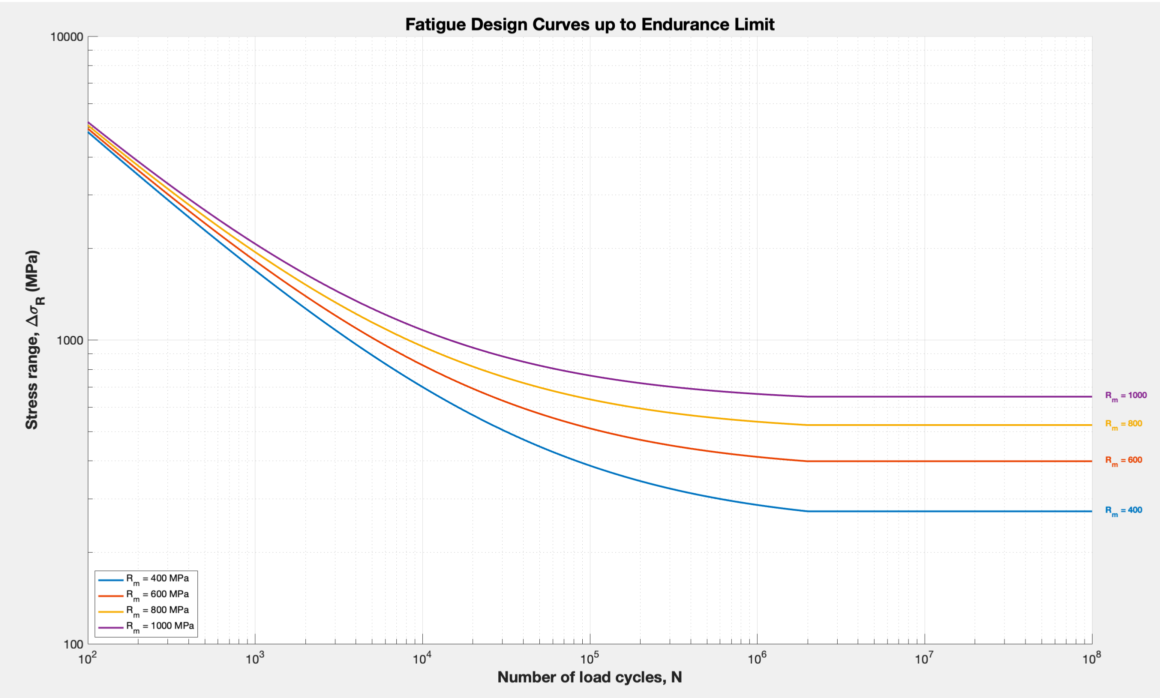

Figure 4.2: Fatigue design curves for unwelded components

The curves were derived from fatigue test data obtained from unnotched polished rolled and forged steel specimens at room temperature, under alternating load control (zero mean load), or for applied strains exceeding yield (low-cycle fatigue), strain control. The failure criterion for the test data which form the curves is (macro) crack initiation (with crack depth of approximately 0.5 to 1.0 mm). The curves incorporate safety factors of 10 on fatigue life and 1.3 on stress range, compared to the mean curve fitted to the original data.

The fatigue design curves are given by

$$N = \left[\frac{46000}{\Delta\sigma_{\mathrm{R}} - 0.63R_m + 11.5}\right]^2, \tag{4.21}$$

for lives up to the endurance limit, σ_{D}, of $2 \cdot 10^6$ cycles.

For cumulative damage calculations using Miner's ruler in Equation (4.27) from an upcoming section, the curves are linear for $N = 2 \cdot 10^6$ to 10^8 cycles, and are given by

$$N = \left[\frac{2.69R_m + 89.72}{\Delta\sigma_{\mathrm{R}}}\right]^{10}. \tag{4.22}$$

4.6 Stresses for Fatigue Assessment of Welded Components (Class 51)

The use of a single S–N curve using absolute stress range has also been proposed in the literature for other pressure-equipment details where fatigue strength is governed primarily by notch effects rather than base material strength. In particular, [2], suggests that recent controlled fatigue data do not support the traditional assumption of improved fatigue performance with increased tensile strength and indicate that a single design curve corresponding to approximately Class 50 is adequate across bolt strength grades, see Figure 4.3.

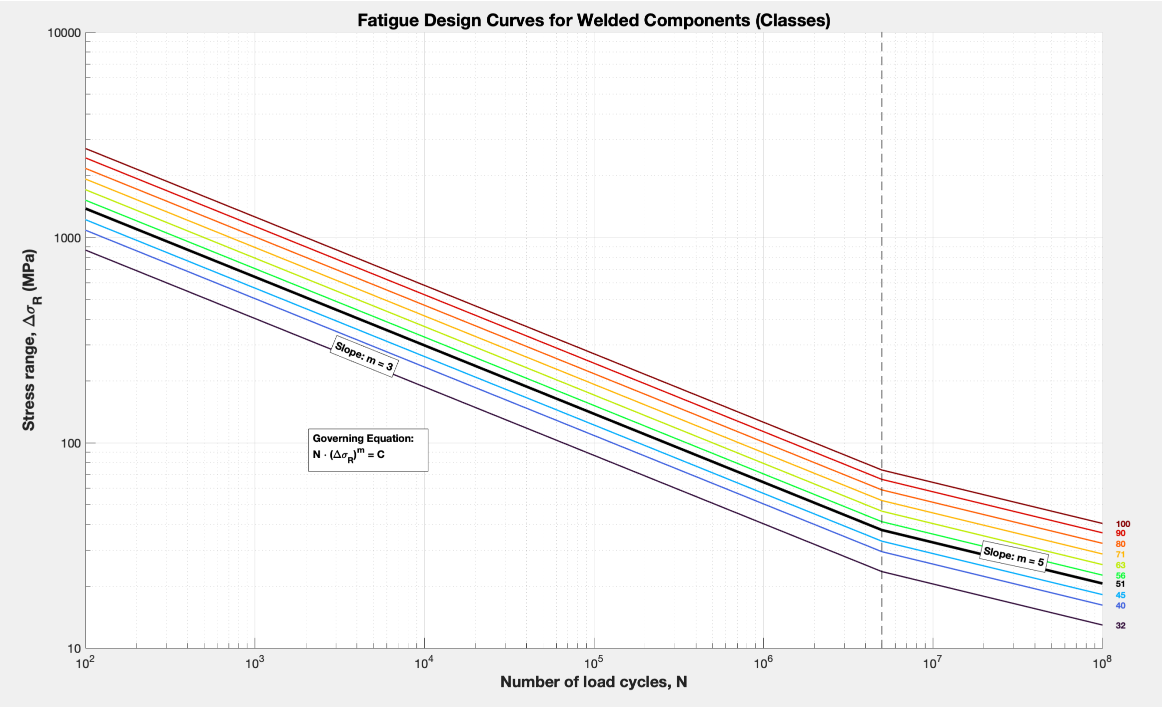

Figure 4.3: Fatigue design curves for welded components.

Maddox in [1] also suggests that it would be better to express the design curve in terms of an absolute stress level. Such a design curve is shown in Figure 4.4, which presents all the relevant results obtained from 20 mm diameter bolts in [12] where the current European Committee for Standardization (CEN) mean and design curves are included, plotted assuming an ultimate tensile strength of $\sigma_{\mathrm{TS}} = 785$ N/mm^2. The class corresponding to the current CEN pressure vessel rules, EN 13445, design curve is Class 41. Regression analysis of the fatigue data assuming $m = 3$ gave a mean -3 standard deviation line corresponding to Class 51, where the class number denotes the reference stress range in MPa at the specified reference life.

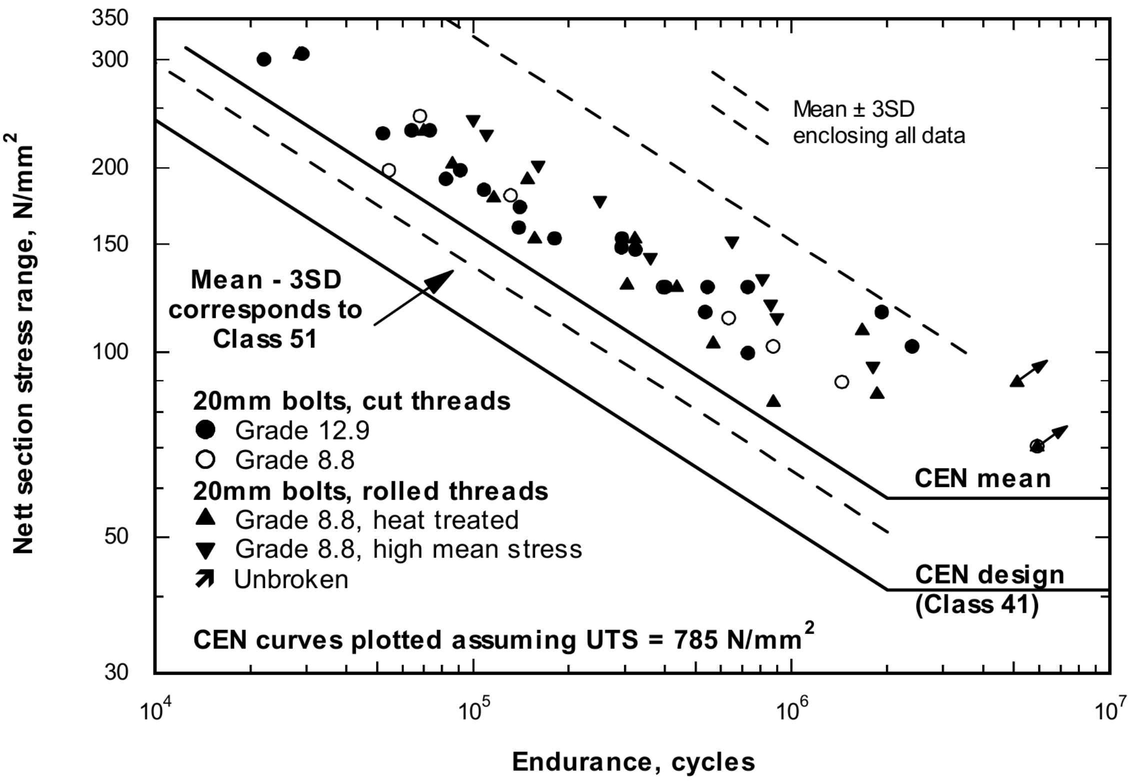

Figure 4.4: Statistical analysis of combined data for steel bolts in tension as a basis for design. [1]

The fatigue assessment of welded components is based on the structural equivalent stress range at the weld detail, combined with a fatigue strength class (FAT/Class) taken from the weld detail tables. The weld class implicitly accounts for the notch effect of the weld geometry; therefore, unlike unwelded components, no additional effective notch factor approach is applied.

4.6.1 Fatigue verification using Class 51

The fatigue life could be determined from the Class 51 S–N curve. The allowable number of cycles, N, corresponding to a calculated structural equivalent stress range, $\Delta\sigma_{\mathrm{eq,struc}}$, is obtained from the appropriate design curve for welded details of Class 51, including the applicable slope and endurance limit defined by the standard for welded joints.

The design curve is described as

$$N \cdot (\Delta\sigma_{\mathrm{R}})^m = C \tag{4.23}$$

where and for Class C,

$$C_1 = C^3 \cdot 2 \cdot 10^6, m_1 = 3.0 \quad \text{used for } 10^2 < N < 5 \cdot 10^6 \tag{4.24}$$

$$C_2 = C^5 \cdot \left(\frac{2}{5}\right)^{\frac{5}{3}} \cdot 5 \cdot 10^6, m_2 = 5.0 \quad \text{used for } 5 \cdot 10^6 < N < 10^8. \tag{4.25}$$

For a fatigue assessment using Class 51, $C = 51$, and the use of either C_1, m_1 or C_2, m_2 depends on the whether the fatigue life is in the high or low cycle range.

4.6.2 Cumulative fatigue damage

The fatigue damage index, D_f, is defined for constant-amplitude loading as the ratio of the specified or actual number of cycles, n_1, to the allowable number of cycles, N_1, i.e. the fatigue life obtained from the appropriate design curve at the corresponding equivalent stress amplitude for the service condition. Thus, D_f is calculated as

$$D_\mathrm{f} = \frac{n_1}{N_1}. \tag{4.26}$$

For cyclic loading with variable stress amplitudes, D_f is given by Miner's summation

$$D_\mathrm{f} = \frac{n_1}{N_1} + \frac{n_2}{N_2} + ... = \sum \frac{n_i}{N_i}. \tag{4.27}$$

4.7 Validation and Known Limitations

The bolt design curve in EN 13445 is based on dedicated fatigue tests on axially loaded bolts, including tests conducted under significant mean tensile stresses, and therefore inherently incorporates the geometric notch effect of the thread root. However, the validation work [9] indicates that the fatigue life of threaded fasteners is largely independent of ultimate tensile strength. When the experimental results are plotted in terms of stress range alone, bolts of different strength classes exhibit essentially identical fatigue behavior. Conversely, normalization by R_m leads to the higher-strength bolts appearing to perform worse.

These findings suggest that the current normalized formulation in EN 13445 lacks a clear physical basis and that a conventional S–N curve expressed directly in terms of stress range may provide a more appropriate representation of bolt fatigue behavior.

Furthermore, the present formulation does not explicitly address the highly multi-axial stress state at the thread root, local contact effects, or load redistribution between engaged threads, all of which are known to influence crack initiation. As a result, the method still treats fatigue primarily through an equivalent nominal stress measure, even when that stress is extracted from a finite element model.

4.8 Design by experimental methods

EN 13445 permits the use of special fatigue tests to validate or modify fatigue design data, following principles similar to those in BS PD 5500. Reduction factors applied to experimentally obtained fatigue lives depend on the number of tests performed and are adopted from AD-Merkblatt procedures, with the stated aim of achieving a reliability level consistent with the standard design curves.

4.9 Implications and development needs

The available validation studies highlight several unresolved issues in the current EN 13445 fatigue framework for bolts, including the role of tensile strength, the interpretation of local multiaxial stress states, and the influence of preload. In particular, there remains a lack of clear guidance on how finite element stress results at the thread root should be related to experimentally derived bolt fatigue data. Improving the consistency between advanced stress analysis methods and bolt-specific fatigue testing therefore represents a key area for future development.

4.10 Annex T Design by Experimental Methods

This clause provides the possibility to validate the design of vessels or vessel parts against pressure loading by experimental methods. The tests are primarily based on burst testing supplemented by other tests such as fatigue tests, where the design is characterized by the determination of the maximum allowable pressure P_s of the vessel or vessel part [10]. Material wise, this clause is applicable to steels according to EN 13445-2, manufactured according to EN 13445-4, inspected and tested according to EN 13445-5 and aluminum and aluminum alloys according to EN 13445-8 with limitations. Currently, the application of this clause is limited to the design of vessels having a maximum allowable temperature at which creep effects may be ignored.

The test plan needs to be defined prior to the actual testing. If the conformity assessment module requires the presence of a notified body, it shall be approved by an organization or a body qualified in the domain of design by experiment. The test plan shall contain essential dimensions and material characteristics of the test part, test conditions, description of instrumentation, and criteria for acceptance or refusal.

For fatigue testing with pressure loading of predominantly cyclic nature ($N_{req} > 500$), two or more tests are required. The pressure shall be cycled between the minimum value P_{min} given by the installation and $P_{min} + P_s$. The geometric mean fatigue life shall be higher than $N_{req} \cdot F$, where F is the test factor that depends on the required probability of survival, the number of test results n, and the standard deviation of $\log N, \sigma$. For the cases with a required fatigue life above 10 000 cycles, it is permissible to accelerate the test by applying a higher cyclic pressure range ΔP. The geometric mean number of cycles that must be endured becomes

$$N_{c,gm} = \left(\frac{P_s}{\Delta P}\right)^3 \cdot N_{req} \cdot F \tag{4.28}$$

Being consistent with the design $\Delta\sigma_R$–N curves in EN 13445-3 Clauses 17 and 18, the required probability of survival is 99.86%. The standard deviation of $\log N$ may be obtained from these tests or other representative tests. The test factor F is derived using the one-sided tolerance limit factor, k (a selection of k tabulated in Table 4.2), such that

$$F = 10^{k\sigma}. \tag{4.29}$$

Table 4.2: Values of the factor k, which correspond to 95 % confidence in 99,86 % survivability. Values for other numbers are given in ISO 12107.

Number of tests	k
2	49.3
3	13.9
4	9.2
5	7.5
6	6.6
7	6.1
8	5.7
9	5.4
10	5.2

The acceptence criteria for these tests are that there are no leaks for the specified number of cycles in any of the tests performed.

The test report of the fatigue tests has to explicitly state acceptence or rejection of the tested vessel or part, and must contain the number of cycles obtained in each test.

In terms of parts qualifying as similar parts, the only variables allowed to change are the length and the diameter. The length has to be longer and the diameter of the similar part has to be smaller than that tested. Other deviations have to be evaluated and clearly stated in the documentation.

4.11 BS 7608

For each design class, the relationship between the applied stress range, S_r, and the number of cycles to failure, N, under constant amplitude loading conditions is of the form:

$$\log N = \log C_\mathrm{o} - dSD - m \log S_\mathrm{r} \tag{4.30}$$

where C_o is the parameter defining the mean line S_r–N relationship, d is the number of standard deviations of log N from the mean S_r–N curve, SD is the standard deviation of log N, and m is the inverse slope of the log S_r–log N curve.

This can be rewritten as:

$$S_\mathrm{r}^m N = C_\mathrm{d} \tag{4.31}$$

where C_d is the parameter defining the S_r–N relationship for d standard deviations of log N from the mean line from:

$$\log C_\mathrm{d} = \log C_\mathrm{o} - dSD \tag{4.32}$$

The curves for axially loaded bolts up to 25 mm diameter are expressed in terms of the stress range on the tensile area. The fatigue strength for bolts with a diameter greater than 25 mm, is reduced by a factor k_tb.

$$S = k_\mathrm{tb} S_\mathrm{B} \tag{4.33}$$

where, for $t > 25$ mm:

$$k_\mathrm{tb} = \left(\frac{t_\mathrm{B}}{t_\mathrm{eff}}\right)^b [1 + 0.18\Omega^{1.4}] \tag{4.34}$$

where t_eff is the bolt diameter under consideration and Ω it the degree of bending.

If the thread rolling is carried out after any heat treatment, the fatigue strength may be increased by 25% and if the bolt is electroplated, the fatigue strength should be reduced by 20%.

5

Fatigue Life Code Calculations for M20 Bolts Under Assembly Loading

EN 13445-3 provides multiple fatigue-assessment routes that can be applied to bolted joints depending on how the stress is defined and how notch effects are treated. In the present thesis, three EN 13445-based routes are compared on a single bolt example to illustrate how method choice and embedded assumptions influence the predicted fatigue life:

- **Method 1:** bolt-specific design curve (Section 4.3), using nominal core-area stress.
- **Method 2:** unwelded component approach (Section 4.5), using a pseudo-elastic local equivalent stress range derived from an effective notch fatigue stress concentration.
- **Method 3:** unwelded component approach using the **Class 51** curve (Section 4.6), which was mentioned as a more accurate design curve.

The comparison is intentionally limited to **fatigue initiation at the first engaged thread** and does not include manufacturing-route effects (e.g. rolling-induced residual stresses) or joint-level phenomena beyond the applied stress concentration factor.

5.1 Applied calculation example

The following calculation example represents an extreme loading case relevant to Alfa Laval heat exchangers, considering assembly loading. The assessment is focused on fatigue crack initiation at the first engaged thread root, which is assumed to be the fatigue-critical location.

5.1.1 Bolt geometry and material data

The bolt is modelled using standard thread geometry measures for an M20 fastener. The tensile stress area is evaluated from the pitch and minor diameters in accordance with the conventional definition in Equation (2.21) with $d_n = 20$ mm, $d_2 = 18.376$ mm, and $d_3 = 16.933$ mm from [13], giving $A_\mathrm{s} = 245$ mm^2 according to Equation (2.21).

Material properties are taken as representative values for property class 10.9: ultimate tensile strength $R_m = 1000$ MPa and 0.2% proof strength $R_{p0.2/T^*} = 940$ MPa at the reference temperature.

5.1.2 Loading and environmental conditions

The bolt is subjected to a cyclic axial force with amplitude $F_\mathrm{z} = 100$ kN and stress ratio $R = F_\mathrm{min}/F_\mathrm{max} = 0$ (zero-based cycling). For axial loading, the nominal stress range based on the tensile stress area is

$$\Delta\sigma_b = \frac{F_z}{A_s} = 408.51 \text{ MPa}. \tag{5.1}$$

The operating temperature is $T = 20$ °C, such that temperature reduction factors in Section 4.3.2 are not activated for the present comparison. Surface condition is represented by an assumed rolled-thread roughness parameter $R_\mathrm{z} = 200$ μm for the surface finish correction used in the unwelded-component route from Table 4.1 for a rolled component.

5.1.3 Representation of the thread-root notch effect

To connect nominal (structural) stress to a local thread-root measure, the theoretical stress concentration factor at the first engaged thread is taken as $K_t = 5.17$, which is taken from [14]. A summary of Lenhoff's article can be found in Appendix A.2.1.

5.2 Method 1: Bolt-specific curve (EN 13445-3, Section 18.12)

The first method evaluates the fastener using the dedicated bolt design curve outlined in EN 13445-3, Section 18.12. Because this empirical curve was derived directly from physical fatigue tests on actual threaded fasteners, the severe stress concentration effect at the thread root is implicitly accounted for within the reference data. Consequently, the analysis relies purely on the nominal axial stress range and requires no explicit local notch penalty.

5.2.1 Nominal stress range and mean stress

For zero-based cycling $R = 0$, the mean stress is

$$\sigma_m = \frac{\Delta\sigma_b}{2} = 204.25 \text{ MPa}. \tag{5.2}$$

5.2.2 Correction factors and fatigue life

The thickness and temperature factors are unity, as per Section 4.5.1.1 and Section 4.3.2,

$$f_{\mathrm{e}} = 1.0, \quad f_{T^*} = 1.0, \quad f_b = f_{\mathrm{e}} \cdot f_{T^*} = 1.0. \tag{5.3}$$

Using the bolt design curve with R_{m} limited to 785 MPa as specified in Section 4.3, the fatigue life is calculated to

$$N_1 = 2,022 \text{ cycles.} \tag{5.4}$$

5.3 Method 2: Unwelded component approach (EN 13445-3, Section 18.11)

The second method assesses the bolt as a general machined structure, applying the unwelded component framework from EN 13445-3, Section 18.11. Unlike the bolt-specific curve, this approach utilizes a generalized material reference curve. Therefore, the geometric severity of the threads must be explicitly penalized by mathematically deriving a fatigue concentration factor (K_f) from the theoretical elastic notch factor (K_t), alongside comprehensive analytical corrections for surface finish and mean stress.

5.3.1 Structural stress and pseudo-elastic local stress range

Following the procedure in Section 4.4, the corresponding linear-elastic peak range at the thread root would be

$$\Delta\sigma_{\text{total}} = K_t \cdot \Delta\sigma_{\text{struc}} = 2,112.0 \;\; \text{MPa.} \tag{5.5}$$

which exceeds the proof strength and indicates local nonlinearity. EN 13445 therefore employs an effective notch approach.

The reference stress range at the endurance limit $2 \cdot 10^6$ cycles from the design curve is

$$\Delta\sigma_{\mathrm{D}} = 0.63 R_m - 11.5 = 651.03 \;\; \text{MPa.} \tag{5.6}$$

The fatigue concentration factor is

$$K_f = 1 + \frac{1.5(K_t - 1)}{1 + 0.5 \max\left(1; K_t \frac{\Delta\sigma_{\text{struc}}}{\Delta\sigma_{\mathrm{D}}}\right)} = 3.39, \tag{5.7}$$

leading to the pseudo-elastic equivalent stress range

$$\Delta\sigma_{\text{eq,t}} = K_f \cdot \Delta\sigma_{\text{struc}} = 3.39 \cdot 408.51 = 1,383.02 \text{ MPa.} \tag{5.8}$$

5.3.2 Correction factors (surface, thickness, temperature, mean stress)

The surface correction factor is calculated according to Section 4.5.1.1,

$$f_s = 0.848. \tag{5.9}$$

Thickness and temperature factors remain unity,

$$f_e = 1.0, \quad f_{T^*} = 1.0. \tag{5.10}$$

Using Section 4.5.2, the mean stress correction factor was calculated to

$$f_m = 0.916. \tag{5.11}$$

The overall correction factor for the unwelded approach is

$$f_u = f_s \cdot f_e \cdot f_{T^*} \cdot f_m = 0.776. \tag{5.12}$$

5.3.3 Fatigue life

Using the EN 13445 unwelded-component curve in Section 4.5.3.1, the fatigue life is calculated to

$$N_2 = 1,563 \text{ cycles.} \tag{5.13}$$

5.4 Method 3: Unwelded component curve Class 51 (EN 13445-3, Section 18.10)

The third method applies the exact same procedural framework as Method 1, evaluating the nominal axial stress range directly without the need to calculate local notch factors. However, rather than utilizing the standard bolt design curve (which artificially forces a dependence on the ultimate tensile strength, capped at $R_m =$ 785 MPa), this approach evaluates the fastener using the constant reference curve for fatigue Class 51 (EN 13445-3, Section 18.10). In this context, the thread profile is not being strictly categorized as a standard welded or unwelded structural detail. Rather, the Class 51 curve is applied because it mathematically represents the design curve that would result if the underlying experimental bolt data were interpreted entirely independently of R_m.

Using the nominal stress range and correction factors derived from Section 5.2, the predicted fatigue life is,

$$N_3 = 3,892 \ \text{ cycles.} \tag{5.14}$$

5.5 Results comparison

The resulting fatigue lives and other relevant parameters for this example are compiled in Table 5.1.

Table 5.1: Comparison of predicted fatigue life and governing parameters using three EN 13445 routes.

Parameter	**Method 1 (Bolt Curve)**	**Method 2 (Unwelded)**	**Method 3 (Class 51)**
Stress measure driving fatigue curve	$\Delta\sigma_b$ (nominal)	$\Delta\sigma_{\mathrm{eq,t}}$ (pseudo-elastic)	$\Delta\sigma_b$ (nominal)
Effective stress range	408.51 MPa	1383.02 MPa	408.51 MPa
Correction factor	$f_b = 1.0$	$f_u = 0.776$	$f_b = 1.0$
Allowable cycles	2,022	1,563	3,892

5.6 Sensitivity Analysis

To illustrate the influence of load level (and the transition toward elastic behaviour), the same comparison is repeated for two reduced external load amplitudes, $F_{\mathrm{amp}} =$ 50 kN (partly plastic) and $F_{\mathrm{amp}} = 25$ kN (fully elastic), and the results are shown in Table 5.2 and Table 5.3.

Table 5.2: Sensitivity study at reduced load amplitude $F_{\mathrm{amp}} = 50$ kN (partly plastic).

Parameter	**Method 1 (Bolt curve)**	**Method 2 (Unwelded)**	**Method 3 (Class 51)**
Effective stress range	204.25 MPa	841.26 MPa	204.25 MPa
Correction factor	$f_b = 1.0$	$f_u = 0.619$	$f_b = 1.0$
Allowable cycles	16,179	2,914	31,134

Table 5.3: Sensitivity study at reduced load amplitude $F_{\mathrm{amp}} = 25$kN (fully elastic).

Parameter	**Method 1 (Bolt curve)**	**Method 2 (Unwelded)**	**Method 3 (Class 51)**
Effective stress range	102.13 MPa	527.19 MPa	102.13 MPa
Correction factor	$f_b = 1.0$	$f_u = 0.691$	$f_b = 1.0$
Allowable cycles	129,430	100,233	249,071

5.7 Interpretation

In the bolt curve from Section 18.12 in EN 13445-3, the thread-root notch effect is treated implicitly through curve calibration. Consequently, nominal stress is used directly. The method is straightforward to apply, but its validity is bounded by the underlying test basis and by the associated assumptions on geometry and loading.

Using the unwelded component route in Section 18.11, the notch effect is introduced explicitly via K_t and K_f, which can produce pseudo-elastic stress ranges that exceed the proof strength. EN 13445 addresses this by combining an effective notch treatment with partly plastic handling of mean stress, which may reduce the mean-stress penalty (i.e. $f_m \to 1$) when local yielding is expected.

With the class curve from Section 18.10 in EN 13445-3, the class-based curve provides a nominal-stress reference for an absolute stress category.

At lower load amplitudes, such that the notch-root response remains elastic, differences between the methods are driven primarily by whether notch effects are embedded in the curve definition (bolt curve) or supplied explicitly by the analyst (unwelded route).

5.8 Proposed extension: LCF block for repeated assembly/disassembly (strain–life)

In Alfa Laval service some bolts experience repeated assembly and disassembly events where the stress history spans from an unloaded state to the maximum operational load. An additional LCF block could be evaluated using a local strain-life approach while retaining the current EN 13445 bolt fatigue assessment for the operational loading.

5.8.1 Block Definition and Trigger Criterion

The total fatigue damage is evaluated using a linear damage accumulation model that explicitly separates the assembly loading from the high-cycle operational loading. This relationship is mathematically expressed as

$$D = D_{\text{ass}} + D_{\text{op}} = \frac{n_{\text{ass}}}{N_{\text{ass}}} + \sum_j \frac{n_{\text{op},j}}{N_{\text{EN}}\left(\Delta\sigma_{\text{op},j}\right)} \tag{5.15}$$

where n_{ass} represents the scheduled number of assembly and disassembly cycles, and N_{ass} is the predicted low-cycle fatigue life for that specific block. For the operational phase, $n_{\text{op},j}$ is the number of applied load cycles at a given stress range j, and N_{EN} denotes the allowable number of cycles derived from the selected EN 13445 S–N reference curve.

To determine whether the assembly block strictly requires this LCF assessment, a local plasticity trigger is introduced. If the local peak equivalent stress at the first engaged thread root—calculated either via finite element analysis or an analytical notch approximation—exceeds a predefined threshold, the assembly macro-cycle must be evaluated as a low-cycle fatigue event. This activation criterion is defined as

$$\sigma_{\text{eq,max,ass}} > \alpha R_{\text{p0.2}/T^*} \tag{5.16}$$

where $R_{\text{p0.2}/T^*}$ is the material yield strength evaluated at the relevant operating temperature, and α represents a chosen calibration margin designed to capture the onset of significant localized yielding.

5.8.2 Local Strain Estimation at the First Engaged Thread

An elastic FE analysis or a structural nominal stress combined with K_t provides an elastic local stress amplitude at the thread root, $\sigma_{e,a}$. The corresponding elastic strain amplitude is

$$\varepsilon_{e,a} = \frac{\sigma_{e,a}}{E}. \tag{5.17}$$

To account for local cyclic plasticity, the elastic estimate is converted to an elasto-plastic local strain amplitude using a cyclic stress-strain relation and a notch rule.

6

Methodology and Proposed Framework

A localized elastoplastic Strain-Life framework is established to evaluate the service life of gasketed plate heat exchanger (GPHE) tightening bolts. Abandoning nominal stress evaluation, the proposed methodology is structured in three sequential steps. First, a non-linear finite element strategy is utilized to capture the physical spring-back mechanism and extract stabilized local strain histories at the fatigue-critical thread root. Second, these numerical results are mathematically implemented into the Coffin-Manson fatigue framework to conduct a local strain-life assessment. Finally, recognizing that numerical models require empirical validation to certify pressurized components, an experimental test strategy is proposed to physically replicate the elastoplastic macro-cycle.

6.1 Finite Element Modeling

Finite element analyses were performed in ANSYS Mechanical APDL 2024 R2. While the numerical framework is geometrically scalable, the analysis was performed for an M20 bolt. The FE work had two purposes. First, an elastic model was used to validate the predicted thread-root stress concentration factor against literature data and to identify the fatigue-critical location. Second, cyclic analyses were used to extract local stress and strain histories at that location for subsequent strain–life assessment.

6.1.1 Model Geometry and Idealization

As illustrated in Figure 6.1, the bolted joint was represented as a two-dimensional axisymmetric assembly consisting of four components: bolt, nut, upper plate, and lower plate. The expanded model is shown in Figure 6.2. The bolt geometry followed the standard ISO metric coarse thread profile. The model was parameterized by nominal bolt diameter so that all studied bolt sizes could be generated from the same APDL script, utilizing the specific geometric dimensions outlined in Table 6.1. For all analyzed cases, the plate thickness was fixed at 20 mm, and the bolt extended two thread pitches below the nut.

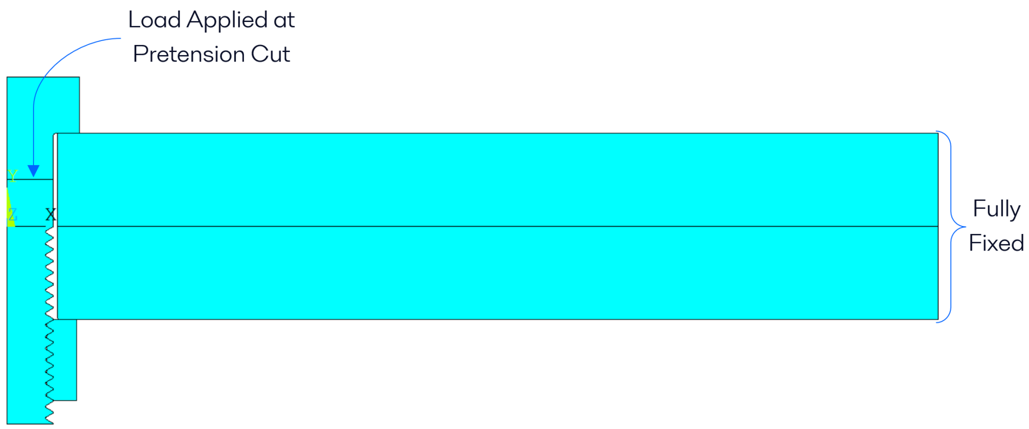

Figure 6.1: Axisymmetric FE model of the bolt–nut–plate assembly.

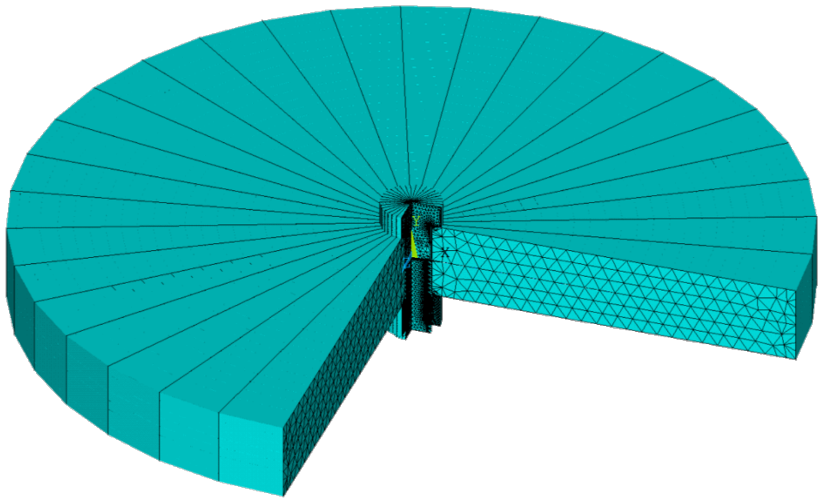

Figure 6.2: Expanded Axisymmetric FE model.

Table 6.1: Bolt model geometric parameters.

Bolt	Pitch (mm)	d_{maj} (mm)	d_{min} (mm)	A_s (mm^2)	Head fillet radius (mm)
M8	1.25	7.866	6.284	36.6	0.4
M12	1.75	11.834	9.619	84.3	0.6
M16	2.00	15.822	13.291	156.7	0.6
M20	2.50	19.791	16.625	244.8	0.8
M24	3.00	23.765	19.969	352.5	0.8

6.1.2 Element formulation and mesh strategy

The structural assembly was discretized using six-node, quadratic triangular elements (PLANE183) with an axisymmetric formulation. These higher-order triangular elements were specifically selected because their shape naturally conforms to the tight, highly curved geometry of the thread root, while their quadratic formulation ensures accurate resolution of the steep stress and strain gradients present at the notch.

The mesh was refined locally in the fatigue-critical regions, specifically the engaged thread roots and the head fillet, as illustrated in Figure 6.3. The engaged bolt thread roots were discretized most finely to accurately resolve the severe local stress gradients, while non-engaged roots, thread peaks, and remote plate regions were meshed more coarsely to maintain computational efficiency. Smooth element size transitions were maintained between neighboring mesh zones to prevent artificial numerical stiffening. The adopted refinement strategy was guided by the thread-root convergence study reported by Pedersen [15], alongside an independent mesh convergence study performed in the present work. A summary of Pedersen's article is found in Appendix A.2.2.

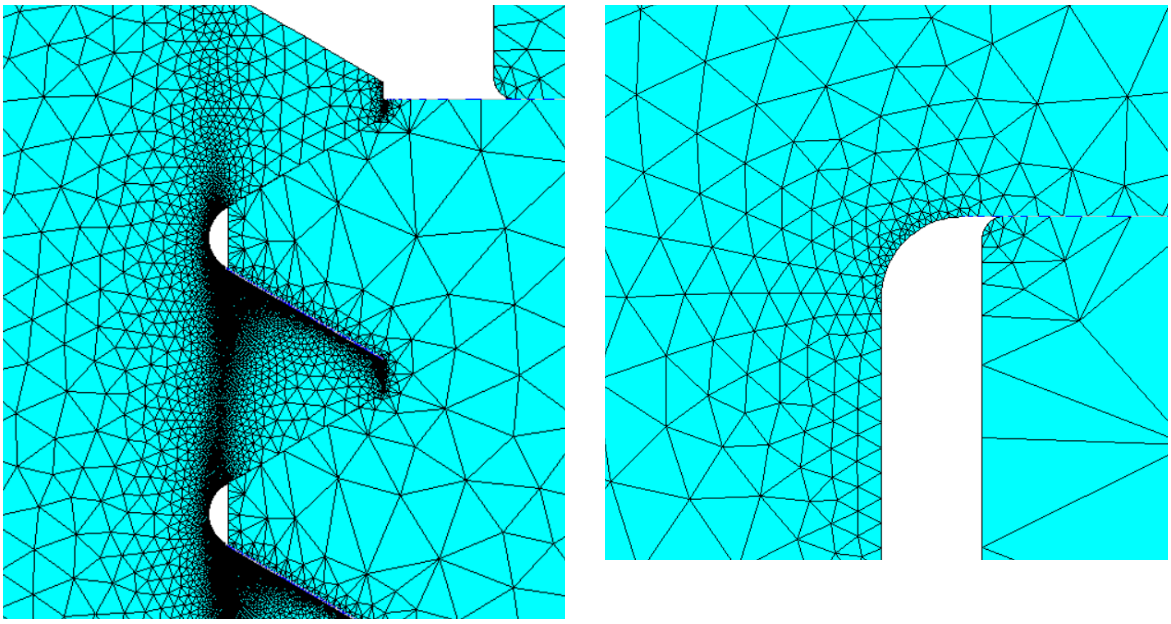

Figure 6.3: Detailed views of the local mesh refinement in the fatigue-critical regions. Left: The engaged thread roots, showing the high-density discretization required to capture the peak notch stress. Right: The bolt head fillet region.

6.1.3 Contact formulation and material data

Augmented Lagrange contact was used for all contact pairs. Contact was defined at the thread flanks, the bolt-head bearing surface, the nut-bearing surface, and the plate interface. A friction coefficient of 0.15 was used on the thread flanks and 0.80 on the remaining contacting surfaces similar to the study in [14] in Appendix A.2.1. In the unwelded-component route this is converted to a fatigue stress concentration factor K_f following EN 13445, reflecting the fact that linear-elastic peak stresses may exceed yield at the notch root and therefore require a pseudo-elastic treatment. Standard bolt clearance of 1 mm was applied between the bolt shank and the plate hole. The plate interface contact used a reduced normal stiffness factor in order to handle the coincident contact surfaces more robustly.

The elastic material properties were taken as $E = 210$ GPa and $\nu = 0.30$ for all components. No residual stresses from thread rolling or manufacturing were included in the FE model.

6.1.4 Loading, boundary conditions, and evaluation procedure

Appropriate axisymmetric boundary conditions were applied along the central axis of revolution, and the outer radial edges of both the upper and lower plates were fully fixed to properly constrain the assembly. The target assembly load was strictly introduced as an axial pretension force applied to the bolt shank using PRETS179 pretension-section elements.

For elastic validation, the nominal thread stress was evaluated as

$$\sigma_0 = \frac{F_b}{A_s} \tag{6.1}$$

where F_b is the applied structural bolt force and A_s is the tensile stress area. The elastic stress concentration factor was then computed as

$$K_t = \frac{\sigma_{\max}}{\sigma_0} \tag{6.2}$$

where $\sigma_{\max}$ is the maximum equivalent von Mises stress in the structural thread-root region, explicitly excluding any artificial numerical stress peaks originating from the contact element nodes.

To separate the reversible elastic response from the plastically stabilized cyclic response, two distinct non-linear cyclic analyses were performed. First, a purely elastic cycling analysis comprising one and a half macro-cycles was carried out. Second, an elastoplastic cyclic analysis was performed assuming ideal plasticity (zero strain hardening), utilizing a bilinear isotropic hardening model with a defined yield strength of $\sigma_y = 940$ MPa.

For the elastoplastic case, the simulated load history consisted of tightening to the target pretension force, complete unloading to zero, reloading, unloading again, and a final reloading phase. The local stress and strain responses at the fatigue-critical thread root were extracted from the final stabilized stages of the cycle history. Both elastic and plastic strain components were recorded, such that the total true strain is defined as

$$\varepsilon_{\text{total}} = \varepsilon_{\text{elastic}} + \varepsilon_{\text{plastic}} \tag{6.3}$$

Crucially, the fatigue-relevant strain amplitude (ε_a) utilized in the subsequent damage calculations was evaluated directly from the stabilized elastoplastic strain range over the final macro-cycle, rather than relying on the peak monotonic strain alone.

6.2 Strain–Life

The finite element work in this thesis is used not only to obtain local stress concentration factors, but also to explore whether a local strain-based interpretation can help explain the discrepancy between code-based fatigue predictions and the long service lives observed in practice. In particular, the strain–life approach is relevant for loading cases in which the local thread-root response may enter the elastoplastic regime, such that a purely elastic stress-based interpretation becomes insufficient.

The total strain amplitude in a stabilized cycle may be written as the sum of an elastic and a plastic contribution,

$$\varepsilon_a = \varepsilon_{\mathrm{e,a}} + \varepsilon_{\mathrm{p,a}} \tag{6.4}$$

and the corresponding strain–life relation is taken in Coffin–Manson–Basquin form from Equation (2.28). In the present work, this formulation is not introduced as a code-replacement design method, but rather as an interpretive tool for local notch-root behaviour. The purpose is to determine whether the local response associated with the maintenance-type loading cycle is more appropriately characterized by a strain-based fatigue framework than by the standardized bolt S–N curve alone.

A central reason for considering strain–life is that the large amplitude maintenance cycle of interest differs fundamentally from the loading situations on which the current standardized bolt fatigue curves are based. In the present application, the relevant assembly-related cycle may be approximated as a large zero-based excursion from an unloaded or disassembled state to full tightening and subsequent peak operating load. Such a cycle may generate a substantial local stress and strain excursion at the first engaged thread root, even if the number of such cycles is low compared with the operational loading.

At the same time, strain–life cannot by itself provide a sufficient basis for product design under EN 13445-3. The code is fundamentally stress-based and relies on standardized fatigue design curves with a defined statistical basis. A local strain-based FE assessment may explain why the current code route appears conservative, especially for zero-based large-amplitude cycles, but it does not in itself provide a directly code-compliant design curve for tightening bolts.

For the finite element based strain–life interpretation, the fatigue-critical quantity is taken as the stabilized local strain amplitude at the first engaged thread root. In the presence of residual stress and residual strain after unloading, this quantity must be evaluated from the stabilized strain range

$$\varepsilon_a = \frac{\varepsilon_{\mathrm{max}} - \varepsilon_{\mathrm{min}}}{2} \tag{6.5}$$

rather than from the peak strain alone. Similarly, if a mean stress correction is included, the corresponding local stress quantities should be taken from the same stabilized cycle,

$$\sigma_a = \frac{\sigma_{\max} - \sigma_{\min}}{2}. \tag{6.6}$$

For Morrow correction, the mean stress σ_m is used directly. For Smith–Watson–Topper correction, the maximum local stress $\sigma_{\max}$ is used together with the strain amplitude ε_a. In this way, the FE-based strain–life approach remains internally consistent with the observed hysteresis behaviour at the fatigue-critical thread root.

6.2.1 Method 4: Strain–life assessment using nominal stress, notch factor, Neuber correction, and cyclic Ramberg–Osgood

The fourth method provides an analytical alternative to non-linear finite element modeling by estimating the localized elastoplastic notch response directly from the nominal structural stress. This approach first scales the nominal axial bolt stress using a theoretical elastic stress concentration factor (K_t). Because this localized pseudo-elastic stress frequently exceeds the material yield limit, Neuber's rule is applied in conjunction with the cyclic Ramberg–Osgood material model. This correction translates the theoretical elastic state into a physically representative elastoplastic stress–strain hysteresis loop. Finally, the corrected local strain amplitude is evaluated using the Coffin–Manson strain–life relation.

This framework is specifically intended for structural scenarios where the macroscopic nominal stress is easily defined, but the localized notch response is driven heavily into the plastic regime. It is particularly relevant for assessing the first engaged thread root of large, high-strength bolts, where relying on a purely elastic notch penalty would yield non-physical peak stresses and result in an overly conservative fatigue life prediction.

For the assembly loading, the nominal stress range is taken as

$$\Delta\sigma_{\text{nom}} = \frac{F_z}{A_s} \tag{6.7}$$

and the corresponding stress amplitude becomes

$$\sigma_{\text{nom,a}} = \frac{\Delta\sigma_{\text{nom}}}{2}. \tag{6.8}$$

The elastic local notch stress amplitude is then approximated as

$$\sigma_{\text{e,a}} = K_t \sigma_{\text{nom,a}}. \tag{6.9}$$

The associated elastic local strain amplitude is

$$\varepsilon_{\text{e,a}} = \frac{\sigma_{\text{e,a}}}{E} \tag{6.10}$$

If the resulting elastic notch stress, $\sigma_{\text{e,a}}$, exceeds the elastic limit of the bolt material, the local response should not be evaluated using the purely elastic notch stress alone.

Instead, an elastoplastic correction is applied. In the present method this is done using Neuber's rule,

$$\sigma_a \varepsilon_a = \sigma_{e'} \frac{a^2}{E} \tag{6.11}$$

together with the cyclic Ramberg–Osgood relation in Equation (2.32).

The two equations are solved iteratively to obtain the corrected local stress and strain amplitudes (σ_a, ε_a). The corresponding plastic strain amplitude is then

$$\varepsilon_{\mathrm{p,a}} = \varepsilon_a - \frac{\sigma_a}{E} \tag{6.12}$$

For a zero-to-maximum cycle, the mean stress is approximated as

$$\sigma_m = \sigma_a \tag{6.13}$$

and the maximum local stress as

$$\sigma_{\max} = 2\sigma_a . \tag{6.14}$$

A temperature correction may then be applied to the strain–life parameters. If f_T denotes the temperature correction factor, the adjusted fatigue coefficients become

$$\sigma_f'^* = f_T \sigma_f' \tag{6.15}$$

$$\varepsilon_f'^* = \frac{\varepsilon_f'}{f_T} \tag{6.16}$$

The fatigue life is finally obtained from the strain–life equation with the Morrow mean stress correction model

$$\varepsilon_a = \left(\frac{\sigma_f'^*}{E}\right)\left(2N_f\right)^b + \varepsilon_f'^*\left(2N_f\right)^c \tag{6.17}$$

with optional mean stress correction. In the present work, either no mean stress correction, Morrow correction, or Smith–Watson–Topper correction may be used, depending on the selected interpretation of the loading cycle and on the available stress information.

The transition between elastic-dominated and plastic-dominated behaviour is estimated from the intersection of the elastic and plastic strain terms, giving

$$2N_t = \left(\frac{\varepsilon_f'^* E}{\sigma_f'^*}\right)^{\frac{1}{b-c}} \tag{6.18}$$

or, in cycles,

$$N_t = \frac{1}{2}\left(\frac{\varepsilon_f'^* E}{\sigma_f'^*}\right)^{\frac{1}{b-c}} \tag{6.19}$$

If the predicted life N_f is smaller than N_t, the response is interpreted as plasticity-dominated LCF. If N_f exceeds N_t, the response is interpreted as elastic-dominated HCF.

6.2.2 Neuber correction combined with cyclic Ramberg–Osgood

Starting from the elastic local notch stress amplitude,

$$\sigma_{e,a} = K_t \sigma_{\mathrm{nom,a}}, \tag{6.20}$$

the corresponding elastic local strain amplitude is

$$\varepsilon_{e,a} = \frac{\sigma_{e,a}}{E}. \tag{6.21}$$

According to Neuber's rule, the elastic notch product is approximately preserved,

$$\sigma_{e,a}\varepsilon_{e,a} = \sigma_a \varepsilon_a, \tag{6.22}$$

which can be written as

$$\frac{\sigma_{e,a}^2}{E} = \sigma_a \varepsilon_a. \tag{6.23}$$

The local elastoplastic stress–strain response is described by the cyclic Ramberg–Osgood relation,

$$\varepsilon_a = \frac{\sigma_a}{E} + \left(\frac{\sigma_a}{K'}\right)^{\frac{1}{n'}}. \tag{6.24}$$

Combining both expressions gives

$$\frac{\sigma_{e,a}^2}{E} = \sigma_a \left[\frac{\sigma_a}{E} + \left(\frac{\sigma_a}{K'}\right)^{\frac{1}{n'}}\right]. \tag{6.25}$$

This nonlinear equation is solved for the local stress amplitude σ_a. The corresponding local strain amplitude is then obtained from

$$\varepsilon_a = \frac{\sigma_a}{E} + \left(\frac{\sigma_a}{K'}\right)^{\frac{1}{n'}}. \tag{6.26}$$

If local yielding occurs, the elastoplastic correction leads to

$$\sigma_a < \sigma_{e,a} \tag{6.27}$$

and

$$\varepsilon_a > \varepsilon_{e,a}, \tag{6.28}$$

i.e. the elastic notch stress is reduced while the local strain is increased.

6.2.3 Method 5: Strain–life assessment directly from local FE strain

This method evaluates fatigue life directly from the local strain response obtained from finite element analysis at the fatigue-critical location, typically the first engaged thread root. Unlike Method 4, no analytical notch correction is required, since the local strain field is taken directly from the finite element solution.

The method is particularly suitable when an elastoplastic finite element model is available and the local stress–strain response can be extracted with sufficient spatial resolution. In such cases, the FE model accounts directly for geometry, contact, and load transfer effects that are difficult to represent by nominal stress methods.

If the loading cycle is defined as zero-to-maximum loading, the local strain amplitude is approximated from the maximum local strain as

$$\varepsilon_a = \frac{\varepsilon_{\text{local,max}}}{2} \tag{6.29}$$

where $\varepsilon_{\text{local,max}}$ denotes the local maximum strain at the critical point during the hysteresis cycle.

If a full elastoplastic load–unload simulation is available, the strain amplitude should instead be evaluated from the strain range over the stabilized hysteresis loop,

$$\varepsilon_a = \frac{\varepsilon_{\text{max}} - \varepsilon_{\text{min}}}{2} \tag{6.30}$$

which is preferable whenever local plasticity causes the unloaded strain state to differ from zero.

Where a mean stress correction is included, the local stress from FE must also be used. For Morrow correction, the mean stress may be approximated as

$$\sigma_m = \frac{\sigma_{\text{local,max}} + \sigma_{\text{local,min}}}{2} \tag{6.31}$$

for a zero-to-maximum cycle. For Smith–Watson–Topper correction, the maximum local stress is used directly,

$$\sigma_{\text{max}} = \sigma_{\text{local,max}} \tag{6.32}$$

A temperature correction may be applied to the fatigue coefficients. If f_T denotes the temperature correction factor, the adjusted fatigue coefficients become

$$\sigma_f'^{*} = f_T \sigma_f' \tag{6.33}$$

$$\varepsilon_f'^{*} = \frac{\varepsilon_f'}{f_T} \tag{6.34}$$

The strain–life equation is then written as

$$\varepsilon_a = \left(\frac{\sigma_f'^{*}}{E}\right)\left(2N_f\right)^b + \varepsilon_f'^{*}\left(2N_f\right)^c \tag{6.35}$$

with optional mean stress correction depending on whether no correction, Morrow correction, or Smith–Watson–Topper correction is adopted.

The transition life between elastic-dominated and plastic-dominated response is again estimated as

$$N_t = \frac{1}{2}\left(\frac{\varepsilon_f'^{*} E}{\sigma_f'^{*}}\right)^{\frac{1}{b-c}} \tag{6.36}$$

and the predicted life N_f is interpreted relative to this value.

6.2.4 Constitutive Modeling: Isotropic vs. Kinematic Hardening

To accurately capture the local elastoplastic response of the thread root during the assembly and disassembly load cycles, rate-independent plasticity models were evaluated. Based on the von Mises yield criterion and an associated flow rule, two distinct hardening rules were compared: Bilinear Isotropic Hardening (BISO) and Bilinear Kinematic Hardening (BKIN). To establish the bounds of the local residual stress state, both models were evaluated under a perfectly plastic assumption beyond initial yield, meaning the tangent modulus was set to approach zero ($E_t \approx 0$).

6.2.4.1 Bilinear Isotropic Hardening (BISO)

The BISO option utilizes a work-hardening rule where the yield surface remains centered at the origin of the stress space and expands uniformly in size as plastic strains accumulate [16]. The yield criterion is defined as

$$f(\{\sigma\}) = \sigma_{\mathrm{eq}} - \sigma_k = 0, \tag{6.37}$$

where σ_{eq} is the von Mises equivalent stress evaluated from the deviatoric stress vector $\{s\}$, and σ_k is the current yield stress, which increases as a function of the accumulated equivalent plastic strain ($\varepsilon_{\mathrm{peq}}$).

This uniform expansion of the elastic domain is illustrated in Figure 6.4. Physically, the BISO model inherently neglects the Bauschinger effect. If the thread root yields heavily in tension during the initial assembly preload, the uniform expansion of the yield surface dictates that a correspondingly massive compressive stress must be applied to induce reverse yielding during unloading. Consequently, the material responds largely elastically during the disassembly phase.

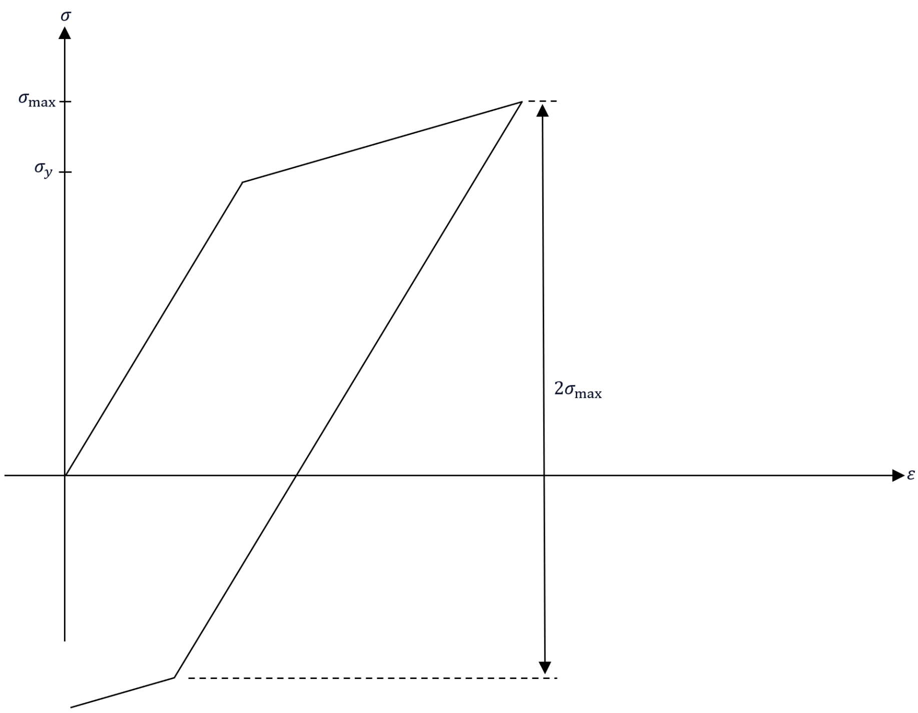

Figure 6.4: Stress-strain behavior of the bilinear isotropic plasticity model (BISO), demonstrating the expansion of the elastic domain without the Bauschinger effect.

6.2.4.2 Bilinear Kinematic Hardening (BKIN)

Conversely, the BKIN model assumes that the yield surface maintains a constant size but translates within the stress space as progressive yielding occurs. This translation is governed by the shift strain and the back stress vector, $\{\alpha\}$, which tracks the shifting center of the yield surface. The equivalent stress is evaluated using the deviatoric stress modified by this translation:

$$\sigma_{\text{eq}} = \sqrt{\frac{3}{2}(\{s\} - \{\alpha\})^T [M](\{s\} - \{\alpha\})}. \tag{6.38}$$

When σ_{eq} equals the constant uniaxial yield stress, σ_y, the material yields. The BKIN yield criterion is expressed as

$$f(\{\sigma\}, \{\alpha\}) = \sigma_{\text{eq}} - \sigma_y = 0. \tag{6.39}$$

The associated flow rule utilizes the Prandtl-Reuss equations, dictating that the increment in plastic strain is normal to the translating yield surface [16]. As shown in Figure 6.5, this translation of the yield surface fundamentally alters the reverse-yielding threshold.

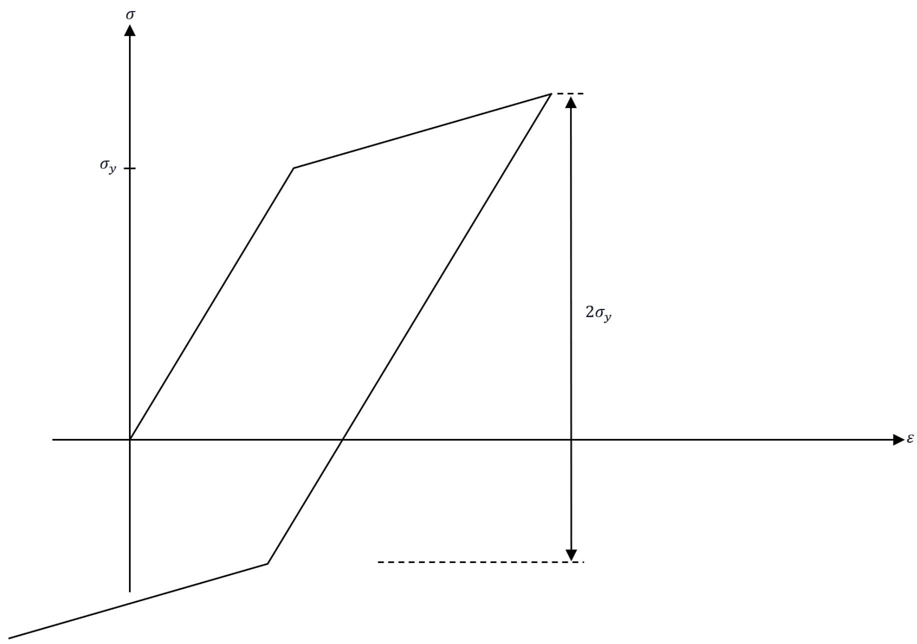

Figure 6.5: Stress-strain behavior of the bilinear kinematic plasticity model (BKIN), illustrating the translation of the yield surface and the premature reverse yielding associated with the Bauschinger effect.

This kinematic translation is strictly necessary to mathematically model the Bauschinger effect in high-strength steels. When the thread root yields in tension during the initial assembly sequence, the yield surface shifts in the tensile direction. Upon macroscopic unloading (disassembly), the local notch is driven into compression by the elastic springback of the surrounding bolt shank. Because the yield surface has translated, reverse yielding occurs prematurely in the compressive domain. This localized reverse yielding dissipates energy and accurately generates the residual compressive stress field that governs the fatigue survival of the fastener during subsequent operational cycles.

6.2.4.3 Equivalence Under Ideal Plasticity (Zero Hardening)

It is critical to note that the distinction between isotropic and kinematic hardening only manifests when the material exhibits strain hardening (i.e., when the tangent modulus $E_t > 0$). If the material is assumed to be perfectly plastic—characterized by zero hardening ($E_t = 0$)—both models yield mathematically identical responses.

Under ideal plasticity, the plastic modulus is zero; therefore, the BISO yield surface cannot expand (σ_k remains rigidly at σ_y), and the BKIN yield surface cannot translate ($\{\alpha\}$ remains zero). Consequently, as depicted in Figure 6.6, both formulations default to a standard elastic-perfectly plastic hysteresis loop. Reverse yielding consistently occurs exactly at $-\sigma_y$, regardless of any prior plastic deformation.

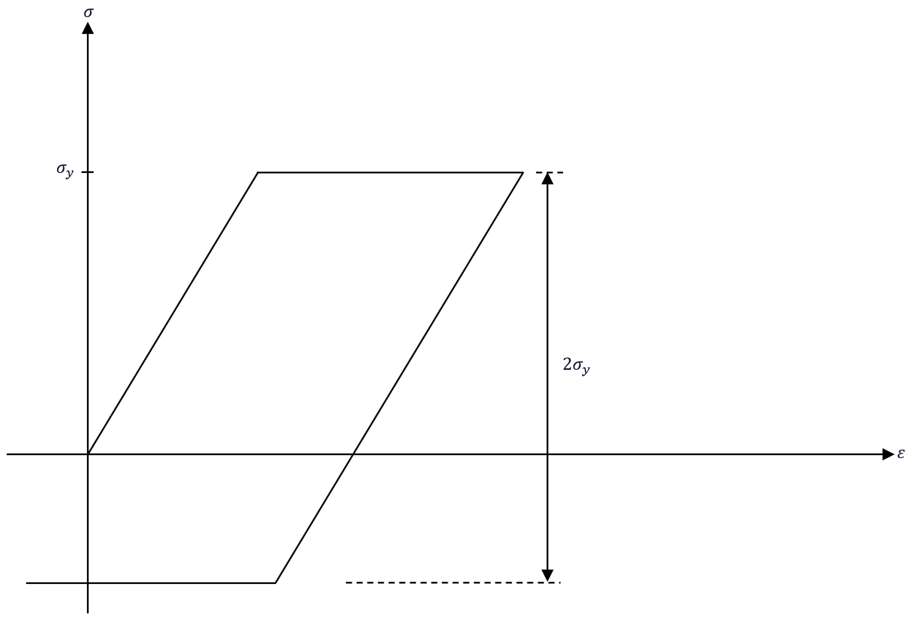

Figure 6.6: Stress-strain response under ideal (perfect) plasticity. With zero hardening ($E_t = 0$), the yield surface neither expands nor translates, resulting in identical theoretical behavior for both BISO and BKIN models.

6.3 Test Plan and Minimal Testing Strategy

Since the current EN 13445-3 bolt fatigue curve is not considered fully representative of the tightening-bolt application studied here, and since the strain-life interpretation alone is not sufficient for product design under the pressure vessel code, a dedicated experimental strategy is required. The purpose of the proposed test program is not to produce a complete final design standard within the scope of this thesis, but to define a realistic and statistically defensible path toward an application-adapted fatigue curve for tightening bolts under zero-based, large-amplitude loading.

The proposed test strategy separates the fatigue problem into two distinct domains. The in-operation case, dominated by repeated pressure fluctuations during service, is primarily a question of how existing bolt fatigue data and design curves are interpreted statistically. By contrast, the assembly and maintenance case is a fundamentally different physical problem. It involves large force amplitudes and a zero-based or near-zero-based loading history that is not well represented by the standardized axial bolt fatigue tests underlying the present EN 13445 curve. It is therefore this second case that necessitates a dedicated, rigorous test plan.

6.3.1 Purpose of the experimental program

The experimental program is intended to answer four primary questions:

- Can large high-strength tightening bolts subjected to repeated zero-based loading achieve fatigue lives significantly higher than those implied by current code curves?
- Is the local fatigue response better represented by a separate design curve for the assembly case than by the current generalized bolt curve?
- What scatter level is obtained under application-relevant test conditions, and what statistical interpretation of the data is appropriate for design use?
- What minimum number of tests is sufficient to establish a technically credible basis for a revised or supplementary fatigue assessment route?

The tests are conceived not as generic bolt fatigue tests, but as validation tests for a specific loading class expected to govern maintenance-related damage in large-scale tightening systems.

6.3.2 Relation to existing standardized bolt tests

The standardized bolt fatigue curves in pressure vessel design are largely based on legacy axial bolt tests, the OTO/HSE work on steel bolts [12]. Unfortunately, they do not fully represent the present maintenance loading case, in which the cycle consists of unloading, re-tightening, and loading up again from a near-zero baseline.

The proposed test plan retains the strong features of standardized axial testing—controlled axial loading and clearly defined failure criteria—while modernizing the statistical design of the experiment to strictly meet current standards, specifically the planning requirements of SS-ISO 12107:2012 [17], and modifying the load history to represent the assembly application.

To accurately represent the target population and minimize unexpected statistical bias, strict random sampling must be enforced. If the tightening bolts are sourced from multiple production batches or display a serial nature (e.g., varying dates of thread rolling), ISO 12107 dictates that specimens must be selected proportionally from each group to properly capture both within-batch and between-batch variance.

Furthermore, the standard requires that the allocation of these specimens to individual test load cases, as well as the order of testing, be randomized. If multiple test rigs are utilized in parallel to expedite the campaign, their mechanical equivalence must be formally verified prior to testing. Specimens must then be distributed equally across the parallel machines and tested in a randomized order to ensure that any systematic rig bias does not skew the final variance and design curve.

6.3.3 Proposed loading concept

The proposed primary test case is an axial zero-based fatigue cycle on a bolt or bolt-like specimen representative of the tightening bolt geometry. The load history should ideally represent the assembly case in simplified form:

- minimum load close to zero, or to the stabilized minimum clamp state judged relevant for the maintenance cycle
- maximum load corresponding to the target assembly plus operating condition
- constant-amplitude cycling at selected force levels
- tension–tension loading only, without compressive reversal

The intended load ratio is therefore close to

$$R = \frac{F_{\min}}{F_{\max}} \approx 0, \tag{6.40}$$

although a small positive minimum force may be necessary in practice to maintain fixture stability and avoid loss of alignment. The selected range should be justified as closely as possible with respect to the cycle definition adopted in the thesis.

6.3.4 Specimen concept

The preferred specimen concept is a full-size or near-full-size bolt assembly using standardized bolts of the same or closely similar type as those used in Alfa Laval tightening systems (M12, M20, M36, M48).

6.3.5 Proposed rig concept

A practical candidate for the experimental setup is a modified Pilgrim Hydrocam tensioner. Since such equipment is already intended for generating controlled axial force in large bolts, it provides a potentially suitable basis for a fatigue rig. However, modification is required before it can be regarded as a repeatable fatigue test machine.

The following rig requirements are identified:

- cyclic axial loading capability with repeatable control over minimum and maximum force
- adequate alignment to avoid bending
- fixtures allowing representative nut and bolt engagement
- sufficient stiffness in the frame and fixtures to prevent uncontrolled compliance
- instrumentation for force measurement and, if feasible, displacement or extension measurement
- safe management of run-out tests and specimen failure.

A modified Hydrocam concept could therefore include:

- a hydraulic loading system capable of repeated controlled force cycling
- integrated load cell or calibrated force measurement
- displacement measurement across the specimen or clamping system.

6.3.6 Test matrix and minimal number of tests

To establish a defensible design curve, the test matrix must be planned precisely in accordance with the regression model guidelines of SS-ISO 12107:2012 (Section 8.5). Unlike other methodologies that cluster specimens at discrete load levels to measure local variance, ISO 12107 explicitly discourages the use of replicate data. Instead, it requires test conditions to be distributed continuously across the stress range of interest.

This continuous distribution is preferred because it more clearly defines whether the fatigue response is linear or curvilinear, and it mitigates against bias by ensuring data are uniformly spread across the S-N curve.

A rigorous test matrix designed to provide statistical authority for a design or reliability curve consists of $n = 30$ total specimens, allocated as follows:

- One reference bolt series representative of the tightening bolts of interest, holding all major variables (diameter, grade, thread manufacturing route) identical.
- No grouped replicates. Each of the 30 specimens is assigned a distinct load (stress) level.
- Test conditions allocated in increments using the double logarithm of stress, rather than linear spacing. Because fatigue results tend to demonstrate significantly more scatter as the stress diminishes, using double-logarithmic increments naturally concentrates a higher density of specimens in the high-life/low-stress regimes, accurately mapping the increasing uncertainty along the length of the curve.
- The stress range should explicitly span from the yield-dominated high-stress regime down to the transition into run-out behaviour.

If the testing budget is strictly limited, SS-ISO 12107 allows for an initial exploratory matrix of $n = 10$ observations. However, 30 observations are required to formally establish a curve intended for structural design or reliability purposes.

6.3.7 Statistical evaluation strategy

The statistical interpretation of the experimental data is a central part of the proposed framework. The present thesis is motivated in part by the view that the current EN 13445 interpretation of bolt fatigue data is overly conservative. A new test program should therefore not only generate data, but also evaluate them using a transparent statistical procedure.

The proposed statistical treatment should follow the established fatigue regression analysis practices detailed in SS-ISO 12107:2012, alongside the guidance of Schneider and Maddox [8]. The main principles are

- fit the fatigue data in log-life versus log-stress form to establish the mean S-N curve
- calculate the continuous tolerance limits or prediction limits along the length of the curve based on the regression of the non-replicated, double-log distributed data points

- define an application-appropriate design curve through a stated survival probability (99.86% for typical pressure vessel code consistency) with a 95% confidence level
- report run-outs explicitly and handle them consistently using censored-data regression methods, such as maximum likelihood estimation.

A particularly important point in the present context is that the revised or supplementary fatigue curve should not be parameterized directly by ultimate tensile strength R_m in the design expression unless the test evidence clearly supports such a dependence. One of the criticisms of current practice is precisely that the relationship between material strength and fatigue design curve may be interpreted too conservatively or too simplistically. For the proposed assembly-case curve, the preferred starting point is therefore a pure, data-driven regression curve for the relevant bolt class and loading mode, rather than a generalized R_m-scaled formulation.

This does not mean that material strength is irrelevant. Rather, it means that its role should be established through test evidence and sensitivity studies, not imposed a priori as the primary design variable. If later datasets show systematic dependence on bolt strength class or manufacturing condition, that dependence can then be introduced explicitly.

6.3.8 Failure criteria and run-outs

For each test, the following outcomes should be recorded:

- number of cycles to failure, if fracture occurs
- failure location
- maximum and minimum load
- any detectable preload or stiffness change during cycling
- fixture observations, alignment issues, or secondary bending indicators

A run-out criterion should be specified in advance, for example at a high cycle count relevant to the intended design regime. Since the present assembly case is expected to involve relatively few severe cycles compared with in-operation loading, the chosen run-out level should reflect the realistic upper bound of maintenance-type cycling rather than an arbitrary very-high-cycle threshold alone. Nevertheless, a higher run-out limit may still be useful for comparison with conventional fatigue-design practice.

6.3.9 Link to FE and strain–life analysis

The FE and strain–life work in this thesis should be used to define and prioritize the test conditions. In particular, the FE model identifies the first engaged thread root as the critical location and provides a way to estimate how nominal load levels map to local stress and strain amplitudes. This allows the experimental load bounds (the maximum and minimum required stresses for the ISO 12107 double-logarithmic distribution) to be selected on a physically informed basis rather than by trial and error alone.

In this way, the FE analysis supports the experimental program in three ways

- by identifying the expected failure location
- by estimating relevant force boundaries for the zero-based cycle
- by helping interpret whether the resulting fatigue behaviour is predominantly elastic or elastoplastic at the thread root.

The experimental program then provides the validation needed to determine whether the strain–life interpretation can be translated into a practical design method.

6.3.10 Proposed outcome of the test program

The intended outcome of the proposed test strategy is not a fully finalized product-standard design curve within the scope of this thesis. Rather, the goal is to establish the foundation for such a curve by:

- defining a representative zero-based fatigue test method for tightening bolts
- identifying a feasible rig concept based on a modified Pilgrim Hydrocam tensioner
- proposing a minimal but mathematically robust test matrix based on ISO 12107 regression guidelines
- defining a transparent statistical evaluation route
- connecting the test program to FE-based local stress and strain analysis

Taken together, this forms a technically defensible path toward an application-adapted fatigue assessment for Alfa Laval tightening bolts, in which the in-operation case and the assembly case may ultimately be treated separately and then combined using cumulative damage concepts.

6.3.11 ISO 12107 Procedure for Test Execution and Curve Estimation

To ensure the resulting data can legally support a structural design curve, the physical execution of the tests and the subsequent mathematical curve fitting must strictly follow the procedural guidelines detailed in SS-ISO 12107:2012 (Annex A.3 and A.4). This procedure governs how the discrete load levels are mathematically calculated, how the tests are physically sequenced, and how the final regression model is selected.

6.3.11.1 1. Double-Logarithmic Load Allocation

As established, the 30 non-replicated specimens must be allocated across the stress range of interest. Because fatigue scatter increases significantly as stress diminishes, a simple linear or single-logarithmic spacing of load levels is inadequate; it leaves the highly variable low-stress regime under-sampled.

ISO 12107 resolves this by mandating double-logarithmic incrementing. Once the maximum and minimum stress boundaries of the assembly load case are defined (informed by the FE analysis), the stress increment for each successive test is calculated using the double logarithm of those bounds. For a 30-specimen campaign, the increment step (Δ) is determined by:

$$\Delta = \frac{\log_{10}[\log_{10}(S_{\max})] - \log_{10}[\log_{10}(S_{\min})]}{29} \tag{6.41}$$

(Note: If the stress or strain values are less than 1.0, the standard requires scaling the values prior to the logarithm to avoid mathematical errors with negative logs).

Applying this increment generates 30 distinct candidate stress levels. This mathematical approach inherently clusters a higher density of test specimens in the high-cycle/low-stress regimes, perfectly mirroring the region where statistical uncertainty is greatest.

6.3.11.2 2. Iterative Test Execution

Rather than blindly executing the 30 tests in their randomized order, the experimental plan must be executed iteratively. The standard requires that a preliminary subset of specimens (e.g., 3 to 5 bolts) be tested first.

The results of these initial tests are plotted against the anticipated S-N response to verify whether the actual fatigue behaviour aligns with the expected bounds. If the bolts fail significantly earlier or later than anticipated, the remaining candidate stress levels in the test matrix are adjusted accordingly. This iterative process of testing, verifying, and adjusting guarantees that by the end of the campaign, the failures are successfully distributed across the entire cycle range of interest without wasting specimens on inappropriate load levels.

6.3.11.3 3. Regression Model Selection (Linear vs. Quadratic)

Current pressure vessel codes, including EN 13445-3, universally assume that the bolt fatigue response is strictly linear on a log-log scale. However, when developing a new data-driven curve, SS-ISO 12107 requires statistical proof that a linear model is appropriate.

Once the test data are generated, both a standard linear model and a curvilinear (quadratic) model must be fitted to the data. The models are evaluated using:

- Residual Analysis: Standardized residuals for both models are plotted against the predicted life. If the linear model's residuals show a distinct curve (the "classic case" where a straight line fails to capture a yielding transition or endurance limit), the quadratic model is preferred.
- General Linear Test (F-test): An F-test is conducted to quantitatively determine if the addition of the quadratic term significantly improves the fit of the data.
- Variance and R^2 Comparison: The standard deviations and correlation coefficients of both models are compared.

If the statistical evaluation proves that the zero-based loading case produces a curvilinear response (which is highly possible given the elasto-plastic thread root yielding at high loads transitioning to purely elastic behaviour at low loads), the quadratic model must be selected as the baseline for calculating the tolerance limits. This ensures the final design curve reflects the true physical behaviour of the tightening bolts, rather than forcing the data into an artificially linear legacy framework.

7

Results

7.1 FEA Results

The finite element results are presented in five steps. First, the numerical convergence of the mesh is examined. Second, the elastic stress concentration factor is compared with literature data to validate the geometry. Third, the local stress distribution is evaluated to confirm the fatigue-critical location. Fourth, the local stress and strain histories are analyzed by comparing purely elastic, Bilinear Isotropic (BISO), and Bilinear Kinematic (BKIN) material models. Finally, the stabilized hysteresis loops are extracted to establish the input for the local strain-life fatigue assessment.

7.1.1 Mesh convergence study

Since the fatigue assessment is governed by highly localized stresses and strains at the first engaged thread root, a mesh convergence study was carried out to ensure that the extracted notch quantities were not unduly influenced by discretization. Particular attention was given to the circular thread-root fillet, where the stress gradient is steep and where the stress concentration factor is defined.

The convergence study was performed for the M20 model by systematically refining the mesh along the thread-root fillet while keeping the overall geometry, contact definitions, and loading conditions unchanged. The refinement parameter was the number of element divisions along the root fillet. The monitored quantity was the elastic thread-root stress concentration factor K_t, evaluated from the maximum Von Mises stress in the first engaged thread root and the nominal thread stress.

The results showed that the global force response converged rapidly, whereas the local thread-root stress required substantially finer discretization. This behaviour is expected for notch-dominated problems, where local peak stresses are more sensitive to mesh density than nominal quantities. With increasing refinement of the root fillet, the calculated value of K_t increased monotonically and approached a stable engineering value. This indicates that coarse meshes underpredict the local peak stress at the thread root and are therefore not suitable for fatigue-relevant stress extraction.

Table 7.1: Mesh convergence study for the M20 thread-root stress concentration factor.

Mesh factor	Divisions along root fillet	K_t
10	20	3.889
5	40	4.104
2.5	80	4.252
1	200	4.304
0.5	400	4.383

As shown in Table 7.1, the predicted stress concentration factor increases from $K_t = 3.889$ for the coarsest mesh to $K_t = 4.383$ for the finest mesh considered. The adopted mesh, corresponding to 200 divisions along the root fillet, gave $K_t = 4.304$, which differs by approximately 1.8% from the finest mesh. This was considered sufficient for the purposes of the present work, since further refinement would significantly increase the computational cost while only modestly changing the fatigue-relevant stress estimate.

7.1.2 Elastic Validation Against Literature

The elastic axisymmetric model was used to determine the thread-root stress concentration factor K_t for bolt sizes M8 to M24. The primary validation case considered here is the M20 bolt. Using the definition

$$K_t = \frac{\sigma_{\max}}{\sigma_0} \tag{7.1}$$

with

$$\sigma_0 = \frac{F_b}{A_s} \tag{7.2}$$

the finite element model gave a stress concentration factor of approximately $K_t \approx 4.304$ for the M20 bolt.

This value is lower than the value reported by Lehnhoff and Bunyard [14] for the corresponding M20 case, but is close to the value reported by Pedersen for an ISO metric thread in an axisymmetric contact model ($K_t = 4.56$). The present result therefore lies within 6% of Pedersen's result.

Differences relative to independent FE models are expected due to varying assumptions regarding exact root geometry, the number of engaged threads, and differences in contact idealization. The primary purpose of this elastic validation is to verify that the FE model produces realistic stress magnitudes prior to introducing elasto-plasticity.

7.1.3 Stress distribution and fatigue-critical location

In all analyzed bolt sizes, the highest local stress occurred at the root of the first engaged thread on the bolt side. This is consistent with established analytical results for axially loaded bolted joints and confirms that the first engaged thread root governs fatigue crack initiation. The stress decreased progressively in the subsequent engaged threads, reflecting the non-uniform load distribution through the nut.

Because the peak stress at the first engaged thread root far exceeded the material's elastic limit during the simulated assembly preload, a purely elastic assessment is physically invalid. The fatigue-critical location was therefore targeted for localized elastoplastic extraction throughout the cyclic analyses.

7.1.4 Local Time-History Response

To investigate the assembly and disassembly macro-cycles, the local thread-root response was evaluated under a perfectly plastic assumption ($E_t \approx 0$). As theoretically established in Figure 6.6, when the strain hardening modulus is zero, the isotropic (BISO) and kinematic (BKIN) hardening formulations yield mathematically identical stress-strain responses. Therefore, the following results are presented using the BISO formulation as the representative case for both models.

Figure 7.1 shows the nodal equivalent (Von Mises) stress at the first engaged thread root at the peak of the initial assembly preload, alongside the completely unloaded state. During assembly, the stress plateaus at the yield limit (940 MPa). Critically, the plastic yielding is highly localized and is entirely encapsulated by the surrounding elastic bolt shank.

Upon complete macroscopic unloading (disassembly), this elastic encapsulation forces the yielded thread root back toward its original geometry. As shown in the right pane of Figure 7.1, despite the global applied assembly force dropping to zero, the local notch remains under a significant residual stress field due to this elastoplastic springback.

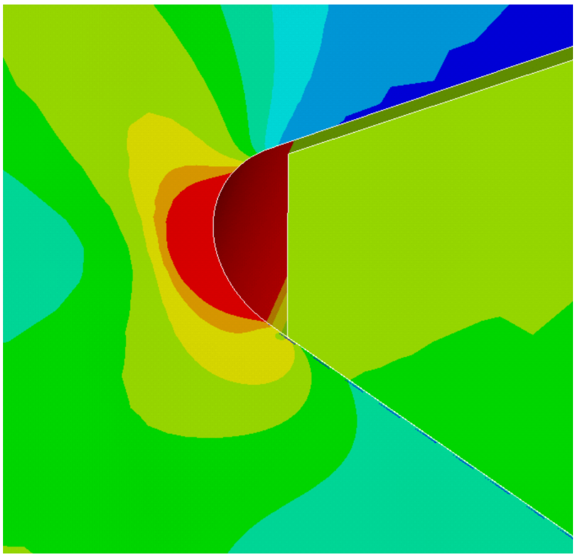

a) Peak assembly load, with yielding localized at the 940 MPa limit.

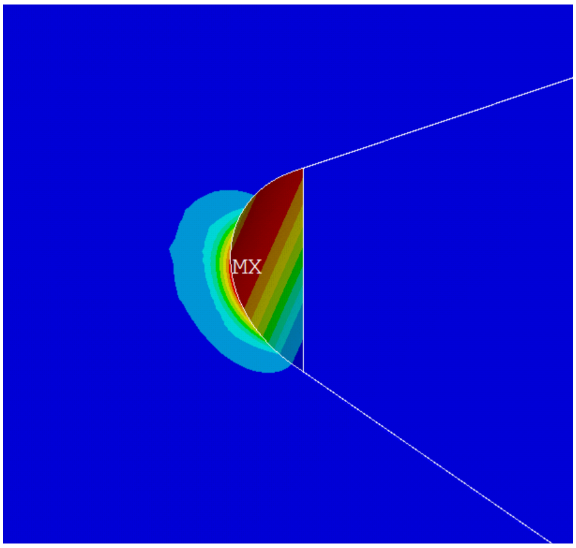

b) Completely unloaded state, revealing the localized residual stress field.

Figure 7.1: Nodal equivalent stress at the first engaged thread root under perfectly plastic conditions.

To accurately capture the severest cyclic response, the specific node exhibiting the maximum residual equivalent stress at the end of the final unloading step was identified as the fatigue-critical location. By tracking this specific node throughout the entire assembly and operational load history, the decoupling of local stress and strain over time becomes evident.

As shown in the total strain charts (Figure 7.7), the thread root takes a permanent plastic set (ε_p) during the initial assembly overload. When the macroscopic load is removed during disassembly, the massive elastic shank forces the permanently deformed thread root back to its original position. As seen in the corresponding stress charts (Figure 7.4), this springback drives the local axial stress deep into the compressive regime.

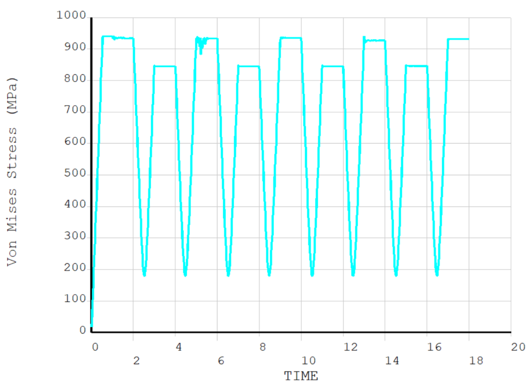

a) Equivalent Stress.

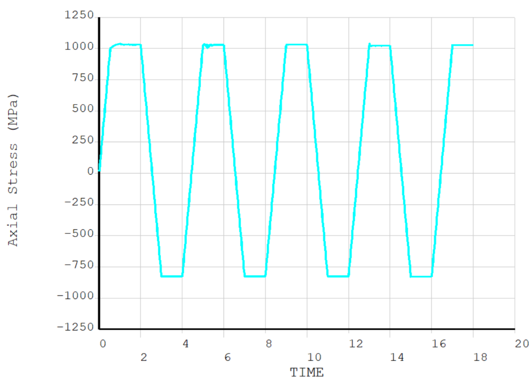

b) Axial Stress.

Figure 7.4: Time history of local stress over the simulated macro-cycles under perfect plasticity. The material demonstrates a significant compressive residual axial stress upon unloading.

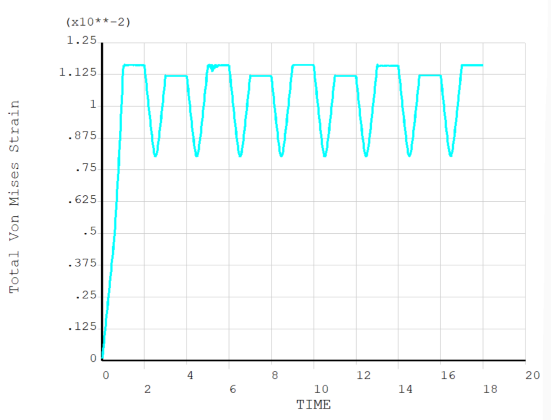

a) Total Equivalent Strain.

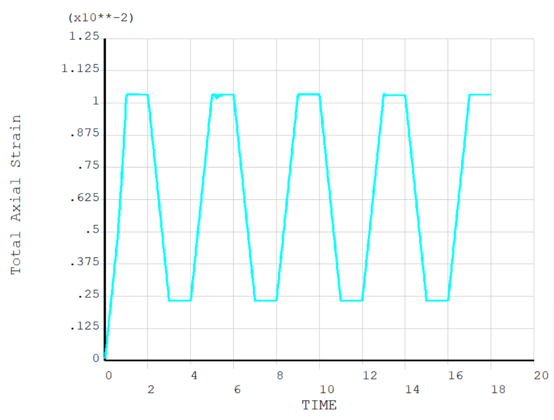

b) Total Axial Strain.

Figure 7.7: Time history of local total strain over the simulated macro-cycles under perfect plasticity. The thread root exhibits a permanent plastic set following the initial assembly overload.

7.1.5 Stabilized Hysteresis and Fatigue Implications

The physical nature of the springback mechanism is best illustrated by the stabilized local stress-strain hysteresis loops (Figure 7.10).

Because the simulation employs ideal plasticity, reverse yielding consistently occurs at the exact magnitude of the compressive yield limit ($-\sigma_y$), regardless of whether the solver uses the BISO or BKIN subroutine. As the elastic shank compresses the notch during disassembly, the material undergoes reverse yielding, forming a closed elastic-perfectly plastic hysteresis loop.

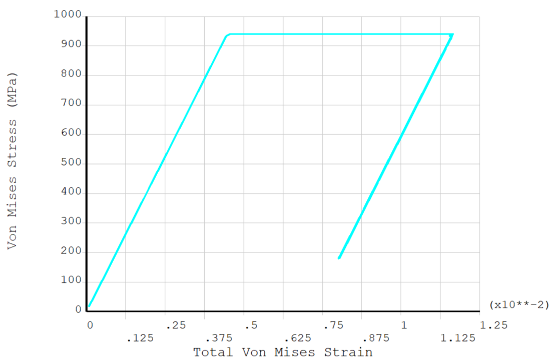

a) Equivalent Stress vs. Equivalent Strain.

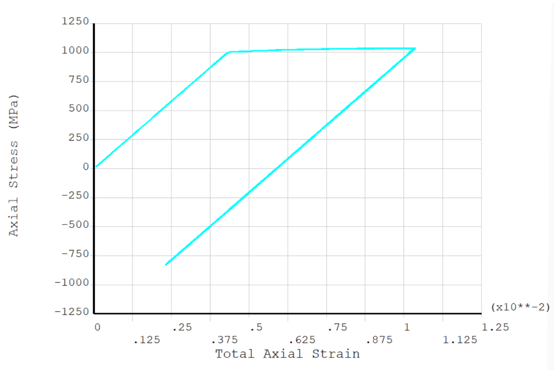

b) Axial Stress vs. Axial Strain.

Figure 7.10: Stabilized local stress-strain hysteresis loops at the critical thread-root node. Under perfect plasticity, the notch undergoes reverse yielding upon unloading, forming a closed loop.

A key observation from these loops is that the absolute local axial stress in the unloaded state is heavily compressive, effectively neutralizing the tensile mean stress of the subsequent operational pressure cycles. Furthermore, the fatigue-damaging part of the cycle is determined by the width of the stabilized loop (the strain amplitude, ε_a), rather than the peak elastic stress.

By bypassing the nominal elastic stress and directly extracting the stabilized strain amplitude (ε_a) from these elastoplastic hysteresis loops, the resulting values serve as the direct, physically accurate inputs for the Strain-Life (Coffin-Manson) fatigue assessment in Method 5.

7.1.6 Influence of Initial Proof Test Overload

In industrial practice, pressure vessels and plate heat exchangers are subjected to a hydrostatic proof test (typically at 1.43 times the design pressure) prior to commissioning. For the tightening bolts, this test pressure manifests as a severe, one-time axial overload (F_{test}) that exceeds the standard operational and assembly maximums ($F_{\max}$).

To evaluate the impact of this initial overload on the subsequent stabilized cyclic behaviour, an additional finite element load history was simulated. In this sequence, the bolt was first loaded to the calculated test pressure state, completely unloaded, and then subjected to the standard assembly macro-cycles. The resulting time histories for local stress and strain are presented in Figure 7.13 and Figure 7.16.

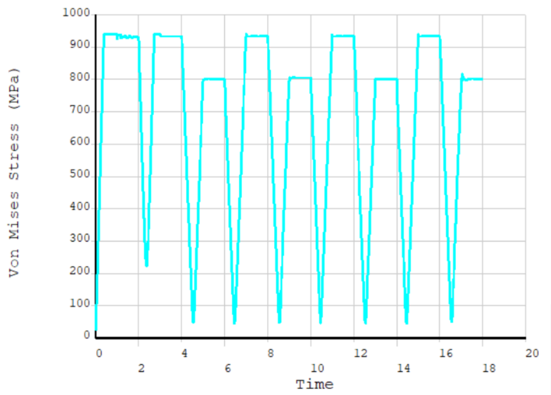

a) Equivalent Stress.

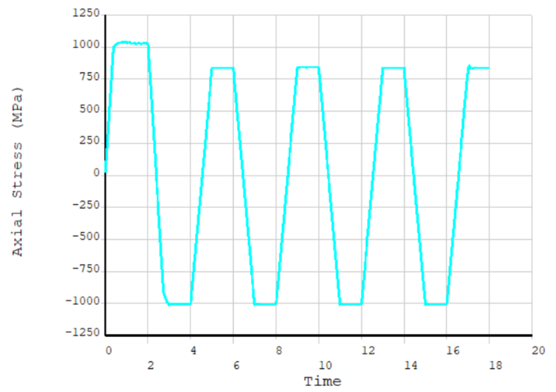

b) Axial Stress.

Figure 7.13: Time history of local stress including an initial proof test overload. The initial overload drives the thread root further into the plastic regime, resulting in a deeper compressive residual axial stress upon unloading compared to the standard assembly cycle.

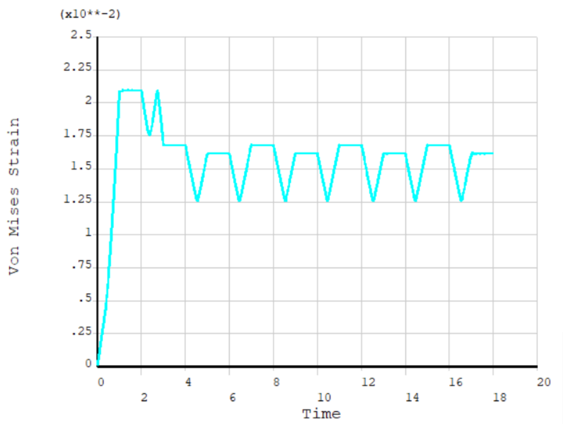

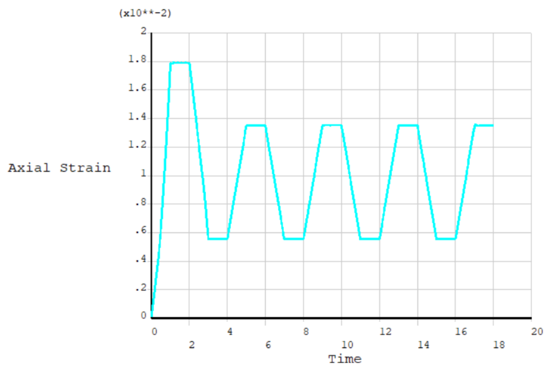

b) Total Axial Strain.

a) Total Equivalent Strain.

Figure 7.16: Time history of local total strain including an initial proof test overload. The first peak establishes a significantly larger permanent plastic set, after which the material shakes down elastically for the subsequent standard macro-cycles.

7.2 Strain–Life Calculations

7.2.1 Material Parameter Selection

To perform the local strain-life assessment, cyclic and fatigue-ductility properties of the bolt material are required. High-strength tightening bolts, such as those conforming to ISO property classes 10.9 or 12.9, are typically manufactured from quenched and tempered low-alloy steels. In the absence of proprietary cyclic test data for the specific fasteners used in the assembly, AISI 4340 steel was selected as a highly representative surrogate material. Its cyclic strain-hardening and fatigue-life parameters are extensively documented in established engineering literature, providing a reliable and physically appropriate benchmark for this elastoplastic evaluation.

7.2.2 Applied Method 4: Analytical Neuber Correction

Using the elastic stress concentration factor $K_t = 5.17$ from [14], an axial load and tensile stress area were chosen such that the nominal stress range is

$$\Delta\sigma_{\text{nom}} = \frac{F_z}{A_s} = 408.5 \;\; \text{MPa} \tag{7.3}$$

The nominal stress amplitude is therefore

$$\sigma_{\text{nom,a}} = \frac{\Delta\sigma_{\text{nom}}}{2} = 204.3 \;\; \text{MPa} \tag{7.4}$$

Applying the theoretical stress concentration factor yields the purely elastic notch stress amplitude:

$$\sigma_{\mathrm{e,a}} = K_t \cdot \sigma_{\mathrm{nom,a}} = 5.17 \cdot 204.3 = 1056.0 \ \ \mathrm{MPa} \tag{7.5}$$

which corresponds to an elastic local stress range of $\Delta\sigma_{\mathrm{local,el}} = 2112.0 \ \ \mathrm{MPa}$.

This theoretically derived stress level lies well above the physical elastic limit of the high-strength bolt material. Therefore, the purely elastic notch result cannot be used directly as the fatigue damage parameter. Instead, a local elastoplastic correction must be applied utilizing Neuber's rule alongside a cyclic Ramberg–Osgood relation.

Because explicit cyclic fatigue parameters for structural fastener grades are rarely published, AISI 4340 steel was selected as the reference material for this assessment. This selection is justified by its strong similarity to the macroscopic mechanical properties of standard grade 10.9 bolts, particularly regarding the monotonic yield stress and ultimate tensile strength (R_m). From established literature for AISI 4340 steel [5], the cyclic mechanical properties are:

$$E = 210,000 \ \ \mathrm{MPa}, \quad K' = 1448 \ \ \mathrm{MPa}, \quad n' = 0.09 \tag{7.6}$$

Neuber's rule dictates that the product of the local stress and strain amplitudes remains constant relative to the elastic prediction:

$$\sigma_a \varepsilon_a = \frac{\sigma_{\mathrm{e,a}}^2}{E} = \frac{1056.0^2}{210000} \approx 5.31 \ \ \mathrm{MPa} \tag{7.7}$$

The cyclic Ramberg–Osgood relation defines the stabilized elastoplastic response as:

$$\varepsilon_a = \frac{\sigma_a}{E} + \left(\frac{\sigma_a}{K'}\right)^{\frac{1}{n'}} = \frac{\sigma_a}{210000} + \left(\frac{\sigma_a}{1448}\right)^{\frac{1}{0.09}} \tag{7.8}$$

Solving Neuber's rule and the Ramberg–Osgood equation iteratively yields the localized elastoplastic stress and strain amplitudes:

$$\sigma_a \approx 840.2 \ \ \mathrm{MPa} \tag{7.9}$$

$$\varepsilon_a \approx 0.0064 \tag{7.10}$$

The plastic strain amplitude is isolated as:

$$\varepsilon_{\mathrm{p,a}} = \varepsilon_a - \frac{\sigma_a}{E} = 0.0064 - \frac{840.2}{210000} \approx 0.0024 \tag{7.11}$$

For the subsequent strain–life assessment, the fatigue parameters for AISI 4340 [5] are:

$$\sigma_f' = 1655 \ \ \mathrm{MPa}, \quad \varepsilon_f' = 0.73, \quad b = -0.076, \quad c = -0.62 \tag{7.12}$$

Assuming a fully reversed cycle (no mean stress correction) and no temperature reduction, the Coffin–Manson strain–life relation becomes:

$$\varepsilon_a = \left(\frac{\sigma'_f}{E}\right)\left(2N_f\right)^b + \varepsilon'^{c}_{f(2N_f)} \tag{7.13}$$

$$0.0064 = \left(\frac{1655}{210000}\right)\left(2N_f\right)^{-0.076} + 0.73\left(2N_f\right)^{-0.62} \tag{7.14}$$

Solving for the number of reversals to failure ($2N_f$) gives a predicted fatigue life of approximately:

$$N_f \approx 1,951 \quad \text{cycles} \tag{7.15}$$

The transition life (N_t), where the elastic and plastic strain amplitudes contribute equally to the total fatigue damage, is calculated as:

$$N_t = \frac{1}{2}\left(\frac{\varepsilon'_f \cdot E}{\sigma'_f}\right)^{\frac{1}{b-c}} = \frac{1}{2}\left(\frac{0.73 \cdot 210000}{1655}\right)^{\frac{1}{-0.076+0.62}} \approx 1,990 \quad \text{cycles} \tag{7.16}$$

Because the calculated fatigue life ($N_f \approx 1951$) lies slightly below the transition life, the material response is heavily influenced by the plastic strain regime, confirming that the local notch experiences significant plastic deformation. This illustrates that a purely elastic notch stress estimate vastly overpredicts the true local stress while simultaneously underestimating the corresponding local strain, proving that an elastoplastic correction is strictly necessary for analytical assessments.

7.2.3 Applied Method 5: Direct FEA Strain Extraction

Instead of relying on analytical notch approximations, this method utilizes the localized elastoplastic response extracted directly from the non-linear finite element model. From the final, plastically stabilized macro-cycle of the FE analysis, the local minimum and maximum strains at the fatigue-critical thread root were determined to be

$$\varepsilon_{\text{local,min}} = 0.00802582, \tag{7.17}$$

$$\varepsilon_{\text{local,max}} = 0.0116162. \tag{7.18}$$

The stabilized strain amplitude is extracted directly from these FE results as

$$\varepsilon_a = \frac{\varepsilon_{\text{local,max}} - \varepsilon_{\text{local,min}}}{2} = 0.001795 \tag{7.19}$$

Similarly, the corresponding local minimum maximum equivalent stress is taken directly from the stabilized FE load history

$$\sigma_{\text{local,min}} = 179.862 \text{ MPa}, \tag{7.20}$$

$$\sigma_{\text{local,max}} = 933.894 \text{ MPa}. \tag{7.21}$$

To account for the assembly loading conditions characterized by a non-zero mean stress, a Morrow-type mean stress correction is applied. The mean stress during the stabilized cycle is approximated as

$$\sigma_m = \frac{\sigma_{\text{local,max}} + \sigma_{\text{local,min}}}{2} = 556.878 \ \ \text{MPa}. \tag{7.22}$$

Using the same AISI 4340 fatigue parameters established previously ([5]), the Morrow-corrected strain–life equation is formulated as

$$\varepsilon_a = \left(\frac{\sigma'_f - \sigma_m}{E}\right)\left(2N_f\right)^b + \varepsilon'_f\left(2N_f\right)^c. \tag{7.23}$$

Substituting the FE-derived local strain amplitude and mean stress yields

$$0.001795 = \left(\frac{1655 - 556.878}{210000}\right)\left(2N_f\right)^{-0.076} + 0.73\left(2N_f\right)^{-0.62} \tag{7.24}$$

Solving this relationship produces a fatigue life on the order of

$$N_f = 1,426,587 \ \ \text{cycles} \tag{7.25}$$

7.2.4 Strain-Life Calculation Summary

The results of the strain–life fatigue assessments are summarized in Table 7.2. The comparison highlights that the predicted allowable life depends strongly on both the method used to obtain the local strain amplitude and the chosen mean stress correction model.

For the present case, the analytical Neuber-based approach (Method 4) gives substantially shorter predicted lives than the direct finite element strain extraction (Method 5). This reflects the fact that the two methods do not represent the local notch-root response in the same way. The Neuber approach estimates the local elastoplastic response from an elastic notch stress and a cyclic stress–strain law, whereas the FE-based method extracts the response directly from the adopted nonlinear model. In the present calculations, the FE model gives a much smaller stabilized strain amplitude ($\varepsilon_a = 0.001795$) than the Neuber approach, leading to a correspondingly much longer predicted fatigue life.

The choice of mean stress correction model has a secondary but still noticeable influence. For both methods, the Smith–Watson–Topper correction gives shorter allowable lives than the Morrow correction, although the dominant source of variation remains the difference between the two strain-extraction methods themselves.

Table 7.2: Summary of the strain–life fatigue assessments for the critical thread root. The table compares the damage parameters and predicted allowable cycles between the analytical Neuber approach (Method 4) and direct non-linear FEA extraction (Method 5) under both SWT and Morrow mean stress corrections.

Parameter	**Method 4 (SWT)**	**Method 4 (Morrow)**	**Method 5 (SWT)**	**Method 5 (Morrow)**
Effective stress amplitude	1383.02 MPa	1383.02 MPa	556.878 MPa	556.878 MPa
Effective strain amplitude	0.006443	0.006443	0.001795	0.001795
Allowable cycles	897	1,951	556,980	1,426,587

A limited material-parameter sensitivity check was also carried out in order to assess whether the use of AISI 4340 as a surrogate material influenced the strain–life results materially. Since the tightening bolts relevant to the present application are manufactured from 42CrMo4, which is more closely related to AISI 4140, the direct FE-based strain–life calculation (Method 5) was repeated using published cyclic fatigue parameters for quenched and tempered AISI 4140 steel. The parameter set used was $\sigma'_f = 1825$ MPa, $b = -0.08$, $\varepsilon'_f = 1.2$, and $c = -0.59$, corresponding to a strength level of approximately $R_m = 1075$ MPa.

The comparison is summarized in Table 7.3. The results show that, although the predicted allowable life changes quantitatively, the overall interpretation remains unchanged, the FE-based strain extraction still produces a much longer fatigue life than the Neuber-based estimate, and the response remains in the high-cycle regime. This indicates that the dominant driver of the predicted life is the stabilized local strain amplitude rather than the specific choice between two broadly similar low-alloy steel parameter sets.

Table 7.3: Limited material sensitivity check for the FE-based strain–life method using published cyclic fatigue parameters for AISI 4340 and AISI 4140.

Parameter	**4340 surrogate**	**4140 surrogate**
Fatigue strength coefficient, σ'_f	1655 MPa	1825 MPa
Fatigue strength exponent, b	−0.076	−0.08
Fatigue ductility coefficient, ε'_f	0.73	1.2
Fatigue ductility exponent, c	−0.62	−0.59
Predicted allowable cycles, Method 5 (SWT)	556,980	1,131,939
Predicted allowable cycles, Method 5 (Morrow)	1,426,587	4,724,043

8

Discussion

The results of the different fatigue evaluation methodologies are synthesized, critically comparing the code-based predictions against the numerical strain–life assessments.

8.1 Sensitivity Analysis

8.1.1 Sensitivity to Load Amplitude in Operational Loading

To illustrate the influence of the external load level, particularly the transition toward purely elastic behaviour characteristic of continuous operational loading, a sensitivity comparison was performed for two reduced external load amplitudes: $F_{\text{amp}} = 50$ kN (partly plastic) and $F_{\text{amp}} = 25$ kN (fully elastic). The allowable cycle predictions from the standard code procedures are presented in Table 5.2 and Table 5.3.

These results demonstrate that for the high-cycle operational loading regime, fatigue assessment using nominal-stress-based curves is generally adequate. The complex local elastoplastic evaluations required for assembly loading are not strictly necessary when the thread root operates primarily within the elastic domain.

However, direct application of the dedicated EN 13445 bolt curve (Method 1) remains conservative. As shown in the tables, Method 3 (Class 51) provides a higher allowable life, yielding 249,071 cycles compared to 129,430 cycles at the 25 kN amplitude, while still relying on established, empirically derived fatigue data. Consequently, the optimal approach for assessing operational loading is to shift the statistical interpretation of the standard bolt curve to a less conservative baseline, such as Class 51.

8.1.2 Sensitivity to Material Parameters in Strain–Life Assessment

The strain–life calculations presented in this work were initially based on published cyclic fatigue parameters for AISI 4340 steel, used as a surrogate. Since the tightening bolts relevant to the present application are manufactured from 42CrMo4, which is more closely related to AISI 4140, an additional comparison was made using published cyclic fatigue parameters for quenched and tempered AISI 4140 steel.

As shown in Table 7.3, replacing the 4340 surrogate with a 4140 parameter set changes the predicted allowable life quantitatively, but not qualitatively. For the FE-based strain extraction (Method 5), the SWT-corrected life increases from 5.56×10^5 to 1.43×10^6 cycles, while the Morrow-corrected life increases from 1.13×10^6 to 4.72×10^6 cycles. Although the numerical value of the predicted life is sensitive to the chosen material parameters, the overall interpretation remains unchanged.

This comparison indicates that the dominant driver of the Method 5 result is not the exact choice of surrogate low-alloy steel, but the small stabilized local strain amplitude predicted by the nonlinear FE model. In other words, the discrepancy between the code-based fatigue assessments and the FE-based strain–life result is influenced more strongly by the extracted cyclic response than by moderate changes in the strain–life parameters of broadly similar quenched and tempered steels.

8.1.3 Sensitivity to Hardening Models

The FE-based strain–life prediction is also influenced by the constitutive hardening model used in the nonlinear analysis. In the present work, the main elastoplastic simulations were carried out using a bilinear isotropic hardening model. Limited comparison indicated that there was little practical difference between a perfectly plastic material response and cases with a small hardening modulus. This suggests that, for the present loading case, the predicted stabilized local strain range is not strongly sensitive to small variations in hardening slope once local yielding has been initiated.

A more noticeable difference would be expected only if a substantially larger hardening modulus were introduced, or if a more advanced cyclic constitutive description such as kinematic hardening or combined nonlinear hardening were used. In such cases, the shape of the stabilized hysteresis loop could change more significantly, which would in turn alter the extracted plastic strain amplitude and the resulting strain–life prediction.

8.1.4 Implications of Proof Test Overloads

The finite element results regarding the initial proof test overload demonstrate a counter-intuitive but highly beneficial mechanism for the long-term fatigue life of the fastener. While the initial test pressure induces a severe plastic penalty at the first engaged thread root, it yields a distinct mechanical advantage for the remainder of the bolt's service life.

Because the notch root is driven further into the plastic regime during the test overload, the elastic springback of the surrounding unyielded shank upon unloading is proportionately greater. This enlarged springback forces the thread root into the deeper state of residual axial compression observed in the FEA results. When the standard assembly and operational cycles are subsequently applied, they operate entirely within this enlarged, protected elastic envelope.

The fundamental consequence is a distinct downward shift in the stabilized mean stress (σ_m). This phenomenon is highly analogous to mechanical presetting or autofrettage. It proves that an initial, controlled overload actually enhances the fatigue capacity of the fastener, provided the material possesses sufficient local ductility to absorb the initial plastic set without initiating a surface crack.

8.2 Limitations and Industrial Relevance

8.2.1 Cycle Definition and Equivalent Strain Reversals

A critical nuance in interpreting the direct finite element extraction (Method 5) lies in the definition of a fatigue cycle within the local multiaxial stress and strain histories. As illustrated in Figure 7.4 and Figure 7.7, while the macroscopic loading consists of a single tension-unloading sequence, the local equivalent stress and total equivalent strain responses exhibit a double-peak behaviour.

During the initial assembly tensioning, the axial stress is highly tensile, causing the equivalent strain to reach its first peak. Upon unloading, the elastic springback of the surrounding macroscopic geometry forces the plastically yielded thread root into severe axial compression. Because equivalent (von Mises) stress and strain are strictly positive scalar magnitudes, this negative axial stress state manifests as a second distinct peak in the equivalent history.

Consequently, if the damage parameter is extracted directly from the equivalent scalar history, one macroscopic assembly cycle effectively induces two distinct local strain reversals. To accurately translate the local cyclic damage back into the number of allowable macroscopic maintenance operations, the fatigue life results predicted by Method 5 must theoretically be at least halved. While this correction meaningfully reduces the absolute numerical prediction, the resulting life still vastly outperforms the EN 13445 empirical predictions and remains firmly in the elastic-dominated high-cycle regime.

8.2.2 Applicability to Non-Preloaded Conditions

Furthermore, it must be emphasized that the results extracted from Method 5 apply specifically to a bolt loading scenario without a constant operational preload, i.e. a zero-based assembly cycle. The absence of a maintained pretension is precisely what allows the bolt to fully unload, triggering the deep elastic springback that locks the thread root into a state of residual compression.

This full unloading forces the material into a highly stable elastic shakedown, which makes the resulting cyclic strain amplitude significantly smaller and drives the predicted fatigue life into the infinite regime. This specific stress–strain behavior would not occur in a bolted joint operating under a constant, high-level pretension. Under continuous operational pretension, the bolt never fully unloads. Consequently, the deep compressive springback effect is absent, the local mean stress remains persistently near the yield limit, and the localized strain amplitude is governed by the joint's operational stiffness ratio rather than the zero-based shakedown mechanics captured in this specific FEA.

8.2.3 Geometric and Manufacturing Idealizations

The large difference between the code-based assessments and the FE-based strain–life prediction highlights the limitations of idealized local modelling for threaded fasteners. The FE model used in the present work assumes a highly regular axisymmetric geometry, ideal contact conditions, and a simplified constitutive description. It therefore does not represent all of the geometric, manufacturing, and assembly-induced features that may influence the real stress and strain state in service.

In practice, tightening bolts in gasketed plate heat exchangers are affected by factors such as manufacturing tolerances, thread-profile variation, load redistribution between engaged threads, and possible secondary bending associated with frame deformation. These effects may alter the local notch-root response substantially. The small stabilized strain amplitude obtained from the present FE model should therefore be interpreted as a model result under idealized assumptions, not as a directly transferable design value.

From an industrial perspective, the direct FE strain–life approach is therefore most valuable as a comparative analysis tool rather than as a stand-alone design method. It can help identify the relative severity of different load definitions, assembly scenarios, or thread geometries, but it would require experimental calibration before being used as the primary basis for product qualification.

8.3 Comparison with Existing Standards

To contextualize the vast differences in the fatigue assessment methodologies, Table 8.1 summarizes the predicted allowable cycles across all five methods for the assembly loading case ($F_{\max} = 100$ kN). Here, the result from method 5 was halved due to the two spikes per cycle as previously discussed. Mean stress correction according to TWS, is shown here, as it was the most conservative of the two corrections.

Table 8.1: Overall comparison of fatigue life predictions across all five assessment methods for the zero-based assembly load case ($F_{\text{max}} = 100$ kN).

Method	Fatigue Basis	Damage Parameter	Mean Stress Correction	Allowable Cycles
Method 1: Dedicated Bolt Curve	Nominal Stress	$\Delta\sigma = 408.5$ MPa	Inherent	2,022
Method 2: Unwelded Component	Elastic Notch Stress	$\Delta\sigma_{\text{eq}} =$ 1,383 MPa	f_u factor	1,563
Method 3: Class 51 Component	Nominal Stress	$\Delta\sigma = 408.5$ MPa	Inherent	3,892
Method 4: Analytical Neuber	Elastoplastic Strain	$\varepsilon_a = 0.00644$	TWS	897
Method 5: FEA Extraction	Elastoplastic Strain	$\varepsilon_a = 0.00154$	TWS	278,490

As demonstrated in the table, the fatigue life predictions generated by the EN 13445-3 standard procedures (Methods 1, 2, and 3) exhibit a consistent order of magnitude, generally predicting failure between 1,000 and 4,000 cycles.

In contrast, the strain–life assessments (Methods 4 and 5) diverge significantly from the standard code predictions. The analytical Neuber approach (Method 4) yields a conservative result due to its reliance on a theoretical elastic stress concentration factor ($K_t = 5.17$). When the pseudo-elastic notch stress is artificially forced into a Ramberg–Osgood correction, it mathematically exaggerates the localized plastic strain, leading to a premature predicted failure.

Conversely, the direct FE extraction (Method 5) yields a much longer predicted fatigue life, vastly outperforming the EN 13445 predictions. The empirical code curves evaluate the component's global fatigue capacity, folding all physical and metallurgical imperfections into the reference curve. The numerical method, however, isolates pure elastoplastic continuum mechanics. Because the idealized FE model shakedowns to a very small stabilized cyclic strain amplitude, the governing Coffin–Manson equation interprets the stabilized state as an essentially infinite-life condition.

8.4 Influence of Gasket Settlement and Preload Relaxation

A further possible explanation for the discrepancy between calculated and observed fatigue life is that the actual bolt force during service and maintenance may be lower than assumed in the analytical and numerical assessments. In the present calculations, the bolts are idealized as reaching a specified assembly state and then experiencing the full subsequent load cycle from that condition. In reality, however, the gasketed plate pack is not perfectly elastic. During first tightening and early operation, the gasket and contacting surfaces may undergo irreversible compression, embedment, and local settling. Part of the imposed frame closure is therefore consumed by permanent deformation in the clamped package rather than by elastic elongation of the bolt.

This means that the same frame-to-pressure-plate displacement may correspond to a lower bolt force after the gasket has taken a permanent set. The resulting stabilized preload, and therefore the mean stress in the bolt, may then be lower than in the idealized assembly case used in the fatigue calculations. If the local thread-root stress or strain depends strongly on the total bolt force, the fatigue-driving response may also be reduced.

This does not imply that preload loss is always beneficial, since reduced clamp force can in some joint configurations increase the fraction of external load transferred into the bolt. The key point is instead that the stabilized service condition may differ materially from the assumed worst-case assembly condition. For the present application, this may contribute to a conservative fatigue prediction.

At present, this remains a hypothesis-based interpretation. No direct measurements of gasket settlement, preload relaxation, or stabilized bolt force after repeated assembly cycles have been included in the present work. A useful continuation would therefore be to measure the relation between frame displacement and bolt force during first assembly and subsequent reassembly.

The concept is illustrated schematically in Figure 8.1, where the first assembly path and the stabilized reassembly path are compared. The figure shows how the same achieved closure may correspond to a lower effective bolt force after gasket settlement.

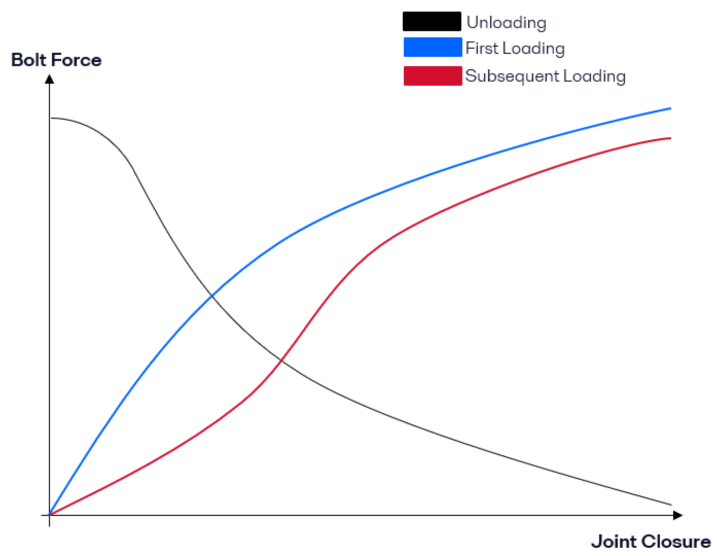

Figure 8.1: Illustration of conceptual load paths for a gasketed heat exchanger assembly. The figure highlights the potential discrepancy between the initial assembly bolt force and the reduced stabilized force following gasket settlement.

9

Conclusions and Recommendations

9.1 Summary of Findings

This thesis investigated the fatigue performance of high-strength tightening bolts in gasketed plate heat exchangers using both standard code-based procedures and local strain–life methods. The aim was to compare the empirical fatigue assessment routes used in EN 13445 with local elastoplastic modelling of the first engaged thread root.

The main findings may be summarized as follows.

- Both analytical and finite element approaches identified the first engaged thread root as the fatigue-critical location and confirmed that the local response is much more severe than the nominal bolt stress alone would suggest.
- The EN 13445-based procedures predicted allowable lives on the order of 10^3 to 10^4 assembly cycles for the applied example case, whereas the FE-based strain–life method predicted much longer lives due to the small stabilized strain amplitude obtained in the present nonlinear model.
- The difference between the numerical strain–life methods was driven primarily by the extracted strain amplitude rather than by the exact fatigue material parameters used. This indicates that the life prediction is highly sensitive to the modelling route used to estimate local cyclic strain.
- The FE-based strain–life result should not be interpreted directly as a product-design life, but rather as evidence that the local cyclic response predicted by the idealized model is much less severe than that implied by the empirical design curves.

9.2 Industrial Implications

For industrial application at Alfa Laval, these findings provide crucial guidance on how to deploy numerical and analytical fatigue tools safely and effectively in product development.

The direct finite element strain–life approach cannot safely replace standard code methods for absolute fatigue life certification without extensive physical calibration. The EN 13445 empirical curves inherently bundle the detrimental effects of thread manufacturing tolerances, galling, and non-uniform load distribution into their reference data. Therefore, the standard code methods remain the most robust and reliable baseline for production design and safety assessments.

However, the non-linear FE framework developed in this work holds significant industrial value as a comparative tool. While it may over-predict absolute cycles to failure, it is highly effective at mapping the mechanical severity of different tightening procedures or exploring geometric optimizations (e.g., modifying thread root radii or pitch profiles).

Furthermore, the hypothesis regarding gasket settlement and preload relaxation introduces a critical consideration for maintenance protocols. If the structural plate pack irreversibly compresses during early operation, the actual stabilized operational cycle will begin from a lower mean stress than the initial assembly overload. Tightening instructions and torque specifications should be evaluated not just for peak assembly closure, but for the true stabilized clamp force, as this dictates the operational mean stress state of the fastener.

9.3 Future Work

To bridge the gap between idealized numerical models and the complex physical reality of bolted heat exchanger assemblies, the following areas are recommended for future investigation.

- The current FE framework utilized a Bilinear Isotropic (BISO) hardening rule. Future numerical studies should implement advanced kinematic or combined cyclic hardening models to accurately capture transient phenomena like cyclic softening and mean stress relaxation, which are highly prevalent in quenched and tempered high-strength steels.
- The axisymmetric assumption should be relaxed in favor of a full 3D sector model. This would allow for the explicit simulation of pressure plate deformation and the resulting flange rotation, capturing the secondary bending stresses induced in the bolt shank and thread roots.
- A comprehensive, full-scale fatigue testing program should be executed to establish an empirical S–N curve specifically for the zero-based, large-amplitude macro-cycles characteristic of the assembly process. Following the rigorous statistical and regression procedures of SS-ISO 12107:2012, this campaign must span the complete dimensional range of operational bolts (e.g., M12 to M48) rather than a single geometry. This will allow for the precise quantification of volumetric size effects—conceptually similar to the legacy OTO testing—and provide a statistically defensible, physically calibrated design curve tailored specifically for the assembly loading of Alfa Laval heat exchangers.

10

References

[1] S. J. Maddox, “Fatigue Design Review: Task 5 — Assembly of Available Fatigue Data Relevant to Pressure Equipment Design: Final Report,” Sep. 2001.

[2] Joint Research Centre (JRC), Institute of Advanced Materials and European Pressure Equipment Research Council (EPERC), Technical Task Force 1, “Pressure components fatigue design, in the framework of Directive 97/23/EC on pressure equipment,” Dec. 2003.

[3] S. Suresh, *Fatigue of Materials, 2nd Edition.* Cambridge University Press, 2016.

[4] J. H. Bickford, *Introduction to the Design and Behavior of Bolted Joints: Non-Gasketed Joints*, Fourth. CRC Press, 2007.

[5] R. G. Budynas and J. K. Nisbett, *Shigley's Mechanical Engineering Design*, 11th ed. New York, NY: McGraw-Hill Education, 2019.

[6] Dansk Standard, “Befæstelseselementer – Mekaniske egenskaber for befæstelseselementer af kulstofstål og legeret stål – Kvalitetsklasser – Del 1: Bolte, skruer og tapskruer med grovog fingevind. Mechanical properties of fasteners made of carbon steel and alloy steel – Part 1: Bolts, screws and studs with specified property classes – Coarse thread and fine pitch thread,” no. DS/EN ISO 898-1. Dansk Standard, Feb. 18, 2013.

[7] “ISO general-purpose metric screw threads – Basic dimensions,” Vernier, Geneva, Switzerland, Apr. 2023.

[8] C. R. A. Schneider and S. J. Maddox, “Best Practice Guide on Statistical Analysis of Fatigue Data,” Cambridge, UK, Jul. 2003.

[9] G. Baylac and D. Koplewicz, “EN 13445 "Unfired pressure vessels": Background to the rules in Part 3 Design,” F-92038 PARIS LA DEFENSE, France, Aug. 2004. [Online]. Available: mailto:guy.baylac@wanadoo.fr

[10] Swedish Institute for Standards, “Tryckkärl (ej eldberörda) – Del 3: Konstruktion (SS-EN 13445-3:2021),” Stockholm, Sweden, 2021.

[11] Swedish Institute for Standards, "Tryckkärl (ej eldberörda) – Del 3: Konstruktion (SS-EN 13445-3:2021/A1:2025)," Stockholm, Sweden, 2025.

[12] Offshore Technology Organisation (OTO), "Fatigue Tests on Steel Bolts," 1997. [Online]. Available: https://www.hse.gov.uk/offshore/structural-integrity-research.htm

[13] "Metriska ISO-gängor för allmän användning — Basmått = ISO general purpose metric screw threads — Basic dimensions (ISO 724:2023, IDT)," no. SS-ISO 724:2023. 2023.

[14] T. F. Lehnhoff and B. A. Bunyard, "Bolt Thread and Head Fillet Stress Concentration Factors," *Journal of Pressure Vessel Technology*, vol. 122, no. 2, pp. 180–185, 2000, doi: 10.1115/1.556168.

[15] N. L. Pedersen, "Optimization of bolt thread stress concentrations," *Structural and Multidisciplinary Optimization*, vol. 46, no. 3, pp. 355–368, 2012, doi: 10.1007/s00158-012-0767-0.

[16] ANSYS, Inc., "Lesson 4: Definition of Plasticity from Experimental Data." [Online]. Available: https://innovationspace.ansys.com/courses/wp-content/uploads/sites/5/2020/12/Lesson-4-Definition-of-Plasticity-from-Experimental-Data.pdf

[17] "Metallic materials – Fatigue testing – Statistical planning and analysis of data," no. SS-ISO 12107:2012. Stockholm, Sweden, 2012.

[18] H. Bartsch and M. Feldmann, "Reassessment of fatigue detail categories of bolts and rods according to EC 3-1-9," *Journal of Constructional Steel Research*, vol. 180, p. 106588, 2021, doi: https://doi.org/10.1016/j.jcsr.2021.106588.

A

Appendix

A.1 OTO 97 067

A.1.1 Introduction

When establishing BS 7608, it was found that the existing design standards were often unclear and relevant test results seemed thin. Based off test results summarized in various Engineering Sciences Data Unit (ESDU) data sheets, the fatigue strength for bolts loaded in tension, uniquely in terms of the ratio:

$$\frac{\text{Stress range on the tensile stress area of the bolt}}{\text{Nominal tensile strength of the bolt material}} \tag{1.1}$$

Implicitly, it was assumed that, for bolts, fatigue strength would increase with increasing tensile strength.

Therefore, the particular S–N curves which were derived for design purposes were of the form

$$\left(\frac{\Delta\sigma_{\mathrm{R}}}{\sigma_{\mathrm{TS}}}\right)^3 N = C, \tag{1.2}$$

with a horizontal cut-off at $N = 2 \cdot 10^6$ cycles. The mean curve was assumed to have $C = 800$, and for the design curve, $C = 400$ with mean -2 standard deviations. For all bolts with sizes up 25 mm diameter, these curves were assumed to be relevant, while the fatigue strength of larger bolts was assumed to reduce in line with the relationship

$$S = S_B\left(\frac{d_B}{d}\right)^{0.25}, \tag{1.3}$$

where S_B is the defined fatigue strength of the bolt with diameter $d_B = 25$ mm and S is the strength of the larger bolt of diameter d mm.

These rules were to be supported by experimental results. It was proposed to investigate the fatigue strength of bolts in tension with reference to the influence of three main variables:

- the tensile strength of the bolt material;
- bolt diameter;
- the method of thread manufacture (i.e. cutting or rolling).

It is generally accepted that rolled threads have a higher fatigue strength than cut threads. The test data to define the magnitude of the improvement is lacking. This is also supported by [18]. The test plan, summarized in Table 1.1, was intended to examine each of these system parameters.

Table 1.1: Summary of test plan in [12]

Series No.	**Variable under Consideration**	**Material Grade**	**Diameter [mm]**	**Thread Form**	**Supplier**	**Testing Machine**
1 (a) 1 (b) 1 (c)	Basic Series	8.8	20	Cut	BNM BNM Prosper	Rig Los Los
2	Bolt diameter	8.8	12	Cut	BNM	Rig
3	Bolt diameter	8.8	36	Cut	BNM	Los
4	Steel grade	12.9	20	Cut	BNM	Rig
5 (a) 5 (b) 5 (c)	Thread form	8.8 8.8 8.8	20 20 20	Rolled Rolled Rolled	BNM BNM Prosper	Rig Los Los

A.1.2 Test Plan

The test plan was arranged to obtain some exploratory results relating to each of the three main variables, as follows in [12]:

- Bolt diameter, by testing bolts of 12 mm, 20 mm and 36 mm diameter, all with cut threads (Series 1,2 and 3). Three series of 20 mm diameter bolts were tested, emanating from two different manufacturers.
- Material grade, by testing bolts of 20 mm diameter of two material grades (8.8 and 12.9) (Series 1 and 4).
- Thread form, by testing bolts 20 mm diameter with both cut and rolled threads (Series 1 and 5). As with the cut threads (see 1 and above), the bolts with rolled threads came from two different manufacturers, and formed separate test series.

The original intention that the tests should be carried out at R $\approx$ 0.15 was subsequently modified and most of the tests were carried out with a higher positive minimum stress of approximately 0.2 times the nominal tensile strength. Here the stress ratio is defined as:

$$R = \frac{\sigma_{\min}}{\sigma_{\max}} \tag{1.4}$$

A.1.3 Testing Method

The tests in [12], were part of a larger test plan tasked with determining the fatigue strength of bolts in sea water. It was decided to make use of the corrosion fatigue testing rigs (with some modifications), which had been used for the UKOSRP tests, and in order to ensure strict comparability some the tests in air were also carried out in those rigs. The tests were normally carried out under axial tension loading. The modifications involved in the test rigs are shown schematically in Figure 1.1. There was also a loose fitting ‘safety bolt’ passing through the cantilever and the top beam near the end of the cantilever - keeping the rig together in case of a sudden failure of the test bolt - that was omitted for clarity.

It was found that it was not possible to obtain sufficient load from from the existing jacks to enable the 36 mm diameter bolts to be tested in the rig due to the increased minimum stress requirement. It was decided to fabricate a special test jig, details shown in Figure 1.2, for these specific tests in a standard Losenhausen hydraulic fatigue testing machine. Some of the air tests on 20 mm diameter bolts were also executed using the Losenhausen machine.

For every test, the objective was establish an S–N curve extending over the range of $\approx 10^5$ to $2 \cdot 10^6$ cycles, where the criterion of failure was taken as complete rupture of the bolt.

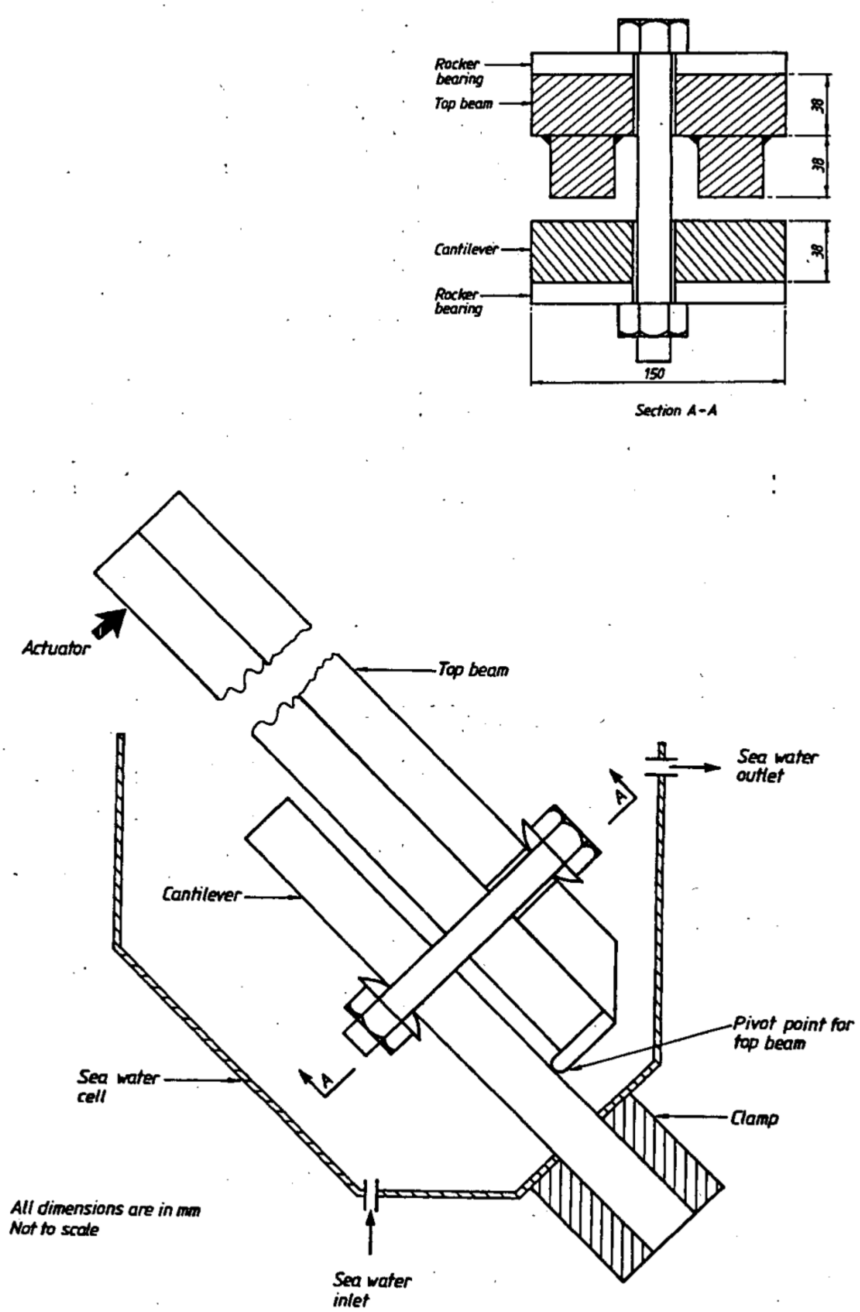

Figure 1.1: Diagram of test arrangement of axially loaded bolts

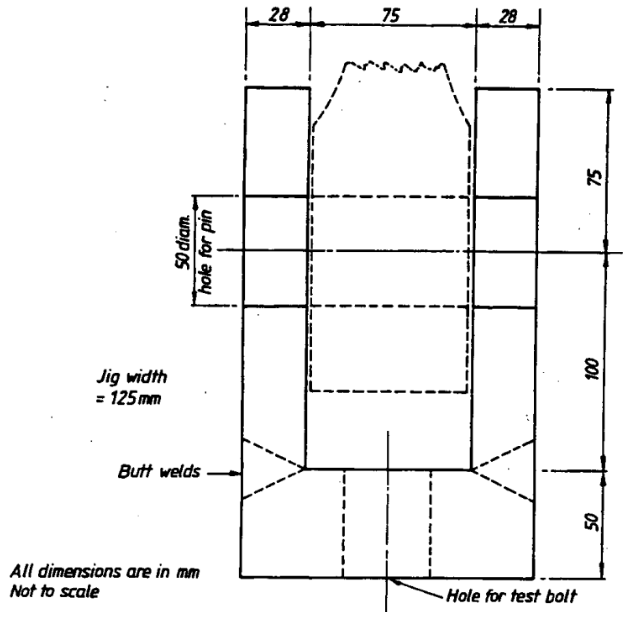

Figure 1.2: Details of jig for testing 36 mm diameter bolts in standard testing machine

A.1.4 Test Specimens

The test plan used steel bolts of Grades 8.8 and 12.9, using bolts typical to the industry at the time - BS 3692 “off the shelf” from BNM of Rotherham. In the cases were only the bolts with rolled threads were literally “off the shelf”, the requirement for cut threads involved those bolts being manufactured to order. However, no records were kept of the particular bar stock used for their manufacture. Tensile tests were carried out by The Welding Institute (TWI) on three specimens from each series, where the results are found in Table 1.2. In all three cases, the tensile properties were above specification. Two series of bolts were obtained from Prosper Engineering, where details of the mechanical properties of the material used to manufacture those bolts are shown in Table 1.3.

Most of the bolts were bent to some extent, as BS 3692 does not include a straightness requirement. Despite not having a formal requirement in the Standard, Industry at the time, worked to the tolerances set out in BS 6322, Part 1 ‘Tolerances for fasteners’. In terms of straightness, for bolts greater than 8 mm diameter, the maximum deflection when two ends of the bolt are placed on a flat table, must not exceed $0.0025l + 0.25$ mm, where l is the bolt length. It was found that all of the 10 bolts in a random sample were well within this required limit and were therefore accepted for testing.

Due to the lack of straightness, the bolt would be loaded by a combined axial force and bending moment, which is seen in Figure 1.3. The bending moment was intended to straighten the bolt and from then on the bending component would remain constant while the axial component increased. This was checked using one bolt of each diameter, statically loading the bolts in the test rig, with each bolt having four strain gauges attached at 90° intervals around the circumference. The bolts in the rig so that the plane of maximum bending was transverse to the longitudinal centerline of the rig.

Table 1.2: Tests by TWI on specimens extracted from bolts supplied by BNM

Bolt	**0.2% Proof stress, [N/mm²]**	**Tensile strength, [N/mm²]**
12 mm diameter, Grade 8.8, cut thread	742	866
20 mm diameter, Grade 8.8, cut thread	776	859
36 mm diameter, Grade 8.8, cut thread	783	914
20 mm diameter, Grade 8.8, rolled thread	868	913
20 mm diameter, Grade 12.9, cut thread	1,315	1,367

Table 1.3: Tests by Prosper Engineering on bolts supplied by them (20 mm diameter, Grade 8.8, cut and rolled threads)

Property	**Value**
Yield stress	865 N/mm²
Tensile strength	971 N/mm²

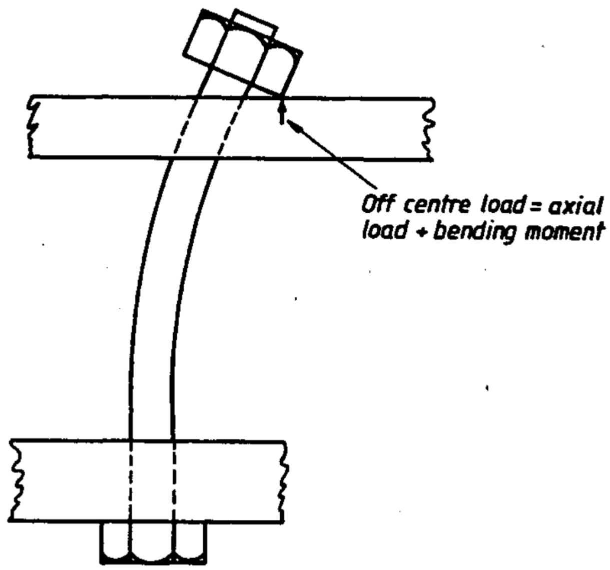

Figure 1.3: Exaggerated schematic showing the influence of the lack of straightness.

A.1.5 Static Loading Tests

The results of the static loading tests are in Figure 1.4, Figure 1.5 and Figure 1.6, which show the output for the two gauges on the plane of maximum curvature plotted against the sum of the outputs for all gauges (i.e. mean strain = 0.25 × the values shown).

In Figure 1.4 for a 12 mm diameter bolt, it is seen that the outputs from the two gauges became approximately parallel to each other at a strain sum of 2,200 (mean strain 550). Figure 1.5 reveals the results for a 20 mm diameter bolt, where the two outputs became parallel at a total value of about 1,600. This was for the second test, as the outputs from the two gauges were still diverging at 2,800 (mean = 700), indicating that small differences in the set can considerably influence the results. Figure 1.6 shows the results of a test on a 36 mm diameter bolt in which the outputs became roughly parallel at a total of about 1,400 (mean = 350).

In most instances, the outputs from the gauges on the two opposite sides of the bolt had become parallel at a mean strain of about 550 (total for four gauges = 2,200). It was decided that all the subsequent tests would be carried out with a maximum stress equal to about 20% proof [i.e. 150 N/mm^2 for which the equivalent strain is about 725 (=2,900 for the sum of the four gauges)].

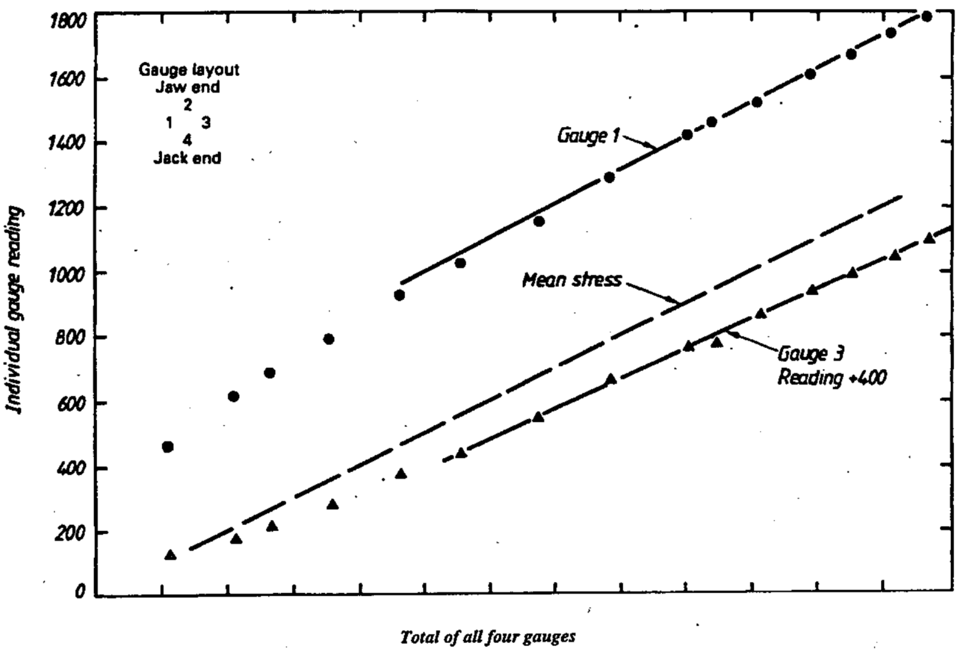

Figure 1.4: Results of static loading test on 12 mm diameter bolt

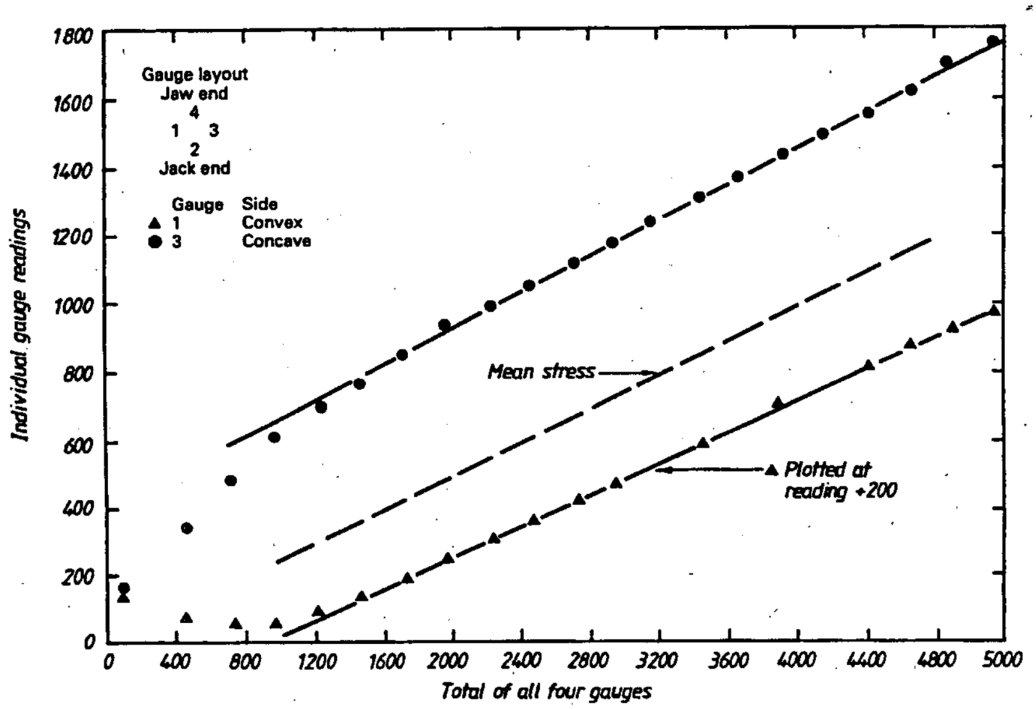

Figure 1.5: Results of static loading test on 20 mm diameter bolt

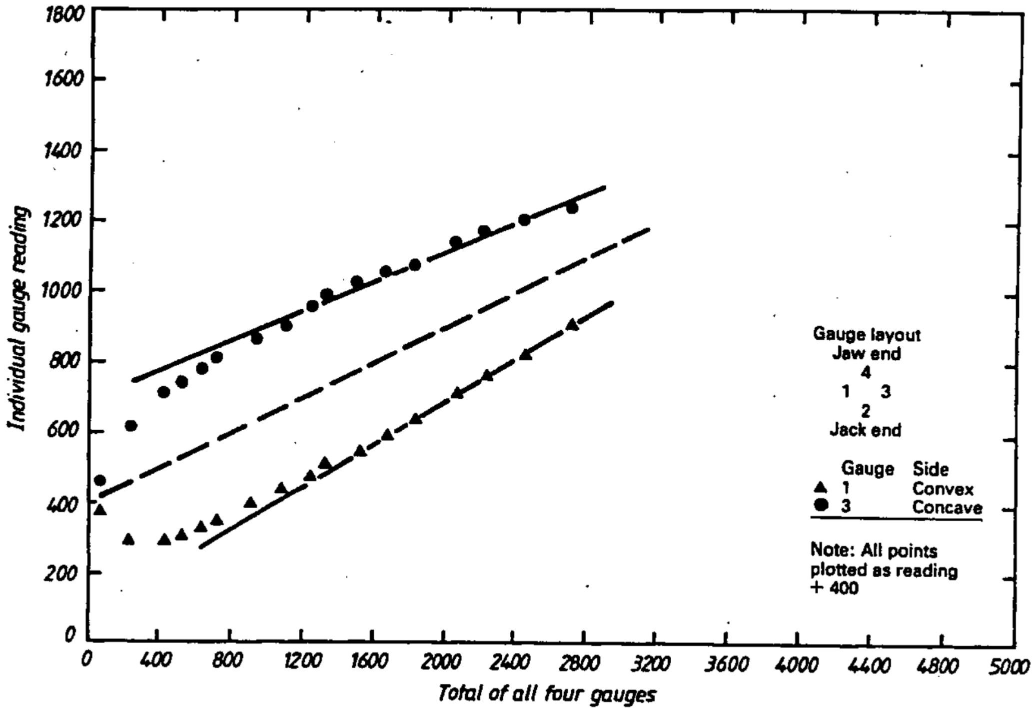

Figure 1.6: Results of static loading test on 36 mm diameter bolt

A.1.6 Fatigue Test Results

The results of the fatigue tests are summarized in Table 1.4 - Table 1.9. Many of the specimens failed right under the bolt head and not in threaded part of the bolt. Most of the 20 mm diameter Grade 8.8 bolts, both with cut and with rolled threads, failed in the cross-section at the entrance to the nut. There were two unusual results in the series with rolled threads, with failure located at the start of the threaded region.

The good correlation for the two series of 20 mm diameter bolts tested in the two machines in Table 1.4 made it reasonable to assume that no significant difference between results would have been introduced by the fact that 12 mm and 36 mm bolts were tested in the rig and the Losenhausen respectively. Comparing the results in Table 1.4, Table 1.5 and Table 1.6, it is clear that there is a significant size effect. However, it isn't consistent. The increase in bolt diameter from 12 mm to 20 mm gave a considerable reduction in life by approximately a factor of 3, as expected. The 36 mm bolts then gave an unexpected increase in fatigue life compared to the 20 mm bolts by a factor of about 1.8. The different failure modes, gave rise to the need of a closer examination of the shapes of the head-to-shank transitions and the threads relating to each test series.

When comparing the results in Table 1.8 series 5(a) to Table 1.4, the cut threads gave the slightly higher strength, where the mode of failure was the same in every case. This went against the convention that bolts with rolled threads should give a higher strength than those with cut threads due to the presence of residual compressive stresses at the surface induced by rolling. Metallurgical examination of some of the bolts revealed that the bolts produced by BNM had been heat treated after thread rolling, which removed the beneficial residual compressive surface stresses. The bolts obtained from Prosper Engineering had been thread rolled after heat treatment, and showed an increase in life by a factor between 4 and 10 depending on stress (see Table 1.9). Both methods of production are acceptable according to BS 3692, however, thread rolling must be carried out after heat treatment for improved fatigue performance.

S–N curves for bolts are usually presented in terms of stress/UTS rather than applied stress. When plotting with stress by itself instead, the two grades of bolt gave identical results. Fatigue design rules for bolts should then be presented in terms of stress alone rather than stress/UTS.

Table 1.4: Test results for 20 mm diameter, Grade 8.8 bolts with cut threads fabricated by BNM (Series 1(a) and (b))

(a) Tests in UKOSRP rig								
Spec. No.	**Error on straightness [mm]**	**Measured strains, ϑ**			**Stress range [N/mm²]**	**Stress range, UTS**	**Cycles to failure, [×10³]**	**Position of failure**
		Min.	**Max.**	**Range**				
805	–	905	1,765	860	178	0.226	52	All specimens failed at
800	–	1,145	1,894	749	155	0.197	91	entrance to nut except
801	–	787	1,483	696	144	0.183	108	where otherwise stated
802	–	1,605	2,209	604	125	0.159	139	
803	–	1,057	1,620	563	116	0.148	292	
806	–	909	1,358	449	91	0.118	535	
804	0.15	825	1,270	445	91	0.117	1,918	Failed under bolt head
807	0.18	799	1,175	376	78	0.10	729	
(b) Tests in Losenhausen machine								
Spec. No.	**Error on straightness [mm]**	**Applied stress [N/ mm²]**			**Stress range [N/mm²]**	**Stress range, UTS**	**Cycles to failure, [×10³]**	**Position of failure**
		Min.	**Max.**	**–**				
814	0.13	160	440	–	280	0.356	14.9	All specimens failed at
813	0.15	160	395	–	235	0.299	22	entrance to nut
808	0.13	160	340	–	180	0.228	64	
810	0.21	160	295	–	135	0.172	140	
815	–	160	280	–	120	0.153	180	
812	–	160	275	–	115	0.146	323	
809	0.29	160	260	–	100	0.127	544	
811	–	160	260	–	100	0.127	728	

Table 1.5: Test results for 12 mm diameter, Grade 8.8 bolts with cut threads tested under axial tension loading in UKOSRP rig (Series 2)

Spec. No.	**Error on straightness [mm]**	**Measured strains, ϑ**			**Stress range [N/mm²]**	**Stress range UTS**	**Cycles to failure [×10³]**	**Position of failure**
		Min.	**Max.**	**Range**				
669	0.15	715	1,844	1,129	233	0.297	118	All specimens failed
668	0.10	749	1,708	959	198	0.253	101	under bolt head
666	0.50	860	1,639	779	160	0.203	366	
667	0.18	1,158	1,746	588	122	0.155	575	
664	0.20	1,047	1,566	519	107	0.137	876	
665	0.20	837	1,253	416	86	0.110	2,949	
670	0.12	631	970	339	70	0.089	8,335	Unbroken

Table 1.6: Test results for 36 mm diameter, Grade 8.8 bolts with cut threads tested under axial tension loading in Losenhausen machine (Series 3)

Spec. No.	**Error on straightness [mm]**	**Applied stresses [N/mm²]**		**Stress range [N/mm²]**	**Stress range UTS**	**Cycles to failure [×10³]**	**Position of failure**
		Min.	**Max.**				
713	0.07	160	365	205	0.261	73	All specimens failed under bolt head
714	0.16	160	340	180	0.229	102	
708	0.12	160	335	175	0.223	113	
710	0.10	160	300	140	0.178	206	
707	–	160	280	120	0.153	321	
706	0.05	160	265	105	0.134	524	
711	0.11	160	255	95	0.121	656	
709	0.12	160	245	85	0.108	1,284	
712	0.10	160	240	80	0.102	2,364	

Table 1.7: Test results for 20 mm diameter, Grade 12.9 bolts with cut threads tested under axial tension loading in UKOSRP rig (Series 4)

Spec. No.	**Error on straightness [mm]**	**Measured strains, ϑ**			**Stress range [N/mm²]**	**Stress range UTS**	**Cycles to failure [×10³]**	**Position of failure**
		Min.	**Max.**	**Range**				
687	0.25	270	1,186	916	190	0.161	68	Under bolt head
684	–	1,936	2,689	753	155	0.132	54.3	Entrance to nut
685	0.20	989	1,669	680	141	0.119	131	Under bolt head
691	0.22	639	1,122	483	100	0.085	395	Under bolt head
688	0.22	1,225	1,654	430	89	0.075	634	Under bolt head
689	0.07	1,110	1,494	384	80	0.068	875	Under bolt head
686	0.11	529	867	338	70	0.059	1,439	Under bolt head
692	0.16	977	1,244	267	55	0.0466	5,906	Unbroken

Table 1.8: Test results for 20 mm diameter, Grade 8.8 bolts with rolled threads fabricated by BNM loading (Series 5(a) and (b))

(a) Tests in UKOSRP rig								
Spec. No.	**Error on straightness [mm]**	**Measured strains, ϑ**			**Stress range [N/mm²]**	**Stress range UTS**	**Cycles to failure [×10³]**	**Position of failure**
		Min.	**Max.**	**Range**				
726	0.07	677	1,445	768	159	0.202	86	All specimens failed at
724	0.08	996	1,643	677	140	0.178	116	entrance to nut except
725	0.05	981	1,559	578	120	0.153	156	where otherwise stated
727	0.12	970	1,456	487	101	0.129	304	
728	0.24	856	1,247	390	81	0.103	567	
729	0.12	635	958	323	67	0.085	1,856	
731	0.07	738	1,053	315	65	0.083	877	At start of bolt head
730	0.10	1,008	1,274	266	55	0.070	5,908	Unbroken
(b) Second batch (tested in Losenhausen machine)								
Spec. No.	**Error on straightness [mm]**	**Applied stress [N/mm²]**			**Stress range [N/mm²]**	**Stress range UTS**	**Cycles to failure [×10³]**	**Position of failure**
		Min.	**Max.**	**–**				
881	0.20	160	400	–	240	0.305	28.5	All specimens failed at
882	0.15	160	340	–	180	0.229	70	entrance to nut except
884	0.11	160	310	–	150	0.190	148	where otherwise stated
883	0.27	160	280	–	120	0.153	322	
886	0.12	160	260	–	100	0.127	436	
888	0.11	160	245	–	85	0.108	1,666	From end of thread
885	0.11	160	230	–	70	0.089	5,113	Unbroken

Table 1.9: Test results for 20 mm diameter, Grade 8.8 bolts manufactured by Prosper Engineering and tested under axial tension loading in Losenhausen machine

Series 1(c) Bolts with cut threads								
Spec. No.	**Error on straightness [mm]**	**Applied stress, [N/mm²]**			**Stress range [N/mm²]**	**Stress range σ_{TS}**	**Cycles to failure [×10³]**	**Position of failure**
		Min.	**Max.**	**–**				
859	0.05	160	400	–	240	0.305	29	All specimens failed
857	0.07	160	340	–	180	0.204	73	at entrance to nut
861	–	160	310	–	150	0.190	82	
858	0.04	160	280	–	120	0.153	293	
860	–	160	260	–	100	0.127	401	
862	0.09	160	240	–	80	0.102	2,390	
Series 5(c) Bolts with rolled threads								
870	0.06	160	460	–	300	0.381	46	Entrance to nut
871	0.08	160	400	–	240	0.305	79	Failed under head
872	0.07	160	360	–	200	0.254	356	Entrance to nut
873	0.05	160	340	–	180	0.229	456	Failed under head
874	–	160	330	–	170	0.216	823	Entrance to nut
869	0.10	160	320	–	160	0.203	2,703	Unbroken end of thread

A.2 Modeling Approaches

A.2.1 Bolt Stress Concentration Factors

Lenhoff et. al. [14] produced a theoretical study using FEA to determine stress concentration factors for the threads and the bolt head fillet in a bolted connection. The FEA models were axisymmetric representations of a bolt and two circular steel plates each 20 mm in thickness. Five different bolt sizes were examined (8, 12, 16, 20 and 24 mm diameter), all grade 10.9 metric bolts with the standard M thread profile. The analysis was made for threads modeled at both the minimum and maximum allowable depths and the fillet modeled at its minimum radius. The results of this work are summarized in Table 1.10 where the maximum K_t for thread is for the first thread and deepest tolerance limit and the minimum K_t for the thread is for the first thread and most shallow tolerance limit.

Table 1.10: Summary of elastic stress concentration factors for fillet and thread

Bolt Size	**K_t, Fillet**	**K_t, Thread**		
		Max.	**Min.**	**Mean**
M8	3.18	4.33	4.80	4.565
M12	3.23	4.32	4.80	4.56
M16	3.63	4.67	5.12	4.895
M20	3.58	4.77	5.17	4.97
M24	3.90	4.82	5.22	5.02

A.2.2 Bolt root shape optimization

Pedersen [15] later investigated the same general problem for metric ISO threads using axisymmetric finite element analysis, but with particular emphasis on the stress concentration at the first engaged thread root and the possibility of reducing it through optimized root geometry. In Pedersen's work, the bolt and nut were modelled as an axisymmetric contact system using concentric thread rings, and the stress concentration factor was defined in terms of the maximum Von Mises stress normalized by the nominal stress based on the stress area.

For the original ISO thread geometry, Pedersen reported thread-root stress concentration factors relative to the tensile stress area in the range $K_t = 4.09$ for M12 up to $K_t = 4.64$ for M24. The corresponding value for the M20 bolt was $K_t = 4.56$, which is somewhat lower than the deeper-thread values reported by Lenhoff et al. but still of the same order. Pedersen showed further that modest changes to the root contour could reduce the local stress concentration by approximately 6–9%, confirming the strong sensitivity of the fatigue-critical notch stress to local thread-root geometry.

The two studies are therefore consistent in showing that the first engaged thread root is the dominant fatigue-critical location in axially loaded bolted joints, and that the corresponding elastic stress concentration factor is high, typically of the order of $K_t \approx 4$–5 for standard metric bolts. At the same time, the reported values are not identical, which reflects the sensitivity of the result to assumptions regarding thread depth, root radius, number of engaged threads, and the exact FE idealization. In particular, Lenhoff et al. explicitly examined the effect of allowable thread depth variation, while Pedersen focused on a standard ISO geometry and its local optimization.